



Decouple charge transfer reactions in the Li-ion battery

Yuxuan Bai^a, Qiu-An Huang^{a,*}, Kai Wu^{b,*}, Juijun Zhang^{a,*}

^a Institute for Sustainable Energy/College of Sciences, Shanghai University, Shanghai 200444, China

^b Ningde Contemporary Innovation Laboratory, Contemporary Amperex Technology Co., Limited, Ningde 352100, Fujian, China

ARTICLE INFO

Article history:

Received 5 January 2024

Revised 3 February 2024

Accepted 4 February 2024

Available online 17 February 2024

Keywords:

Electrochemical impedance spectroscopy
Unified impedance model
Charge transfer reactions
Solid/electrolyte diffusion
Porous electrode
EIS-Toolbox@LIB

ABSTRACT

In the development of Li-ion batteries (LIBs) with high energy/power density, long cycle-life, fast charging, and high safety, an insight into charge transfer reactions is required. Although electrochemical impedance spectroscopy (EIS) is regarded as a powerful diagnosis tool, it is not a direct but an indirect measurement. With respect to this, some critical questions need to be answered: (i) why EIS can reflect the kinetics of charge transfer reactions; (ii) what the inherent logical relationship between impedance models under different physical scenes is; (iii) how charge transfer reactions compete with each other at multiple scales. This work aims at answering these questions via developing a theory framework so as to mitigate the blindness and uncertainty in unveiling charge transfer reactions in LIBs. To systematically answer the above questions, this article is organized into a three-in-one (review, tutorial, and research) type and the following contributions are made: (i) a brief review is given for impedance model development of the LIBs over the past half century; (ii) an open source code toolbox is developed based on the unified impedance model; (iii) the competitive mechanisms of charge transfer reactions are unveiled based on the developed EIS-Toolbox@LIB. This work not only clarifies theoretical fundamentals, but also provides an easy-to-use open source code for EIS-Toolbox@LIB to optimize fast charge/discharge, mitigate cycle aging, and improve energy/power density.

© 2024 Science Press and Dalian Institute of Chemical Physics, Chinese Academy of Sciences. Published by ELSEVIER B.V. and Science Press. All rights reserved.



Yuxuan Bai is currently a Ph.D. candidate at Institute for Sustainable Energy/College of Sciences, Shanghai University. He received his B.E. degree (2018) in Mechanical Design, Manufacturing, and Automation, and Master's degree (2021) in Vehicle Engineering from Xi'an University of Architecture and Technology, China. His research mainly focuses on electrochemical modeling and simulation.



Kai Wu is a professorate senior engineer and chief scientist of Contemporary Amperex Technology Co., Limited (CATL). Dr. Wu received B.Sc. in 1989 and M.Sc. in 1992 both from Shanghai Jiao Tong University (SJTU) and both in Naval Architecture Engineering. Dr. Wu also received Ph.D. from Shanghai Jiao Tong University (SJTU) and in Applied Chemistry. Since June 2023, Dr. Wu is a director for both National Engineering Research Center of Electrochemical Energy Storage and National Energy Battery Technology Research Center.



Qiu-An Huang is an associate professor at Institute for Sustainable Energy/ College of Sciences, Shanghai University. Dr. Huang received B.Sc. in 1997 from Beijing University of Chemical Technology (BUCT) and Ph.D. in 2009 from Huazhong University of Science and Technology (HUST), both in Control Theory and Control Engineering. Dr. Huang's research interest is focused on electrochemical impedance spectroscopy (EIS): theoretical modeling, fast measurement, and intelligent diagnosis for electrochemical energy storage and conversion devices.



Juijun Zhang is a Professor in Fuzhou University Institute for New Energy Materials / College of Materials Science and Engineering. Dr. Zhang is a Fellow of the Canadian Academy of Engineering, Fellow of the Academy of Science of the Royal Society of Canada, Fellow of the Engineering Institute of Canada, Fellow of the International Society of Electrochemistry, Fellow of the Royal Society of Chemistry, Fellow of the International Association of Advanced Materials, and an International Academician of the Chinese Academy of Engineering. Dr. Zhang received his B.S. and M.Sc. in Electrochemistry from Peking University in 1982 and 1985, respectively, and his Ph.D. in Electrochemistry from Wuhan University in 1988. Dr. Zhang's main research areas are Electrochemistry, Electrocatalysts, Fuel cells, Lithium batteries, Metal-air batteries, Supercapacitors, and H₂O/CO₂ electrolysis.

* Corresponding authors.

E-mail addresses: hqahqahqa@163.com (Q.-A. Huang), Wuk@catl.com (K. Wu), jiujun.zhang@i.shu.edu.cn (J. Zhang).

1. Introduction

1.1. Research background

Achieving Li-ion batteries (LIBs) with high-energy/power density, long cycling life, fast charging, and high safety is the necessary requirement for electric vehicles [1–9]. The high-performance LIBs might be achieved through the following efforts: (i) unveiling the factors limiting mass diffusion, charge transport, and charge transfer reaction [10–14] so as to optimize battery design [15,16] and process control [17,18] for a fast-charging capability; (ii) monitoring the battery status to guarantee safe operating for electric vehicles [19–24]; (iii) identifying model parameters to reveal kinetic properties and aging mechanisms [25–29]; (iv) understanding charge storage and transport mechanisms so as to maximize energy density and power output [30,31].

One of the keys of the above efforts is to gain a deep insight into charge transport through the solid electrolyte interlayer (SEI) film at the LIB anode [5,7], charge conductance/mass diffusion in the solid/electrolyte bulk [32,33], and charge transfer reaction at the solid/electrolyte interface [34]. In fact, all the above processes can be collectively referred to as charge transfer reactions, which is the focus of this work. In order to achieve the above goals, there have already been quite a few experimental characterizations [35–37] and theoretical calculations [4,38,39]. Among them, electrochemical impedance spectroscopy (EIS) might be regarded as one of powerful tools because of its advantages of wide bandwidth, high accuracy, and non-destructive diagnosis [7,9,40,41].

1.2. Literature review

Models are the core in analyzing and understanding the EIS data for impedance-based processes. Regarding modeling, several models for porous electrodes may be summarized as follows: (i) Transmission line model (TLM) for porous electrodes. Levie [42,43] first developed TLM for porous electrodes. Most recently, Huang et al. [44] extended the TLM for capacitance energy storage from single pore to porous electrode. (ii) The extended TLM for porous electrodes. Newman and Tiedemann [45] summarized the theory for porous electrodes for LIBs. Under the macro-homogeneous assumption, Paasch et al. [46] extended TLM to a more generalized case with a finite-thickness electrode and resistive solid/electrolyte phases. (iii) Charge/discharge model for intercalation electrodes. Newman et al. [47–49] developed a galvanostatic charge/discharge model for half and full cells, and the model has considered the diffusion in both solid matrix and electrolyte phase for porous intercalation electrodes. (iv) Numerical solution of impedance model for intercalation electrodes. By ignoring the electrolyte diffusion impedance, Newman et al. [50] developed impedance models for porous intercalation electrodes. Later, the solid/electrolyte diffusion impedance was considered for the full cell [51]. (v) Analytical solution of impedance model for intercalation electrodes. White et al. [52,53] developed an analytical solution of the impedance model without ignoring the solid/electrolyte diffusion. Later, it was degenerated by ignoring Li⁺ concentration gradient in the separator [54]. (vi) Spatial-resolved impedance model for intercalation electrodes. Plett et al. [55] built a set of exact closed-form impedance equations for a full cell with spatial-resolved frequency responses. Later, it was extended to be time-resolved and three-dimensional (3D) spatial-resolved [56].

If considering the diffusion in the solid/electrolyte phases and electronic resistance of the active particle material, impedance models reviewed above for porous electrodes can also be classified into five cases: (i) Model Doyle-Fuller-Newman (DFN) [51–53,55]. Model DFN comes from the physical model, which considers the

solid/electrolyte diffusion impedance and the electronic resistance of the solid phase. (ii) Model A [54]. Model DFN can be degenerated into Model A under the condition that Li⁺ concentration gradient of the electrolyte phase is ignored in the separator region. (iii) Model B [50]. Model A can be degenerated into Model B under the condition that Li⁺ concentration gradient of the electrolyte phase is ignored in the whole electrode. (iv) Model C [57]. Model B can be degenerated into Model C under the condition that the electrical resistance of the solid phase is ignored in the whole electrode. (v) Others (Models D–F) [42–46,58]. If the solid diffusion impedance is ignored in Models A–C, Models D–F can be obtained, respectively.

In the present work, Model DFN and Models A–F as the DFN-like impedance models are considered. The impedance model advancement for porous electrodes is summarized in Table 1.

There are also other classification methods for impedance models of porous electrodes: (i) Spatial dimension. Impedance models for porous electrodes have different spatial dimensions, for instance, one-dimensional (1D) [42,43,45,46,58], pseudo-two-dimensional (P2D) [50–55,57,59,60], and 3D [56]. (ii) Temporal dimension. In addition to traditional static impedance models reviewed above, there are dynamic impedance models [56,61] for porous intercalation electrodes. In short, dynamic EIS can capture transient information which static EIS cannot do. (iii) Phenomenological dimension. The equivalent circuit model (ECM) is phenomenological and loses specific physicochemical meanings [62,63]; however, it is still widely used due to its simplicity and ease of use. Physics-based ECMs are developed for LIBs as well [64–66]. In contrast, physics-based impedance models are rooted in strict mathematical derivation; therefore, their model parameters have rigorous physicochemical meanings [55,56,67–69]. In addition to physics-based ECMs, there are TLMs [70–73]. To some extent, TLMs are much closer to physics-based impedance models than ECMs.

With the advancement of the impedance model for porous electrodes, numerous valuable tutorials/reviews and researches have emerged, which are briefly reviewed as follows: (i) Tutorial and review for impedance models [5,7,9,73–78]. Lots of valuable reviews or tutorials for impedance models of porous electrodes have been reported, facilitating readers to understand the fundamentals as well as to track the development frontiers. (ii) Parameter identification. Parameter identification is important to the degradation prediction for LIBs [25], ranging from ECM [79] and single particle model [27,80,81] to physical impedance model [21,26,66,82,83]. These identification results are comparable [84,85]. (iii) Revealing rate limiting factors. To design fast-charging LIBs, it is required to identify rate limiting factors [11,86]. EIS can be used to reveal rate-determining steps [87–89], for example, revealing mass diffusion limiting, charge transport limiting, and transfer reaction limiting [90–94]. (iv) Cycling aging mechanisms. LIBs are deteriorated with respect to cycling aging [95–101]. EIS can be used to investigate aging mechanisms under different operating temperatures [102–104], charge rate [105], over-discharge/overcharge [106,107], cycle number [108], and short circuit [109,110]. (v) Status monitoring and prediction. The safety of electric vehicles mainly relies on LIBs [111,112]. In turn, LIBs safety consists of safe electrolytes [113], safety design [114], and safe operation [22]. Furthermore, safe operating relies on state prediction [104,115,116] and state control [21,23]. EIS might play a critical role in the operando monitoring and prediction for the above goals [77,117,118].

1.3. Research motivation

This work builds a theory framework to mitigate the blindness and uncertainty in unveiling the competitive mechanisms of charge

Table 1

Summary of impedance models from porous insertion electrode to full cell for LIBs.

Model	Author	Year	Solution	Component	Diffusion	Dimension	Ref.
Model DFN	J. Newman	2000	Numerical	Full cell	s + e	P2D	[51]
	R.E. White	2002	Numerical	Half cell	s + e	P2D	[59]
	V.R. Subramanian	2018	Numerical	Full/half cell	s + e	P2D	[60]
	R.E. White	2007	Analytical	Half cell	s + e	P2D	[52]
	R.E. White	2008	Analytical	Full cell	s + e	P2D	[53]
	G.L. Plett	2020	Analytical	Full cell	s + e	P2D	[55]
Model A	J. Huang	2016	Analytical	Single electrode	s + e	P2D	[54]
Model B	J. Newman	2000	Analytical	Single electrode	s	P2D	[50]
Model C	B. Roling	2020	Analytical	Single electrode	s	P2D	[57]
Model D	R.E. White	2004	Analytical	Symmetric electrode	e	1D	[58]
Model E	J. Newman	1975	Analytical	Single electrode	-	1D	[45]
	G. Paasch	1993	Analytical	Single electrode	-	1D	[46]
Model F	R. de Levie	1963	Analytical	Single electrode	-	1D	[42]
	R. de Levie	1964	Analytical	Single electrode	-	1D	[43]

Note: P2D denotes pseudo-two-dimensional; 1D denotes one-dimensional; s/e denotes solid/electrolyte phase.

transfer reactions in LIBs by using EIS data analysis through modeling. As reviewed above, great achievements have been made during the last several decades, involving theoretical modeling, in-situ measurements, and intelligent diagnosis. No doubt, the charging/discharging processes in a LIB involve not only mass diffusion and charge transport in the bulk phases of solid or electrolyte but also charge transfer reaction at the solid/electrolyte interface, ranging from particle to electrode and to full cell. Furthermore, the inherent characteristics such as nonselectivity, nonlinearity, competition, and overlapping can make the EIS diagnosis a rather complicated approach.

Compared to the urgent requirements, till now, progresses achieved with the EIS approach for LIBs are still relatively fragmented, although those diagnosis efforts have been made based on various impedance models under different physical scenes, non-standard measurement techniques, and non-uniform identification methods. As a result, it is difficult to share and compare those diagnosis results from different research groups, in particular for the competitive mechanisms of charge transfer reactions from particle to electrode and to full cell. If used improperly, the EIS diagnosis is not an opportunity but a pitfall.

In order to address the above challenges and mitigate the blindness and uncertainty in unveiling the competitive mechanisms of charge transfer reactions in LIBs through the EIS approach, two core questions are addressed in the present work: (i) Unifying impedance models of porous insertion electrodes for LIBs under different physical scenes, such as with or without considering the diffusion in the pore electrolyte in the separator region, the diffusion in the electrode matrix or the pore electrolyte in the electrode region, and the electronic conductance resistance in the electrode matrix. (ii) Building the theory framework for EIS diagnosis to unveil the competitive mechanisms of charge transfer reactions in LIBs with respect to the parameter changes involving kinetics, thermodynamics, transport, and geometry. The established theory framework can offer a theoretical method on how to separate the solid/electrolyte diffusion impedance in LIBs.

1.4. Paper organization

This paper is organized as follows. In Section 2, the LIB impedance models under different physical scenes are unified based on the systematic deduction with the complex phasor method. Corresponding to the unified impedance model, an open source code for the EIS-Toolbox@LIB in Matlab is available from Supporting Information. In Section 3, the competitive mechanisms of charge transfer reactions in LIBs are numerically analyzed based on the unified impedance model with respect to the parameter change involving kinetics, thermodynamics, transport, and geometry. In

addition, the sensitivity of the solid/electrolyte diffusion impedance of LIBs in the negative electrode to 11 battery parameters is quantitatively analyzed. In Section 4, the main conclusions are summarized for the present work.

2. Deduction, unification, and implementation of impedance models for LIBs

In this section, the impedance models over the past half century for LIBs are unified under different physical scenes via a complete model deduction with the complex phasor method. Based on the unified impedance model, an EIS-Toolbox@LIB is developed in Matlab.

2.1. Deduction of the DFN impedance model with the complex phasor method

2.1.1. Governing equation of impedance models

DFN-like impedance models for LIBs are based on the concentrated solution theory, porous electrode theory, and Butler-Volmer kinetics [47–49]. Fig. 1 shows governing equations (GEs) with initial boundary conditions (IBCs) [51–53,55,60], where Subscripts e and s denote the electrolyte phase and solid matrix phase, respectively; Subscripts 1, 2, 3, and 4 denote the negative electrode, positive electrode, separator, and full cell, respectively.

In addition, some supplements to GEs with ICBs shown in Fig. 1 are illustrated as follows.

$$D_{e,\text{eff}1} \frac{\partial c_{e1}(x, t)}{\partial x} \Big|_{x=L_1} = D_{e,\text{eff}3} \frac{\partial c_{e3}(x, t)}{\partial x} \Big|_{x=L_1} = \zeta_1(t) \quad (1-3)$$

$$D_{e,\text{eff}3} \frac{\partial c_{e3}(x, t)}{\partial x} \Big|_{x=L_1+L_3} = D_{e,\text{eff}2} \frac{\partial c_{e2}(x, t)}{\partial x} \Big|_{x=L_1+L_3} = \zeta_2(t) \quad (6-2)$$

The current through the electrolyte phase and the active material phase in Region 1, 2, or 3 is expressed by

$$i_e(x, t) = -\kappa_{\text{eff}} \frac{\partial \phi_e(x, t)}{\partial x} - \kappa_{D,\text{eff}} \frac{\partial \ln c_e(x, t)}{\partial x} \quad (13-1)$$

$$i_s(x, t) = -\sigma_{\text{eff}} \frac{\partial \phi_s(x, t)}{\partial x} = i(t) - i_e(x, t) \quad (13-2)$$

In Fig. 1, the relationship between j and j_F in Region 1 or 2 is expressed by

$$j(x, t) = j_F(x, t) + j_{dl}(x, t) + \frac{C_{sei}}{F} \frac{\partial}{\partial t} (\phi_s(x, t) - \phi_e(x, t)) \quad (14-1)$$

and j_{dl} in Region 1 or 2 is defined as

$$j_{\text{dl}}(x, t) = \frac{C_{\text{dl}}}{F} \frac{\partial}{\partial t} (\phi_s(x, t) - \phi_{\text{sf}}(x, t)) \quad (14-2)$$

ϕ_{sf} is related to ϕ_e in Region 1 or 2, which can be expressed as

$$\phi_{\text{sf}}(x, t) - \phi_e(x, t) = F(j_{\text{dl}}(x, t) + j_F(x, t))R_{\text{sei}} \quad (14-3)$$

where $C_{\text{sei}1}$ and $R_{\text{sei}1}$ in Region 1 are defined as

$$C_{\text{sei}1} \stackrel{\text{def}}{=} \varepsilon_{\text{sei}1}(\delta_{\text{sei}1} + r_{s1})/(\delta_{\text{sei}1}r_{s1}) \text{ and } R_{\text{sei}1} \stackrel{\text{def}}{=} \rho_{\text{sei}1}\delta_{\text{sei}1}r_{s1}/(\delta_{\text{sei}1} + r_{s1}).$$

2.1.2. Definition of impedance models for LIBs

Before deducing DFN-like impedance models for LIBs, the following assumptions may be made [51,119]: (i) LIBs are uniform and homogeneous; (ii) responses are linear; (iii) a complex sinusoidal signal is imposed on LIBs under the static condition, i.e., the open-circuit condition; (iv) transient responses are explicitly ignored; (v) no side reactions happen under complex sinusoidal signal excitation; (vi) different kinds of currents are measurable and separable.

In this work, the complete phasor method is used to deduce the DFN-like impedance models for LIBs in a more concise and readable method [44]. Firstly, $i(t)$ imposed on LIBs is defined as

$$i(t) = \sqrt{2}I \exp(j\omega t) \quad (15-1)$$

$$I = \frac{i_{app}}{A} \exp(j\varphi_0) \text{ and } \varphi_0 = 0 \quad (15-2)$$

where I is the phasor of complex sinusoidal current density signal $i(t)$.

In order to eliminate the influence of the initial value from the time domain to the phasor domain, the debiased response variable is defined as [120]

$$\tilde{\varphi}(x, t) \stackrel{\text{def}}{=} \varphi(x, t) - \varphi(x, 0) \quad (16-1)$$

Eq. (16-1) results in $\tilde{\varphi}(x, 0) = 0$. Herein, $\varphi(x, t)$ collectively refers to variables of $c_s(x, t)$ or $\phi_s(x, t)$ in Region 1 or 2 and $c_e(x, t)$ in Region 1, 2, or 3.

Based on the above assumptions, under the excitation of complex sinusoidal current signal $i(t)$, response variables in Eqs. (1-1)–(14-3) for LIBs can be expressed as

$$\psi(x, t) = \sqrt{2}\dot{\Psi}(x, j\omega)\exp(j\omega t) \quad (16-2)$$

where $\dot{\Psi}(x, j\omega)$ denotes the complex phasor of the time domain variables of $\tilde{c}_s(x, t)$, $\tilde{\phi}_s(x, t)$, $\phi_{\text{sf}}(x, t)$, $j(x, t)$, $j_{\text{dl}}(x, t)$, or $j_F(x, t)$ in Region 1 or 2, and $\tilde{c}_e(x, t)$ or $\phi_e(x, t)$ in Region 1, 2, or 3.

Till now, LIBs impedance model containing $Z_1(s)$ for negative electrode, $Z_2(s)$ for positive electrode, $Z_3(s)$ for separator, and $Z_4(s)$ for full cell can be defined as follows.

$$Z_1(s) \stackrel{\text{def}}{=} -\frac{\dot{\Phi}_{e1}(L_1, s) - \dot{\Phi}_{s1}(0, s)}{\dot{I}(s)} \quad (17-1)$$

$$Z_2(s) \stackrel{\text{def}}{=} -\frac{\dot{\Phi}_{e2}(L_4, s) - \dot{\Phi}_{s2}(L_1 + L_3, s)}{\dot{I}(s)} \quad (17-2)$$

$$Z_3(s) \stackrel{\text{def}}{=} -\frac{\dot{\Phi}_{e3}(L_1 + L_3, s) - \dot{\Phi}_{e3}(L_1, s)}{\dot{I}(s)} \quad (17-3)$$

$$Z_4(s) \stackrel{\text{def}}{=} -\frac{\dot{\Phi}_{s2}(L_4, s) - \dot{\Phi}_{s1}(0, s)}{\dot{I}(s)} \quad (17-4)$$

The detailed definitions for parameters in the above equations refer to Supporting Information.

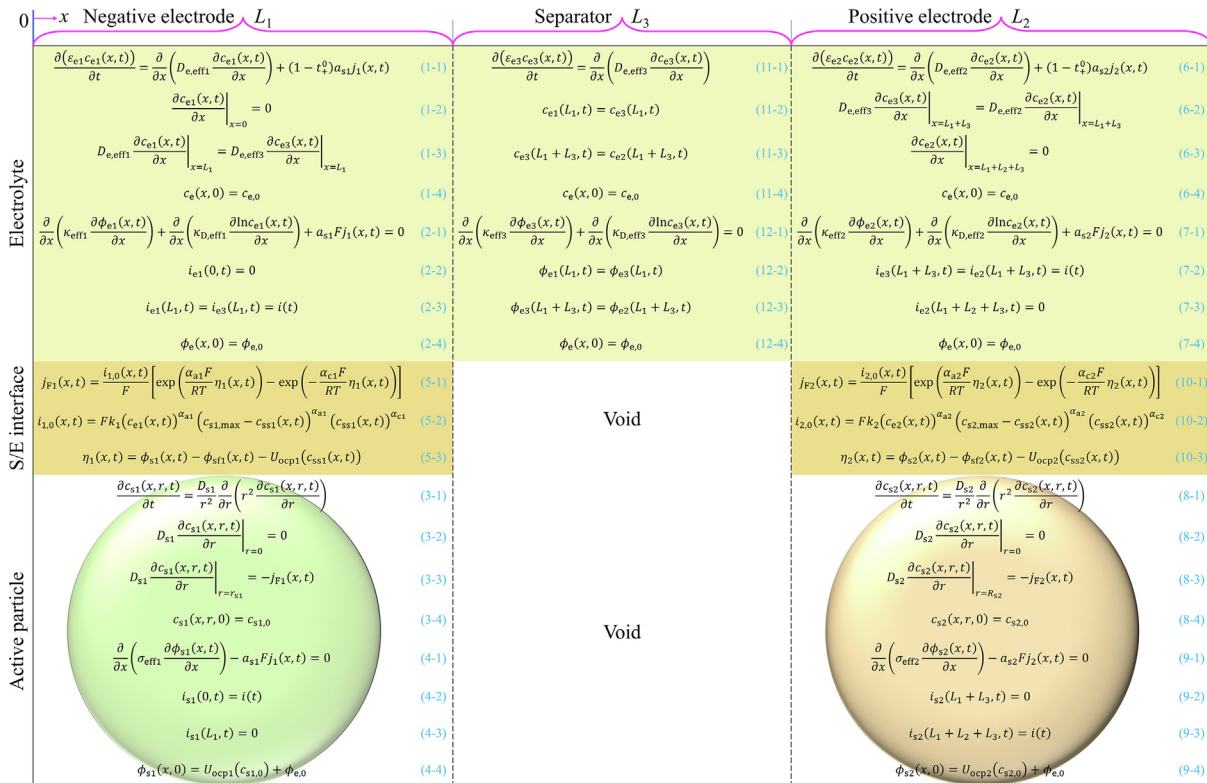


Fig. 1. Governing equations with initial boundary conditions for LIBs. The definitions of the parameters are listed in Supporting Information.

2.1.3. Glimpse of impedance models from particle to electrode and to full cell

Different from the previous method [53], a glimpse of impedance models and impedance spectra is given directly before a complete deduction. In the porous electrode, each spherical particle is surrounded by a resistive film as shown in Fig. 2(a and b) [50,84,121]. Fig. 2 shows impedance models and impedance spectra for LIBs from solid diffusion, Faradaic behavior, and whole process all in the particle, electrode, and full cell. Herein, the discharging mode is used to illustrate the flow of various currents and the current density $\dot{I}_{\text{int}1} = Fj_1$ and $\dot{I}_{\text{int}1} = \dot{I}_{\text{dl}1} + \dot{I}_{\text{F1}} + \dot{I}_{\text{sei}1}$. The detailed definitions for parameters in Fig. 2 refer to Supporting Information.

Starting from the solid-phase mass conservation Eqs. (3-1)–(3-4) or (8-1)–(8-4) [122], the transfer function about $c_{s1}(x, r_s, t)$ and $j_{F1}(x, t)$ can be obtained [123]

$$\dot{C}_{ss1}(x, s) = -\frac{r_{s1}}{D_{s1} Y_{s1}(s)} \quad (18-1)$$

$$Y_{s1}(s) \stackrel{\text{def}}{=} \frac{r_{s1} \sqrt{s/D_{s1}} - \tanh(r_{s1} \sqrt{s/D_{s1}})}{\tanh(r_{s1} \sqrt{s/D_{s1}})} \quad (18-2)$$

where $\dot{C}_{ss1}(x, s)$ is the complex phasor for $c_{s1}(x, r_s, t)$, $j_{F1}(x, s)$ is the complex phasor for $j_{F1}(x, t)$, and Y_{s1} is the dimensionless transfer function.

In order to solve $j_{F1}(x, s)$ by linearizing the Butler-Volmer equation for the solid/electrolyte interfacial kinetics, an equilibrium operational setpoint is defined for a Taylor-series expansion [55].

$$p^* = \{c_{s1}(x, t) = c_{s1,0}, c_{e1}(x, t) = c_{e,0}, \phi_{s1}(x, t) - \phi_{sf1}(x, t) = U_{\text{ocp}1}(c_{s1,0}), j_{F1}(x, t) = 0\} \quad (19-1)$$

where

$$c_{s1,0} = c_{s1,\text{max}} \times \theta_{s1,0} \\ = c_{s1,\text{max}} \times [\text{SOC}_0 \times (\theta_{1,100\%} - \theta_{1,0\%}) + \theta_{1,0\%}] \quad (19-2)$$

With Taylor-series expansion, the open-circuit-potential can be linearized as

$$U_{\text{ocp}1}(c_{ss1}(x, t)) \approx U_{\text{ocp}1}(c_{s1,0}) + \left. \frac{\partial U_{\text{ocp}1}}{\partial c_{ss1}} \right|_{c_{s1,0}} \tilde{c}_{ss1}(x, t) \quad (19-3)$$

The linearized Butler-Volmer Eq. (5-1) around the setpoint p^* using a Taylor-series expansion can be obtained based on the assumption Eq. (19-1).

$$\tilde{j}_{F1}(x, t)F \approx \frac{(\alpha_{a1} + \alpha_{c1})F}{RT} \left(\tilde{\phi}_{s1}(x, t) - \phi_{sf1}(x, t) - \left. \frac{\partial U_{\text{ocp}1}}{\partial c_{ss1}} \right|_{c_{s1,0}} \tilde{c}_{ss1}(x, t) \right) \quad (20-1)$$

Rearranging Eq. (20-1) yields

$$\tilde{\phi}_{s1}(x, t) - \phi_{sf1}(x, t) = FR_{ct1}j_{F1}(x, t) + \left. \frac{\partial U_{\text{ocp}1}}{\partial c_{ss1}} \right|_{c_{s1,0}} \tilde{c}_{ss1}(x, t) \quad (20-2)$$

where the exchange current density and charge transfer resistance at the interface of the particle/sei film are defined as $i_{1,0}(x, 0) \stackrel{\text{def}}{=} Fk(c_{e,0})^{\alpha_{a1}}(c_{s1,\text{max}} - c_{s1,0})^{\alpha_{a1}}(c_{s1,0})^{\alpha_{c1}}$ and $R_{ct1} \stackrel{\text{def}}{=} RT/[i_{1,0}(x, 0)(\alpha_{a1} + \alpha_{c1})F]$, respectively.

Transforming Eq. (20-2) into the complex phasor field and combining Eq. (18-1) yield

$$\dot{\Phi}_{s1}(x, s) - \dot{\Phi}_{sf1}(x, s) = F \left(R_{ct1} + \frac{R_{\text{diff}1}}{Y_{s1}(s)} \right) j_{F1}(x, s) \quad (21)$$

where the solid-phase diffusion resistance in the particle is defined as $R_{\text{diff}1} \stackrel{\text{def}}{=} -(\partial U_{\text{ocp}1}/\partial c_{ss1})|_{c_{s1,0}} \times r_{s1}/(FD_{s1})$.

Considering the effect of double layer capacitance in Eq. (14-2), Eq. (22-1) can be obtained.

$$\frac{\dot{\Phi}_{s1}(x, s) - \dot{\Phi}_{sf1}(x, s)}{F \left[\dot{j}_{\text{dl}1}(x, s) + \dot{j}_{\text{F1}}(x, s) \right]} = \frac{1}{sC_{\text{dl}1} + \frac{1}{R_{ct1} + \frac{R_{\text{diff}1}}{Y_{s1}(s)}}} \quad (22-1)$$

Considering the effect of sei film in Eqs. (14-1) and (14-3), Eqs. (22-2) and (22-3) can be obtained.

$$\frac{\dot{\Phi}_{s-e1}(x, s)}{F \left[\dot{j}_{\text{dl}1}(x, s) + \dot{j}_{\text{F1}}(x, s) \right]} = R_{\text{sei}1} + \frac{1}{sC_{\text{dl}1} + \frac{1}{R_{ct1} + \frac{R_{\text{diff}1}}{Y_{s1}(s)}}} \quad (22-2)$$

$$\frac{\dot{\Phi}_{s-e1}(x, s)}{Fj_{F1}(x, s)} = \frac{1}{sC_{\text{sei}1} + \frac{1}{R_{\text{sei}1} + \frac{1}{sC_{\text{dl}1} + \frac{1}{R_{ct1} + \frac{R_{\text{diff}1}}{Y_{s1}(s)}}}}} \quad (22-3)$$

Till now, the relationship between complex impedances of $z_{d1}(s)$, $z_{F1}(s)$, and $z_{\text{int}1}(s)$ for the solid-diffusion, the Faradaic behavior, and the whole process in the particle of negative electrode, respectively, could be concluded as follows.

$$z_{d1}(s) \stackrel{\text{def}}{=} \frac{R_{\text{diff}1}}{Y_{s1}(s)} \quad (23-1)$$

$$z_{F1}(s) \stackrel{\text{def}}{=} \frac{1}{sC_{\text{dl}1} + \frac{1}{R_{ct1} + z_{d1}(s)}} \quad (23-2)$$

$$z_{\text{int}1}(s) \stackrel{\text{def}}{=} \frac{1}{sC_{\text{sei}1} + \frac{1}{R_{\text{sei}1} + z_{F1}(s)}} \quad (23-3)$$

Now, except for the impedance model at the electrode scale, the schematic diagram, circuit model, and impedance spectroscopy from solid diffusion, Faradaic behavior, and whole process all in the particle are obtained. This kind of visual characterization is useful for identifying the aging mechanisms with the EIS approach after battery cycling [84].

2.1.4. Deduction of impedance models with the complex phasor method

Based on the deduced impedance model for the particle, impedance models for porous insertion electrodes can be solved by using the complex phasor method. Fig. 3 shows the deduction flowchart of the DFN impedance model for LIBs, consisting of six boxes from Box I to Box VI and five actions including EXCITE, SIMPLIFY, NONDIMENSIONALIZE, SOLVE, and DEFINE.

Action I: EXCITE

Action I is to impose the complex sinusoidal current signal to GEs with IBCs for LIBs.

Action II: SIMPLIFY

Action II is to simply GEs with IBCs for LIBs via two steps. One is to reduce the number of variables for GEs with IBCs, and the other is to convert partial differential equations in the time domain to ordinary differential equations in the complex phasor field.

The natural logarithm can be approximated as

$$\ln(c_{e1}(x, t)) = \ln(c_{e,0} + \tilde{c}_{e1}(x, t)) \approx \ln c_{e,0} + \frac{\tilde{c}_{e1}(x, t)}{c_{e,0}} \quad (24-1)$$

Subtracting Eq. (2-1) from Eq. (4-1) yields a new equation, and substituting Eq. (24-1) into this new equation yields

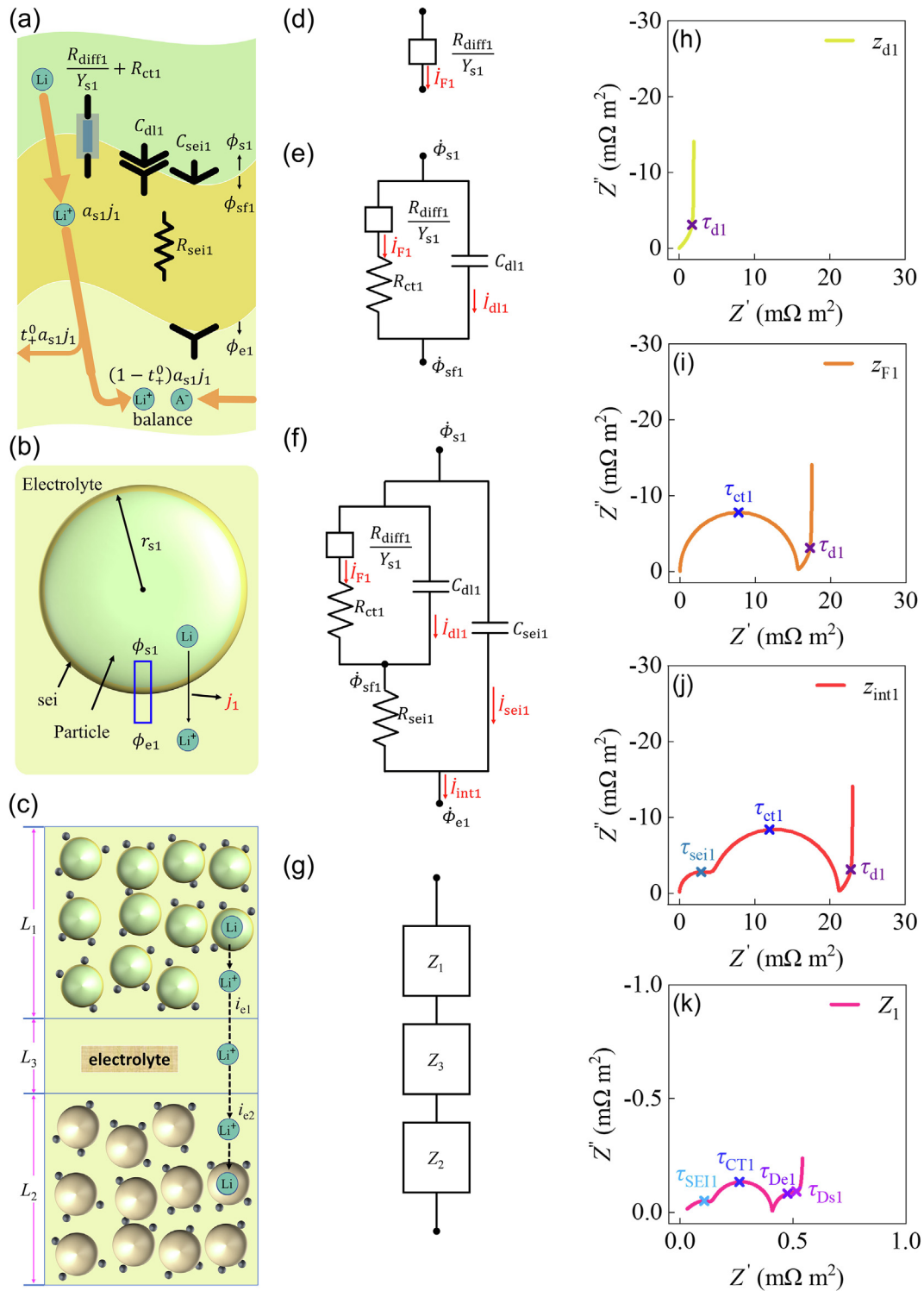


Fig. 2. Impedance models and impedance spectra for LIBs. Schematic diagrams for (a) the interface of the active particle/sei film/the surrounding electrolyte, (b) the active particle immersed in the electrolyte, and (c) LIB. Impedance models for (d) solid diffusion in the active particle, (e) Faradic behavior in the active particle, (f) whole process in the active particle, and (g) all processes in the full cell. The corresponding impedance spectra for (h) z_{d1} , (i) z_{F1} , (j) z_{int1} , and (k) Z_1 .

$$\frac{\partial^2 \phi_{s-e1}(x, t)}{\partial x^2} \approx a_{s1} F \left(\frac{1}{\sigma_{eff1}} + \frac{1}{\kappa_{eff1}} \right) j_1(x, t) + \frac{\kappa_{D,eff1}}{\kappa_{eff1} C_{e,0}} \frac{\partial^2 \tilde{C}_{e1}(x, t)}{\partial x^2} \quad (24-2)$$

$$\frac{\partial^2 \phi_{s-e2}(x, t)}{\partial x^2} \approx a_{s2} F \left(\frac{1}{\sigma_{eff2}} + \frac{1}{\kappa_{eff2}} \right) j_2(x, t) + \frac{\kappa_{D,eff2}}{\kappa_{eff2} C_{e,0}} \frac{\partial^2 \tilde{C}_{e2}(x, t)}{\partial x^2} \quad (24-3)$$

The result similar to Eq. (24-2) can be obtained for the positive electrode

Transforming Eq. (1-1) into the complex phasor field and combining the result with Eq. (23-3) can yield the following equation

$$\frac{\partial^2 \dot{C}_{e1}(x, s)}{\partial x^2} = \frac{\varepsilon_{e1}}{D_{e,eff1}} s \dot{C}_{e1}(x, s) - \frac{a_{s1}(1-t_0^+)}{D_{e,eff1}} \frac{\dot{\Phi}_{s-e1}(x, s)}{Fz_{int1}(s)} \quad (25-1)$$

Transforming Eq. (24-2) into the complex phasor field and combining the result with Eqs. (23-3) and (25-1) can yield the following equation.

$$\begin{aligned} \frac{\partial^2 \dot{\Phi}_{s-e1}(x, s)}{\partial x^2} &= \frac{\kappa_{D,eff1}}{\kappa_{eff1} c_{e,0}} \frac{\varepsilon_{e1}}{D_{e,eff1}} s \dot{C}_{e1}(x, s) \\ &+ \left(\frac{1}{\sigma_{eff1}} + \frac{1}{\kappa_{eff1}} \right) \frac{a_{s1}}{z_{int1}(s)} \dot{\Phi}_{s-e1}(x, s) - \frac{\kappa_{D,eff1}}{\kappa_{eff1} c_{e,0}} \frac{a_{s1}(1-t_0^+)}{D_{e,eff1} Fz_{int1}(s)} \dot{\Phi}_{s-e1}(x, s) \end{aligned} \quad (25-2)$$

The results are similar to Eqs. (25-1) and (25-2) can be obtained for the positive electrode.

$$\frac{\partial^2 \dot{C}_{e2}(x, s)}{\partial x^2} = \frac{\varepsilon_{e2}}{D_{e,eff2}} s \dot{C}_{e2}(x, s) - \frac{a_{s2}(1-t_0^+)}{D_{e,eff2}} \frac{\dot{\Phi}_{s-e2}(x, s)}{Fz_{int2}(s)} \quad (25-3)$$

$$\begin{aligned} \frac{\partial^2 \dot{\Phi}_{s-e2}(x, s)}{\partial x^2} &= \frac{\kappa_{D,eff2}}{\kappa_{eff2} c_{e,0}} \frac{\varepsilon_{e2}}{D_{e,eff2}} s \dot{C}_{e2}(x, s) \\ &+ \left(\frac{1}{\sigma_{eff2}} + \frac{1}{\kappa_{eff2}} \right) \frac{a_{s2}}{z_{int2}(s)} \dot{\Phi}_{s-e2}(x, s) - \frac{\kappa_{D,eff2}}{\kappa_{eff2} c_{e,0}} \frac{a_{s2}(1-t_0^+)}{D_{e,eff2} Fz_{int2}(s)} \dot{\Phi}_{s-e2}(x, s) \end{aligned} \quad (25-4)$$

The gradient BCs of Eqs. (1-2), (1-3), (6-2), and (6-3) can be rewritten in the complex phasor form

$$\frac{\partial \dot{C}_{e1}(x, s)}{\partial x} \Big|_{x=0} = 0 \quad (26-1)$$

$$D_{e,eff1} \frac{\partial \dot{C}_{e1}(x, s)}{\partial x} \Big|_{x=L_1} = \dot{\xi}_1(s) \quad (26-2)$$

$$D_{e,eff2} \frac{\partial \dot{C}_{e2}(x, s)}{\partial x} \Big|_{x=L_1+L_3} = \dot{\xi}_2(s) \quad (26-3)$$

$$\frac{\partial \dot{C}_{e2}(x, s)}{\partial x} \Big|_{x=L_4} = 0 \quad (26-4)$$

where $\dot{\xi}_1(s)$ and $\dot{\xi}_2(s)$ are the complex phasors for $\zeta_1(t)$ and $\zeta_2(t)$, which are calculated later according to the continuity BCs for $c_e(x, t)$.

Subtracting Eq. (13-1) from Eq. (13-2), combining with Eqs. (2-2), (2-3), (4-2), (4-3), (24-1), and (1-2), and transforming into complex phasor field can yield new BCs for Eq. (25-2).

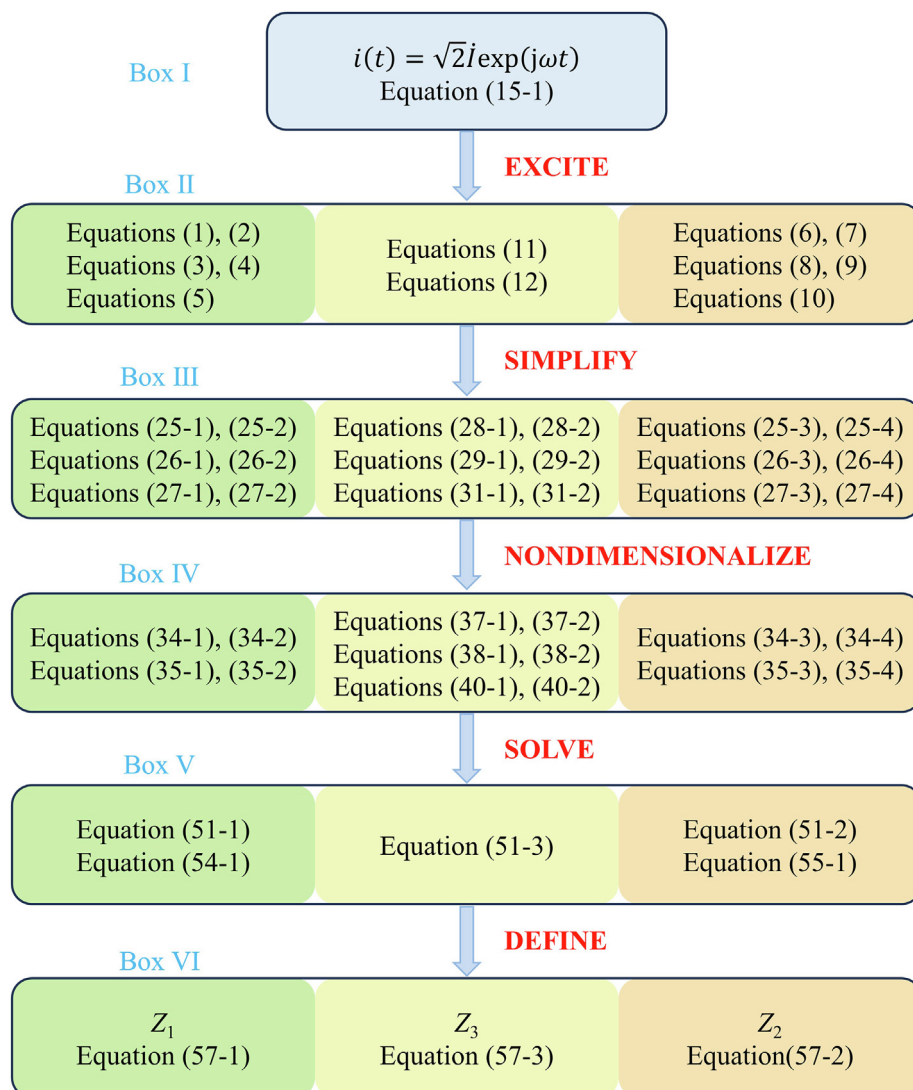


Fig. 3. The deduction flowchart of the DFN impedance model for LIBs.

$$\frac{\partial \dot{\Phi}_{s-e1}(x, s)}{\partial x} \Big|_{x=0} = -\frac{\dot{I}(s)}{\sigma_{eff1}} \quad (27-1)$$

$$\frac{\partial \dot{\Phi}_{s-e1}(x, s)}{\partial x} \Big|_{x=L_1} = \frac{\kappa_{D,eff1}}{\kappa_{eff1}C_{e,0}} \frac{\partial \dot{C}_{e1}(x, s)}{\partial x} \Big|_{x=L_1} + \frac{\dot{I}(s)}{\kappa_{eff1}} \quad (27-2)$$

Subtracting Eq. (13-1) from Eq. (13-2), combining with Eqs. (7-2), (7-3), (9-2), (9-3), (24-1), and (6-3), and transforming into the complex phasor field can yield new BCs for Eq. (25-4).

$$\frac{\partial \dot{\Phi}_{s-e2}(x, s)}{\partial x} \Big|_{x=L_1+L_3} = \frac{\kappa_{D,eff2}}{\kappa_{eff2}C_{e,0}} \frac{\partial \dot{C}_{e2}(x, s)}{\partial x} \Big|_{x=L_1+L_3} + \frac{\dot{I}(s)}{\kappa_{eff2}} \quad (27-3)$$

$$\frac{\partial \dot{\Phi}_{s-e2}(x, s)}{\partial x} \Big|_{x=L_4} = -\frac{\dot{I}(s)}{\sigma_{eff2}} \quad (27-4)$$

The mass conservation of Eq. (11-1) can be rewritten in the complex phasor form

$$\epsilon_{e3}s\dot{C}_{e3}(x, s) = D_{e,eff3} \frac{\partial^2 \dot{C}_{e3}(x, s)}{\partial x^2} \quad (28-1)$$

Combined with Eq. (2-3) or (7-2), the charge conservation of Eq. (12-1) can be rewritten in the complex phasor form

$$-\kappa_{eff3} \frac{\partial \dot{\Phi}_{e3}(x, s)}{\partial x} - \frac{\kappa_{D,eff3}}{C_{e,0}} \frac{\partial \dot{C}_{e3}(x, s)}{\partial x} = \dot{I}(s) \quad (28-2)$$

The gradient BCs of Eqs. (1-3) and (6-2) can be rewritten in the complex phasor form

$$D_{e,eff3} \frac{\partial \dot{C}_{e3}(x, s)}{\partial x} \Big|_{x=L_1} = \dot{\xi}_1(s) \quad (29-1)$$

$$D_{e,eff3} \frac{\partial \dot{C}_{e3}(x, s)}{\partial x} \Big|_{x=L_1+L_3} = \dot{\xi}_2(s) \quad (29-2)$$

The continuity BCs of Eqs. (11-2) and (11-3) can be rewritten in the complex phasor form

$$\dot{C}_{e1}(L_1, s) = \dot{C}_{e3}(L_1, s) \quad (30-1)$$

$$\dot{C}_{e3}(L_1 + L_3, s) = \dot{C}_{e2}(L_1 + L_3, s) \quad (30-2)$$

The continuity BCs of Eqs. (12-2) and (12-3) can be rewritten in the complex phasor form

$$\dot{\Phi}_{e1}(L_1, s) = \dot{\Phi}_{e3}(L_1, s) \quad (31-1)$$

$$\dot{\Phi}_{e3}(L_1 + L_3, s) = \dot{\Phi}_{e2}(L_1 + L_3, s) \quad (31-2)$$

Zero reference potential for LIBs is set as

$$\dot{\Phi}_{e3}(L_1 + L_3, s) = 0 \quad (32)$$

Action III: Nondimensionalize

Action III is to nondimensionalize GEs with IBCs for LIBs via defining the dimensionless variables.

To rewrite the above simplified GEs with IBCs in a more concise form and to follow the previous method [53], the dimensionless variables are defined as

$$\begin{aligned} \bar{C}_{e1}(\bar{x}_1, \bar{s}_1) &= \frac{\kappa_{D,eff1}}{\kappa_{eff1}C_{e,0}} \frac{\sigma_{eff1}}{L_1} \frac{\dot{C}_{e1}(x, s)}{\dot{I}} \text{ and } \bar{C}_{e2}(\bar{x}_2, \bar{s}_2) \\ &= \frac{\kappa_{D,eff2}}{\kappa_{eff2}C_{e,0}} \frac{\sigma_{eff2}}{L_2} \frac{\dot{C}_{e2}(x, s)}{\dot{I}} \end{aligned} \quad (33-1)$$

$$\bar{\Phi}_{s-e1}(\bar{x}_1, \bar{s}_1) = -\frac{\sigma_{eff1}}{L_1} \frac{\dot{\Phi}_{s-e1}(x, s)}{\dot{I}} \text{ and } \bar{\Phi}_{s-e2}(\bar{x}_2, \bar{s}_2) \quad (33-2)$$

$$= -\frac{\sigma_{eff2}}{L_2} \frac{\dot{\Phi}_{s-e2}(x, s)}{\dot{I}} \quad (33-2)$$

$$\bar{x}_1 = \frac{x}{L_1} \text{ and } \bar{x}_2 = \frac{x - (L_1 + L_3)}{L_2} \quad (33-3)$$

$$\bar{s}_1 = \frac{\epsilon_{e1}L_1^2}{D_{e,eff1}}s \text{ and } \bar{s}_2 = \frac{\epsilon_{e2}L_2^2}{D_{e,eff2}}s \quad (33-4)$$

$$\Theta_{II} = -\frac{\kappa_{D,eff1}(1 - t_0^+)}{\kappa_{eff1}C_{e,0}FD_{e,eff1}Z_{int1}} \text{ and } \Theta_{II2} = -\frac{\kappa_{D,eff2}(1 - t_0^+)}{\kappa_{eff2}C_{e,0}FD_{e,eff2}Z_{int2}} \quad (33-5)$$

$$\Theta_{III} = \frac{a_{s1}L_1^2}{\sigma_{eff1}Z_{int1}} \left(1 + \frac{\sigma_{eff1}}{\kappa_{eff1}} \right) \text{ and } \Theta_{III2} = \frac{a_{s2}L_2^2}{\sigma_{eff2}Z_{int2}} \left(1 + \frac{\sigma_{eff2}}{\kappa_{eff2}} \right) \quad (33-6)$$

The detailed definitions for parameters in the above equations refer to Supporting Information.

Based on Eqs. (33-1)–(33-6), Eqs. (25-1)–(25-4) can be rewritten in the dimensionless form

$$\frac{\partial^2 \bar{C}_{e1}(\bar{x}_1, \bar{s}_1)}{\partial \bar{x}_1^2} = \bar{s}_1 \bar{C}_{e1}(\bar{x}_1, \bar{s}_1) - \Theta_{II} \bar{\Phi}_{s-e1}(\bar{x}_1, \bar{s}_1) \quad (34-1)$$

$$\frac{\partial^2 \bar{\Phi}_{s-e1}(\bar{x}_1, \bar{s}_1)}{\partial \bar{x}_1^2} = -\bar{s}_1 \bar{C}_{e1}(\bar{x}_1, \bar{s}_1) + (\Theta_{II} + \Theta_{III}) \bar{\Phi}_{s-e1}(\bar{x}_1, \bar{s}_1) \quad (34-2)$$

$$\frac{\partial^2 \bar{C}_{e2}(\bar{x}_2, \bar{s}_2)}{\partial \bar{x}_2^2} = \bar{s}_2 \bar{C}_{e2}(\bar{x}_2, \bar{s}_2) - \Theta_{II2} \bar{\Phi}_{s-e2}(\bar{x}_2, \bar{s}_2) \quad (34-3)$$

$$\frac{\partial^2 \bar{\Phi}_{s-e2}(\bar{x}_2, \bar{s}_2)}{\partial \bar{x}_2^2} = -\bar{s}_2 \bar{C}_{e2}(\bar{x}_2, \bar{s}_2) + (\Theta_{II2} + \Theta_{III2}) \bar{\Phi}_{s-e2}(\bar{x}_2, \bar{s}_2) \quad (34-4)$$

Similarly, the gradient BCs of Eqs. (26-1)–(26-4) and Eqs. (27-1)–(27-4) can be rewritten in the dimensionless form

$$\begin{aligned} \frac{\partial \bar{C}_{e1}(\bar{x}_1, \bar{s}_1)}{\partial \bar{x}_1} \Big|_{x_{-1}=0} &= 0 \text{ and } \frac{\partial \bar{C}_{e1}(\bar{x}_1, \bar{s}_1)}{\partial \bar{x}_1} \Big|_{x_{-1}=1} \\ &= -\frac{\Theta_{II}}{\Theta_{II1}} \frac{\left(1 + \frac{\sigma_{eff1}}{\kappa_{eff1}} \right)}{(1 - t_0^+)} F \frac{\dot{\xi}_1}{\dot{I}} \end{aligned} \quad (35-1)$$

$$\begin{aligned} \frac{\partial \bar{\Phi}_{s-e1}(\bar{x}_1, \bar{s}_1)}{\partial \bar{x}_1} \Big|_{x_{-1}=0} &= 1 \text{ and } \frac{\partial \bar{\Phi}_{s-e1}(\bar{x}_1, \bar{s}_1)}{\partial \bar{x}_1} \Big|_{x_{-1}=1} \\ &= -\frac{\partial \bar{C}_{e1}(\bar{x}_1, \bar{s}_1)}{\partial \bar{x}_1} \Big|_{x_{-1}=1} - \frac{\sigma_{eff1}}{\kappa_{eff1}} \end{aligned} \quad (35-2)$$

$$\left. \frac{\partial \bar{C}_{e2}(\bar{x}_2, \bar{s}_2)}{\partial \bar{x}_2} \right|_{\bar{x}_2=0} = - \frac{\Theta_{l2}}{\Theta_{ll2}} \frac{\left(1 + \frac{\sigma_{eff2}}{\kappa_{eff2}}\right)}{\left(1 - t_0^+\right)} F \\ \times \frac{\dot{\zeta}_2}{I} \text{ and } \left. \frac{\partial \bar{C}_{e2}(\bar{x}_2, \bar{s}_2)}{\partial \bar{x}_2} \right|_{\bar{x}_2=1} = 0 \quad (35-3)$$

$$\left. \frac{\partial \bar{\Phi}_{s-e2}(\bar{x}_2, \bar{s}_2)}{\partial \bar{x}_2} \right|_{\bar{x}_2=0} = - \left. \frac{\partial \bar{C}_{e2}(\bar{x}_2, \bar{s}_2)}{\partial \bar{x}_2} \right|_{\bar{x}_2=0} \\ - \frac{\sigma_{eff2}}{\kappa_{eff2}} \text{ and } \left. \frac{\partial \bar{\Phi}_{s-e2}(\bar{x}_2, \bar{s}_2)}{\partial \bar{x}_2} \right|_{\bar{x}_2=1} = 1 \quad (35-4)$$

For the separator region, the dimensionless variables are defined as

$$\bar{C}_{e3}(\bar{x}_3, \bar{s}_3) = - \frac{\kappa_{D,eff3}}{c_{e,0}L_3} \frac{\dot{C}_{e3}(x, s)}{I} \quad (36-1)$$

$$\bar{\Phi}_{e3}(\bar{x}_3, \bar{s}_3) = - \frac{\kappa_{eff3}}{L_3} \frac{\dot{\Phi}_{e3}(x, s)}{I} \quad (36-2)$$

$$\bar{x}_3 = \frac{x - L_1}{L_3} \quad (36-3)$$

$$\bar{s}_3 = \frac{\dot{c}_{e3}L_3^2}{D_{e,eff3}} s \quad (36-4)$$

$$\Theta_{ll3} = - \frac{\kappa_{D,eff3}}{D_{e,eff3}c_{e,0}F} \quad (36-5)$$

Based on the dimensionless variables as defined in Eqs. (36-1)–(36-5), Eqs. (28-1) and (28-2) can be rewritten in the dimensionless form

$$\left. \frac{\partial^2 \bar{C}_{e3}(\bar{x}_3, \bar{s}_3)}{\partial \bar{x}_3^2} \right. = \bar{s}_3 \bar{C}_{e3}(\bar{x}_3, \bar{s}_3) \quad (37-1)$$

$$\left. \frac{\partial \bar{\Phi}_{e3}(\bar{x}_3, \bar{s}_3)}{\partial \bar{x}_3} \right. + \left. \frac{\partial \bar{C}_{e3}(\bar{x}_3, \bar{s}_3)}{\partial \bar{x}_3} \right. = 1 \quad (37-2)$$

Similarly, the gradient BCs of Eqs. (29-1) and (29-2) can be rewritten in the dimensionless form

$$\left. \frac{\partial \bar{C}_{e3}(\bar{x}_3, \bar{s}_3)}{\partial \bar{x}_3} \right|_{\bar{x}_3=0} = \Theta_{ll3}F \frac{\dot{\zeta}_1}{I} \quad (38-1)$$

$$\left. \frac{\partial \bar{C}_{e3}(\bar{x}_3, \bar{s}_3)}{\partial \bar{x}_3} \right|_{\bar{x}_3=1} = \Theta_{ll3}F \frac{\dot{\zeta}_2}{I} \quad (38-2)$$

The continuity BCs of Eqs. (30-1) and (30-2) can be rewritten in the dimensionless form

$$\left. - \frac{\Theta_{ll1}}{\Theta_{l1}} \frac{L_1(1 - t_0^+)}{\left(1 + \frac{\sigma_{eff1}}{\kappa_{eff1}}\right)FD_{e,eff1}} \bar{C}_{e1}(1, \bar{s}_1) \right. \\ = \frac{1}{\Theta_{ll3}F} \frac{L_3}{D_{e,eff3}} \bar{C}_{e3}(0, \bar{s}_3) \quad (39-1)$$

$$\left. - \frac{\Theta_{ll2}}{\Theta_{l2}} \frac{L_2(1 - t_0^+)}{\left(1 + \frac{\sigma_{eff2}}{\kappa_{eff2}}\right)FD_{e,eff2}} \bar{C}_{e2}(0, \bar{s}_2) \right. \\ = \frac{1}{\Theta_{ll3}F} \frac{L_3}{D_{e,eff3}} \bar{C}_{e3}(1, \bar{s}_3) \quad (39-2)$$

The continuity BCs of Eqs. (31-1) and (31-2) can be rewritten as

$$\dot{\Phi}_{e1}(\bar{x}_1 = 1, \bar{s}_1) = \dot{\Phi}_{e3}(\bar{x}_3 = 0, \bar{s}_3) \quad (40-1)$$

$$\dot{\Phi}_{e3}(\bar{x}_3 = 1, \bar{s}_3) = \dot{\Phi}_{e2}(\bar{x}_2 = 0, \bar{s}_2) \quad (40-2)$$

The zero reference potential of Eq. (32) can be rewritten in the dimensionless form

$$\bar{\Phi}_{e3}(1, \bar{s}_3) = 0 \quad (41)$$

Action IV: SOLVE

Action IV is to solve two sets of dimensionless differential equation systems. Firstly, the coupled linear differential Eqs. (34-1)–(34-4) with BCs of Eqs. (35-1)–(35-4) can be solved with a similarity matrix transformation method [58]. System of Eqs. (34-1)–(34-4) can be rewritten as the matrix form $\partial^2 y / \partial \bar{x}^2 = \mathbf{A}y$. Follow the previous solving method [52,53], the general solution of Eqs. (34-1) and (34-2) for the negative electrode can be obtained.

$$\bar{C}_{e1}(\bar{x}_1, \bar{s}_1) = B_{l1} \cosh(\sqrt{\lambda_{l1}} \bar{x}_1) + B_{ll1} \sinh(\sqrt{\lambda_{l1}} \bar{x}_1) \\ + B_{ll1} \cosh(\sqrt{\lambda_{ll1}} \bar{x}_1) + B_{lV1} \sinh(\sqrt{\lambda_{ll1}} \bar{x}_1) \quad (42-1)$$

$$\bar{\Phi}_{s-e1}(\bar{x}_1, \bar{s}_1) = \frac{\bar{s}_1 - \bar{\lambda}_{l1}}{\Theta_{l1}} \left[B_{l1} \cosh(\sqrt{\lambda_{l1}} \bar{x}_1) + B_{ll1} \sinh(\sqrt{\lambda_{l1}} \bar{x}_1) \right] \\ + \frac{\bar{s}_1 - \bar{\lambda}_{ll1}}{\Theta_{ll1}} \left[B_{ll1} \cosh(\sqrt{\lambda_{ll1}} \bar{x}_1) + B_{lV1} \sinh(\sqrt{\lambda_{ll1}} \bar{x}_1) \right] \quad (42-2)$$

$$\bar{\lambda}_{l1} = \frac{1}{2} \left(\bar{s}_1 + \Theta_{l1} + \Theta_{ll1} + \sqrt{\bar{s}_1^2 + 2\bar{s}_1(\Theta_{l1} - \Theta_{ll1}) + (\Theta_{l1} + \Theta_{ll1})^2} \right) \quad (42-3)$$

$$\bar{\lambda}_{ll1} = \frac{1}{2} \left(\bar{s}_1 + \Theta_{l1} + \Theta_{ll1} - \sqrt{\bar{s}_1^2 + 2\bar{s}_1(\Theta_{l1} - \Theta_{ll1}) + (\Theta_{l1} + \Theta_{ll1})^2} \right) \quad (42-4)$$

Similar to the above method, the general solution of Eqs. (34-3) and (34-4) for the positive electrode can be obtained.

$$\bar{C}_{e2}(\bar{x}_2, \bar{s}_2) = B_{l2} \cosh(\sqrt{\lambda_{l2}} \bar{x}_2) + B_{ll2} \sinh(\sqrt{\lambda_{l2}} \bar{x}_2) \\ + B_{ll2} \cosh(\sqrt{\lambda_{ll2}} \bar{x}_2) + B_{lV2} \sinh(\sqrt{\lambda_{ll2}} \bar{x}_2) \quad (42-5)$$

$$\bar{\Phi}_{s-e2}(\bar{x}_2, \bar{s}_2) = \frac{\bar{s}_2 - \bar{\lambda}_{l2}}{\Theta_{l2}} \left[B_{l2} \cosh(\sqrt{\lambda_{l2}} \bar{x}_2) + B_{ll2} \sinh(\sqrt{\lambda_{l2}} \bar{x}_2) \right] \\ + \frac{\bar{s}_2 - \bar{\lambda}_{ll2}}{\Theta_{ll2}} \left[B_{ll2} \cosh(\sqrt{\lambda_{ll2}} \bar{x}_2) + B_{lV2} \sinh(\sqrt{\lambda_{ll2}} \bar{x}_2) \right] \quad (42-6)$$

$$\bar{\lambda}_{l2} = \frac{1}{2} \left(\bar{s}_2 + \Theta_{l2} + \Theta_{ll2} + \sqrt{\bar{s}_2^2 + 2\bar{s}_2(\Theta_{l2} - \Theta_{ll2}) + (\Theta_{l2} + \Theta_{ll2})^2} \right) \quad (42-7)$$

$$\bar{\lambda}_{ll2} = \frac{1}{2} \left(\bar{s}_2 + \Theta_{l2} + \Theta_{ll2} - \sqrt{\bar{s}_2^2 + 2\bar{s}_2(\Theta_{l2} - \Theta_{ll2}) + (\Theta_{l2} + \Theta_{ll2})^2} \right) \quad (42-8)$$

where λ_{I} and λ_{II} are the eigenvalues of Matrix A.

By substituting Eqs. (42-1), (42-2), (42-5) and (42-6) into BCs of Eqs. (35-1)–(35-4), the coefficients B_{I} , B_{II} , B_{III} , and B_{IV} can be obtained.

For $\bar{C}_{\text{e}1}(\bar{x}_1, \bar{s}_1)$ and $\bar{\Phi}_{\text{s-e}1}(\bar{x}_1, \bar{s}_1)$

$$B_{\text{II}} = \frac{\Theta_{\text{II}}}{\sqrt{\lambda_{\text{II}}}(\lambda_{\text{II}} - \lambda_{\text{III}})\sinh(\sqrt{\lambda_{\text{II}}})} \\ \times \left[\cosh(\sqrt{\lambda_{\text{II}}}) + \frac{\sigma_{\text{eff}1}}{\kappa_{\text{eff}1}} - \frac{(\bar{s}_1 + \Theta_{\text{II}} - \lambda_{\text{III}})\sigma_{\text{eff}1}Fz_{\text{int}1}}{L_1^2 a_{\text{s}1}(1 - t_0^+)} \frac{\dot{\xi}_1}{\dot{I}} \right] \quad (43-1)$$

$$B_{\text{II}1} = -\frac{\Theta_{\text{II}}}{\sqrt{\lambda_{\text{II}}}(\lambda_{\text{II}} - \lambda_{\text{III}})} \quad (43-2)$$

$$B_{\text{III}1} = -\frac{\Theta_{\text{II}}}{\sqrt{\lambda_{\text{III}}}(\lambda_{\text{II}} - \lambda_{\text{III}})\sinh(\sqrt{\lambda_{\text{III}}})} \\ \times \left[\cosh(\sqrt{\lambda_{\text{III}}}) + \frac{\sigma_{\text{eff}1}}{\kappa_{\text{eff}1}} - \frac{(\bar{s}_1 + \Theta_{\text{II}} - \lambda_{\text{II}})\sigma_{\text{eff}1}Fz_{\text{int}1}}{L_1^2 a_{\text{s}1}(1 - t_0^+)} \frac{\dot{\xi}_1}{\dot{I}} \right] \quad (43-3)$$

$$B_{\text{IV}1} = \frac{\Theta_{\text{II}}}{\sqrt{\lambda_{\text{III}}}(\lambda_{\text{II}} - \lambda_{\text{III}})} \quad (43-4)$$

For $\bar{C}_{\text{e}2}(\bar{x}_2, \bar{s}_2)$ and $\bar{\Phi}_{\text{s-e}2}(\bar{x}_2, \bar{s}_2)$

$$B_{\text{I}2} = -\frac{\Theta_{\text{I}2}}{\sqrt{\lambda_{\text{I}2}}(\lambda_{\text{I}2} - \lambda_{\text{II}2})\sinh(\sqrt{\lambda_{\text{I}2}})} - \frac{B_{\text{II}2}}{\tanh(\sqrt{\lambda_{\text{I}2}})} \quad (44-1)$$

$$B_{\text{II}2} = \frac{\Theta_{\text{I}2}}{\sqrt{\lambda_{\text{I}2}}(\lambda_{\text{I}2} - \lambda_{\text{II}2})} \left[\frac{\sigma_{\text{eff}2}}{\kappa_{\text{eff}2}} - \frac{(\bar{s}_2 + \Theta_{\text{I}2} - \lambda_{\text{II}2})\sigma_{\text{eff}2}Fz_{\text{int}2}}{L_2^2 a_{\text{s}2}(1 - t_0^+)} \frac{\dot{\xi}_2}{\dot{I}} \right] \quad (44-2)$$

$$B_{\text{III}2} = \frac{\Theta_{\text{I}2}}{\sqrt{\lambda_{\text{I}2}}(\lambda_{\text{I}2} - \lambda_{\text{II}2})\sinh(\sqrt{\lambda_{\text{I}2}})} - \frac{B_{\text{IV}2}}{\tanh(\sqrt{\lambda_{\text{I}2}})} \quad (44-3)$$

$$B_{\text{IV}2} = -\frac{\Theta_{\text{I}2}}{\sqrt{\lambda_{\text{I}2}}(\lambda_{\text{I}2} - \lambda_{\text{II}2})} \left[\frac{\sigma_{\text{eff}2}}{\kappa_{\text{eff}2}} - \frac{(\bar{s}_2 + \Theta_{\text{I}2} - \lambda_{\text{I}2})\sigma_{\text{eff}2}Fz_{\text{int}2}}{L_2^2 a_{\text{s}2}(1 - t_0^+)} \frac{\dot{\xi}_2}{\dot{I}} \right] \quad (44-4)$$

The general solution of Eq. (37-1) can be resolved directly.

$$\bar{C}_{\text{e}3}(\bar{x}_3, \bar{s}_3) = B_{\text{I}3}\cosh\left(\sqrt{\bar{s}_3}\bar{x}_3\right) + B_{\text{II}3}\sinh\left(\sqrt{\bar{s}_3}\bar{x}_3\right) \quad (45)$$

Substituting Eq. (45) into BCs of Eqs. (38-1) and (38-2) yields

$$B_{\text{I}3} = \frac{\Theta_{\text{III}3}F}{\sqrt{\bar{s}_3}\sinh(\sqrt{\bar{s}_3})} \left[\frac{\dot{\xi}_2}{\dot{I}} - \frac{\dot{\xi}_1}{\dot{I}} \cosh\left(\sqrt{\bar{s}_3}\right) \right] \quad (46-1)$$

$$B_{\text{II}3} = \frac{\Theta_{\text{III}3}F}{\sqrt{\bar{s}_3}} \frac{\dot{\xi}_1}{\dot{I}} \quad (46-2)$$

Substituting Eq. (45) into Eq. (37-2) and integrating the newly obtained equation, the integration result can be combined with Eq. (41) to yield

$$\bar{\Phi}_{\text{e}3}(\bar{x}_3, \bar{s}_3) = \bar{C}_{\text{e}3}(1, \bar{s}_3) - \bar{C}_{\text{e}3}(\bar{x}_3, \bar{s}_3) + (\bar{x}_3 - 1) \quad (47)$$

Till now, the solution expressions of $\bar{C}_{\text{e}i}(\bar{x}_i, \bar{s}_i)$ ($i = 1, 2, 3$) are known. However, among them both $\dot{\xi}_1$ and $\dot{\xi}_2$ are still unknown. The continuity BCs of Eqs. (39-1) and (39-2) are used to evaluate $\dot{\xi}_1$ and $\dot{\xi}_2$.

Substituting $\bar{C}_{\text{e}1}(1, \bar{s}_1)$, $\bar{C}_{\text{e}2}(0, \bar{s}_2)$, $\bar{C}_{\text{e}3}(0, \bar{s}_3)$, and $\bar{C}_{\text{e}3}(1, \bar{s}_3)$ according to Eqs. (42-1), (42-5), and (45) into Eqs. (39-1) and (39-2) yields

$$\Lambda_{\text{II}1} \frac{\dot{\xi}_1}{\dot{I}} - \Lambda_{\text{III}3} \frac{\dot{\xi}_2}{\dot{I}} = \Lambda_{\text{II}} \quad (48-1)$$

$$\Lambda_{\text{III}3} \frac{\dot{\xi}_1}{\dot{I}} - \Lambda_{\text{II}2} \frac{\dot{\xi}_2}{\dot{I}} = -\Lambda_{\text{I}2} \quad (48-2)$$

where the coefficients Λ_{II} , $\Lambda_{\text{II}1}$, $\Lambda_{\text{II}2}$, $\Lambda_{\text{II}3}$, and $\Lambda_{\text{III}3}$ are given as

$$\Lambda_{\text{II}} = -\frac{l_1^3 a_{\text{s}1}(1 - t_0^+)}{D_{\text{e,eff}1}\sigma_{\text{eff}1}(\lambda_{\text{II}} - \lambda_{\text{III}})Fz_{\text{int}1}} \left[\frac{1}{\sqrt{\lambda_{\text{II}}}\sinh(\sqrt{\lambda_{\text{II}}})} - \frac{1}{\sqrt{\lambda_{\text{II}}}\sinh(\sqrt{\lambda_{\text{II}}})} \right. \\ \left. + \frac{\sigma_{\text{eff}1}}{\kappa_{\text{eff}1}} \left(\frac{1}{\sqrt{\lambda_{\text{II}}}\tanh(\sqrt{\lambda_{\text{II}}})} - \frac{1}{\sqrt{\lambda_{\text{II}}}\tanh(\sqrt{\lambda_{\text{II}}})} \right) \right] \quad (49-1)$$

$$\Lambda_{\text{II}1} = \frac{l_1}{D_{\text{e,eff}1}(\lambda_{\text{II}} - \lambda_{\text{III}})} \left[\frac{\bar{s}_1 + \Theta_{\text{II}} - \lambda_{\text{III}}}{\sqrt{\lambda_{\text{II}}}\tanh(\sqrt{\lambda_{\text{II}}})} - \frac{\bar{s}_1 + \Theta_{\text{II}} - \lambda_{\text{II}}}{\sqrt{\lambda_{\text{III}}}\tanh(\sqrt{\lambda_{\text{III}}})} \right] \\ + \Lambda_{\text{III}3} \cosh\left(\sqrt{\bar{s}_3}\right) \quad (49-2)$$

$$\Lambda_{\text{I}2} = -\frac{l_2^3 a_{\text{s}2}(1 - t_0^+)}{D_{\text{e,eff}2}\sigma_{\text{eff}2}(\lambda_{\text{I}2} - \lambda_{\text{II}2})Fz_{\text{int}2}} \left[\frac{1}{\sqrt{\lambda_{\text{I}2}}\sinh(\sqrt{\lambda_{\text{I}2}})} - \frac{1}{\sqrt{\lambda_{\text{I}2}}\sinh(\sqrt{\lambda_{\text{I}2}})} \right. \\ \left. + \frac{\sigma_{\text{eff}2}}{\kappa_{\text{eff}2}} \left(\frac{1}{\sqrt{\lambda_{\text{I}2}}\tanh(\sqrt{\lambda_{\text{I}2}})} - \frac{1}{\sqrt{\lambda_{\text{I}2}}\tanh(\sqrt{\lambda_{\text{I}2}})} \right) \right] \quad (49-3)$$

$$\Lambda_{\text{II}2} = \frac{l_2}{D_{\text{e,eff}2}(\lambda_{\text{I}2} - \lambda_{\text{II}2})} \left[\frac{\bar{s}_2 + \Theta_{\text{I}2} - \lambda_{\text{II}2}}{\sqrt{\lambda_{\text{I}2}}\tanh(\sqrt{\lambda_{\text{I}2}})} - \frac{\bar{s}_2 + \Theta_{\text{I}2} - \lambda_{\text{I}2}}{\sqrt{\lambda_{\text{II}2}}\tanh(\sqrt{\lambda_{\text{II}2}})} \right] \\ + \Lambda_{\text{III}3} \cosh\left(\sqrt{\bar{s}_3}\right) \quad (49-4)$$

$$\Lambda_{\text{III}3} = \frac{l_3}{D_{\text{e,eff}3}\sqrt{\bar{s}_3}\sinh(\sqrt{\bar{s}_3})} \quad (49-5)$$

Resolving Eqs. (48-1) and (48-2) yields

$$\frac{\dot{\xi}_1}{\dot{I}} = \frac{\Lambda_{\text{II}} + \frac{\Lambda_{\text{I}2}}{\Lambda_{\text{II}2}}\Lambda_{\text{III}3}}{\Lambda_{\text{II}1} - \frac{1}{\Lambda_{\text{II}2}}\Lambda_{\text{III}3}^2} \quad (50-1)$$

$$\frac{\dot{\xi}_2}{\dot{I}} = \frac{\Lambda_{\text{I}2} + \frac{\Lambda_{\text{II}}}{\Lambda_{\text{II}1}}\Lambda_{\text{III}3}}{\Lambda_{\text{II}2} - \frac{1}{\Lambda_{\text{II}1}}\Lambda_{\text{III}3}^2} \quad (50-2)$$

Till now, $\bar{C}_{\text{e}1}(\bar{x}_1, \bar{s}_1)$, $\bar{C}_{\text{e}2}(\bar{x}_2, \bar{s}_2)$, $\bar{\Phi}_{\text{s-e}1}(\bar{x}_1, \bar{s}_1)$, $\bar{\Phi}_{\text{s-e}2}(\bar{x}_2, \bar{s}_2)$, and $\bar{C}_{\text{e}3}(\bar{x}_3, \bar{s}_3)$ are all solved. Thus, $\bar{\Phi}_{\text{e}3}(\bar{x}_3, \bar{s}_3)$ can also be obtained by substituting $\bar{C}_{\text{e}3}(\bar{x}_3, \bar{s}_3)$ into Eq. (47). With all these variables solved, $\dot{C}_{\text{e}1}(x, s)$, $\dot{C}_{\text{e}2}(x, s)$, $\dot{\Phi}_{\text{s-e}1}(x, s)$, $\dot{\Phi}_{\text{s-e}2}(x, s)$, $\dot{C}_{\text{e}3}(x, s)$, and $\dot{\Phi}_{\text{e}3}(x, s)$ can all be obtained in reverse with respect to Eqs. (33-1)–(33-6) and (36-1)–(36-5). Herein, the dimensionless variables \bar{x} and \bar{s} are used and the transfer functions of $\dot{\Phi}_{\text{s-e}1}(\bar{x}_1, \bar{s}_1)$, $\dot{\Phi}_{\text{s-e}2}(\bar{x}_2, \bar{s}_2)$, and $\dot{\Phi}_{\text{e}3}(\bar{x}_3, \bar{s}_3)$ can be shown as follows

$$\frac{\dot{\Phi}_{s-e1}(\bar{x}_1, \bar{s}_1)}{I} = -\frac{L_1}{\sigma_{eff1}} \left\{ \frac{\bar{s}_1 - \lambda_{l1}}{\Theta_{l1}} [B_{l1} \cosh(\sqrt{\lambda_{l1}} \bar{x}_1) + B_{ll1} \sinh(\sqrt{\lambda_{l1}} \bar{x}_1)] + \frac{\bar{s}_1 - \lambda_{ll1}}{\Theta_{ll1}} [B_{ll1} \cosh(\sqrt{\lambda_{ll1}} \bar{x}_1) + B_{lv1} \sinh(\sqrt{\lambda_{ll1}} \bar{x}_1)] \right\} \quad (51-1)$$

$$\frac{\dot{\Phi}_{s-e2}(\bar{x}_2, \bar{s}_2)}{I} = -\frac{L_2}{\sigma_{eff2}} \left\{ \frac{\bar{s}_2 - \lambda_{l2}}{\Theta_{l2}} [B_{l2} \cosh(\sqrt{\lambda_{l2}} \bar{x}_2) + B_{ll2} \sinh(\sqrt{\lambda_{l2}} \bar{x}_2)] + \frac{\bar{s}_2 - \lambda_{ll2}}{\Theta_{ll2}} [B_{ll2} \cosh(\sqrt{\lambda_{ll2}} \bar{x}_2) + B_{lv2} \sinh(\sqrt{\lambda_{ll2}} \bar{x}_2)] \right\} \quad (51-2)$$

$$\frac{\dot{\Phi}_{e3}(\bar{x}_3, \bar{s}_3)}{I} = -\frac{L_3}{\kappa_{eff3}} \left[\Gamma_{ll3} - B_{l3} \cosh(\sqrt{\bar{s}_3} \bar{x}_3) - B_{ll3} \sinh(\sqrt{\bar{s}_3} \bar{x}_3) + (\bar{x}_3 - 1) \right] \quad (51-3)$$

where

$$\Gamma_{ll3} = B_{l3} \cosh(\sqrt{\bar{s}_3}) + B_{ll3} \sinh(\sqrt{\bar{s}_3}) \quad (51-4)$$

Next, the solid-phase potential in the electrode will be solved. Transforming Eq. (4-1) into the complex phasor field and combining the result with Eq. (23-3) to yield

$$\frac{\partial^2 \dot{\Phi}_{s1}(x, s)}{\partial x^2} = \frac{a_{s1} F}{\sigma_{eff1}} j_1(x, s) = \frac{a_{s1} F}{\sigma_{eff1}} \frac{\dot{\Phi}_{s-e1}(x, s)}{F Z_{int1}} \quad (52-1)$$

The BC of Eq. (4-2) combined with Eq. (13-2) can be rewritten in the complex phasor form

$$\frac{\partial \dot{\Phi}_{s1}(x, s)}{\partial x} \Big|_{x=0} = -\frac{\dot{I}}{\sigma_{eff1}} \quad (52-2)$$

Based on Eqs. (33-2)–(33-4), Eqs. (52-1) and (52-2) can be rewritten in the dimensionless form

$$\frac{\partial^2 \dot{\Phi}_{s1}(\bar{x}_1, \bar{s}_1)}{\partial \bar{x}_1^2} = -\frac{L_1^3 a_{s1}}{\sigma_{eff1}^2 Z_{int1}} \dot{\Phi}_{s-e1}(\bar{x}_1, \bar{s}_1) \dot{I} \quad (53-1)$$

$$\frac{\partial \dot{\Phi}_{s1}(\bar{x}_1, \bar{s}_1)}{\partial \bar{x}_1} \Big|_{x_1=0} = -\frac{L_1}{\sigma_{eff1}} \dot{I} \quad (53-2)$$

$\dot{\Phi}_{s1}(x, s) = \dot{\Phi}_{e1}(x, s) + \dot{\Phi}_{s-e1}(x, s)$ combined with the continuity BC of Eq. (40-1) to yield

$$\dot{\Phi}_{s1}(\bar{x}_1 = 1, \bar{s}_1) = \dot{\Phi}_{e1}(\bar{x}_3 = 0, \bar{s}_3) + \dot{\Phi}_{s-e1}(\bar{x}_1 = 1, \bar{s}_1) \quad (53-3)$$

Upon integrating Eq. (53-1) twice and combining Eq. (42-2), the transfer function of $\dot{\Phi}_{s1}(\bar{x}_1, \bar{s}_1)$ is evaluated as follows

$$\frac{\dot{\Phi}_{s1}(\bar{x}_1, \bar{s}_1)}{I} = -\frac{L_1^3 a_{s1}}{\sigma_{eff1}^2 Z_{int1} \Theta_{l1}} \left\{ \frac{\bar{s}_1 - \lambda_{l1}}{\lambda_{l1}} [B_{l1} \cosh(\sqrt{\lambda_{l1}} \bar{x}_1) + B_{ll1} \sinh(\sqrt{\lambda_{l1}} \bar{x}_1)] + \frac{\bar{s}_1 - \lambda_{ll1}}{\lambda_{ll1}} [B_{ll1} \cosh(\sqrt{\lambda_{ll1}} \bar{x}_1) + B_{lv1} \sinh(\sqrt{\lambda_{ll1}} \bar{x}_1)] \right\} + H_{l1} \bar{x}_1 + H_{ll1} \quad (54-1)$$

Using the gradient BC of Eq. (53-2), H_{l1} is evaluated to be

$$H_{l1} = -\frac{L_1}{\sigma_{eff1}} \left[1 - \frac{L_1^2 a_{s1}}{\sigma_{eff1} Z_{int1} \Theta_{l1}} \left(\frac{\bar{s}_1 - \lambda_{l1}}{\sqrt{\lambda_{l1}}} B_{ll1} + \frac{\bar{s}_1 - \lambda_{ll1}}{\sqrt{\lambda_{ll1}}} B_{lv1} \right) \right] = -\frac{L_1}{\kappa_{eff1} + \sigma_{eff1}} \quad (54-2)$$

Using Eq. (53-3), H_{ll1} is evaluated to be

$$H_{ll1} = -\frac{L_1}{\sigma_{eff1} \Theta_{l1}} \left[(\bar{s}_1 - \lambda_{l1}) \Gamma_{l1} + (\bar{s}_1 - \lambda_{ll1}) \Gamma_{ll1} \right] + \frac{L_1^2 a_{s1}}{\sigma_{eff1}^2 Z_{int1} \Theta_{l1}} \left(\frac{\bar{s}_1 - \lambda_{l1}}{\lambda_{l1}} \Gamma_{l1} + \frac{\bar{s}_1 - \lambda_{ll1}}{\lambda_{ll1}} \Gamma_{ll1} \right) - H_{l1} + \frac{L_1}{\kappa_{eff1}} (1 + B_{l3} - \Gamma_{ll3}) \quad (54-3)$$

where Γ_{l1} and Γ_{ll1} are given as

$$\Gamma_{l1} = B_{l1} \cosh(\sqrt{\lambda_{l1}}) + B_{ll1} \sinh(\sqrt{\lambda_{l1}}) \quad (54-4)$$

$$\Gamma_{ll1} = B_{ll1} \cosh(\sqrt{\lambda_{ll1}}) + B_{lv1} \sinh(\sqrt{\lambda_{ll1}}) \quad (54-5)$$

The results are similar to Eqs. (54-1)–(54-3) can be obtained for the positive electrode

$$\frac{\dot{\Phi}_{s2}(\bar{x}_2, \bar{s}_2)}{I} = -\frac{L_2^3 a_{s2}}{\sigma_{eff2}^2 Z_{int2} \Theta_{l2}} \left\{ \frac{\bar{s}_2 - \lambda_{l2}}{\lambda_{l2}} [B_{l2} \cosh(\sqrt{\lambda_{l2}} \bar{x}_2) + B_{ll2} \sinh(\sqrt{\lambda_{l2}} \bar{x}_2)] + \frac{\bar{s}_2 - \lambda_{ll2}}{\lambda_{ll2}} [B_{ll2} \cosh(\sqrt{\lambda_{ll2}} \bar{x}_2) + B_{lv2} \sinh(\sqrt{\lambda_{ll2}} \bar{x}_2)] \right\} + H_{l2} \bar{x}_2 + H_{ll2} \quad (55-1)$$

$$H_{l2} = -\frac{L_2}{\sigma_{eff2}} \left(1 - \frac{\bar{s}_2 L_2^2 a_{s2}}{\sigma_{eff2} \lambda_{l2} \lambda_{ll2} Z_{int2}} \right) = -\frac{L_2}{\kappa_{eff2} + \sigma_{eff2}} \quad (55-2)$$

$$H_{ll2} = -\frac{L_2}{\sigma_{eff2} \Theta_{l2}} \left[(\bar{s}_2 - \lambda_{l2}) B_{l2} + (\bar{s}_2 - \lambda_{ll2}) B_{ll2} \right] + \frac{L_2^3 a_{s2}}{\sigma_{eff2}^2 Z_{int2} \Theta_{l2}} \left(\frac{\bar{s}_2 - \lambda_{l2}}{\lambda_{l2}} B_{l2} + \frac{\bar{s}_2 - \lambda_{ll2}}{\lambda_{ll2}} B_{ll2} \right) \quad (55-3)$$

Action V: DEFINE

Action V is to define impedance models based on the solved $\dot{\Phi}_{s-e1}(\bar{x}_1, \bar{s}_1)$, $\dot{\Phi}_{s-e2}(\bar{x}_2, \bar{s}_2)$, $\dot{\Phi}_{s1}(\bar{x}_1, \bar{s}_1)$, $\dot{\Phi}_{s2}(\bar{x}_2, \bar{s}_2)$, and $\dot{\Phi}_{e3}(\bar{x}_3, \bar{s}_3)$.

Based on Eqs. (33-3), (33-4), (36-3) and (36-4), Eqs. (17-1)–(17-4) can be rewritten as

$$Z_1(s) \stackrel{\text{def}}{=} -\frac{\dot{\Phi}_{s1}(\bar{x}_1 = 1, \bar{s}_1) - \dot{\Phi}_{s-e1}(\bar{x}_1 = 1, \bar{s}_1) - \dot{\Phi}_{s1}(\bar{x}_1 = 0, \bar{s}_1)}{\dot{I}(s)} \quad (56-1)$$

$$Z_2(s) \stackrel{\text{def}}{=} -\frac{\dot{\Phi}_{s2}(\bar{x}_2 = 1, \bar{s}_2) - \dot{\Phi}_{s-e2}(\bar{x}_2 = 1, \bar{s}_2) + \dot{\Phi}_{s-e2}(\bar{x}_2 = 0, \bar{s}_2)}{\dot{I}(s)} \quad (56-2)$$

$$Z_3(s) \stackrel{\text{def}}{=} -\frac{\dot{\Phi}_{e3}(\bar{x}_3 = 1, \bar{s}_3) - \dot{\Phi}_{e3}(\bar{x}_3 = 0, \bar{s}_3)}{\dot{I}(s)} \quad (56-3)$$

$$Z_4(s) \stackrel{\text{def}}{=} -\frac{\dot{\Phi}_{s2}(\bar{x}_2 = 1, \bar{s}_2) - \dot{\Phi}_{s1}(\bar{x}_1 = 0, \bar{s}_1)}{\dot{I}(s)} \quad (56-4)$$

Model DFN can be finally obtained by combining Eqs. (56-1)–(56-4) with Eqs. (51-1)–(51-3), (54-1), and (55-1)

$$Z_1(s) = \frac{L_1}{\kappa_{eff1} + \sigma_{eff1}} - \frac{L_1}{\sigma_{eff1} \Theta_{l1}} \left[(\bar{s}_1 - \lambda_{l1}) \Gamma_{l1} + (\bar{s}_1 - \lambda_{ll1}) \Gamma_{ll1} \right] + \frac{L_1^3 a_{s1}}{\sigma_{eff1}^2 Z_{int1} \Theta_{l1}} \left[\frac{\bar{s}_1 - \lambda_{l1}}{\lambda_{l1}} (\Gamma_{l1} - B_{l1}) + \frac{\bar{s}_1 - \lambda_{ll1}}{\lambda_{ll1}} (\Gamma_{ll1} - B_{ll1}) \right] \quad (57-1)$$

$$Z_2(s) = \frac{L_2}{\kappa_{\text{eff}2} + \sigma_{\text{eff}2}} + \frac{L_2}{\sigma_{\text{eff}2}\Theta_{\text{II}2}} \left[\left(\bar{s}_2 - \lambda_{\text{II}2} \right) B_{\text{II}2} + \left(\bar{s}_2 - \lambda_{\text{II}2} \right) B_{\text{III}2} \right] \\ + \frac{L_2^3 a_{s2}}{\sigma_{\text{eff}2}^2 z_{\text{int}2} \Theta_{\text{II}2}} \left[\frac{\bar{s}_2 - \lambda_{\text{II}2}}{\lambda_{\text{II}2}} (\Gamma_{\text{II}2} - B_{\text{II}2}) + \frac{\bar{s}_2 - \lambda_{\text{II}2}}{\lambda_{\text{II}2}} (\Gamma_{\text{III}2} - B_{\text{III}2}) \right] \quad (57-2)$$

$$Z_3(s) = \frac{L_3}{\kappa_{\text{eff}3} + \sigma_{\text{eff}3}} + \frac{L_3}{\kappa_{\text{eff}3}\Theta_{\text{III}3}} \\ \times \frac{\Theta_{\text{III}3} F}{\sqrt{\bar{s}_3}} \left(\frac{1}{\sinh(\sqrt{\bar{s}_3})} - \frac{1}{\tanh(\sqrt{\bar{s}_3})} \right) \left(\frac{\dot{\xi}_1}{I} + \frac{\dot{\xi}_2}{I} \right) \quad (57-3)$$

$$Z_4(s) = \frac{L_3^3 a_{s2}}{\sigma_{\text{eff}2}^2 z_{\text{int}2} \Theta_{\text{II}2}} \left(\frac{\bar{s}_2 - \lambda_{\text{II}2}}{\lambda_{\text{II}2}} \Gamma_{\text{II}2} + \frac{\bar{s}_2 - \lambda_{\text{II}2}}{\lambda_{\text{II}2}} \Gamma_{\text{III}2} \right) - H_{\text{II}2} - H_{\text{III}2} \\ - \frac{L_3^3 a_{s1}}{\sigma_{\text{eff}1}^2 z_{\text{int}1} \Theta_{\text{II}1}} \left(\frac{\bar{s}_1 - \lambda_{\text{II}1}}{\lambda_{\text{II}1}} B_{\text{II}1} + \frac{\bar{s}_1 - \lambda_{\text{II}1}}{\lambda_{\text{II}1}} B_{\text{III}1} \right) + H_{\text{III}1} \quad (57-4)$$

The above deduction has been briefly summarized in Fig. 3.

In Eq. (57-1) for $Z_1(s)$, the independent variable is the Laplace variable s , and the undetermined coefficients $\Theta_{\text{II}1}$, $\Theta_{\text{III}1}$, $\lambda_{\text{II}1}$ & $\lambda_{\text{III}1}$ and $\dot{\xi}_1$, $\Gamma_{\text{II}1}$, $B_{\text{II}1}$, $B_{\text{III}1}$ & $B_{\text{IV}1}$ can be defined as

$$\Gamma_{\text{II}} \left(\lambda_{\text{II}1}, \lambda_{\text{III}1}, \Theta_{\text{II}1}, \Theta_{\text{III}1}, \frac{\dot{\xi}_1}{I} \right) = B_{\text{II}1} \cosh(\sqrt{\lambda_{\text{II}1}}) \\ + B_{\text{II}1} \sinh(\sqrt{\lambda_{\text{II}1}}) \quad (58-1)$$

$$\Gamma_{\text{III}1} \left(\lambda_{\text{II}1}, \lambda_{\text{III}1}, \Theta_{\text{II}1}, \Theta_{\text{III}1}, \frac{\dot{\xi}_1}{I} \right) = B_{\text{III}1} \cosh(\sqrt{\lambda_{\text{III}1}}) \\ + B_{\text{IV}1} \sinh(\sqrt{\lambda_{\text{III}1}}) \quad (58-2)$$

$$B_{\text{II}1} \left(\lambda_{\text{II}1}, \lambda_{\text{III}1}, \Theta_{\text{II}1}, \Theta_{\text{III}1}, \frac{\dot{\xi}_1}{I} \right) = \frac{\Theta_{\text{II}1}}{\sqrt{\lambda_{\text{II}1}} (\lambda_{\text{II}1} - \lambda_{\text{III}1}) \sinh(\sqrt{\lambda_{\text{II}1}})} \\ \left[\cosh(\sqrt{\lambda_{\text{II}1}}) + \frac{\sigma_{\text{eff}1}}{\kappa_{\text{eff}1}} - \frac{Fz_{\text{int}1} \sigma_{\text{eff}1} (\bar{s}_1 + \Theta_{\text{II}1} - \lambda_{\text{II}1})}{L_1^2 a_{s1} (1 - t_0^+)} \frac{\dot{\xi}_1}{I} \right] \quad (58-3)$$

$$B_{\text{II}11} \left(\lambda_{\text{II}1}, \lambda_{\text{III}1}, \Theta_{\text{II}1}, \Theta_{\text{III}1} \right) = - \frac{\Theta_{\text{II}1}}{\sqrt{\lambda_{\text{II}1}} (\lambda_{\text{II}1} - \lambda_{\text{III}1})} \quad (58-4)$$

$$B_{\text{III}11} \left(\lambda_{\text{II}1}, \lambda_{\text{III}1}, \Theta_{\text{II}1}, \Theta_{\text{III}1}, \frac{\dot{\xi}_1}{I} \right) = - \frac{\Theta_{\text{II}1}}{\sqrt{\lambda_{\text{II}1}} (\lambda_{\text{II}1} - \lambda_{\text{III}1}) \sinh(\sqrt{\lambda_{\text{III}1}})} \\ \left[\cosh(\sqrt{\lambda_{\text{III}1}}) + \frac{\sigma_{\text{eff}1}}{\kappa_{\text{eff}1}} - \frac{Fz_{\text{int}1} \sigma_{\text{eff}1} (\bar{s}_1 + \Theta_{\text{II}1} - \lambda_{\text{II}1})}{L_1^2 a_{s1} (1 - t_0^+)} \frac{\dot{\xi}_1}{I} \right] \quad (58-5)$$

$$B_{\text{IV}11} \left(\lambda_{\text{II}1}, \lambda_{\text{III}1}, \Theta_{\text{II}1}, \Theta_{\text{III}1} \right) = \frac{\Theta_{\text{II}1}}{\sqrt{\lambda_{\text{II}1}} (\lambda_{\text{II}1} - \lambda_{\text{III}1})} \quad (58-6)$$

where

$$\Theta_{\text{II}1} = - \frac{\kappa_{\text{D,eff}1} (1 - t_0^+) a_{s1} L_1^2}{\kappa_{\text{eff}1} c_{\text{e},0} F D_{\text{e,eff}1} z_{\text{int}1}} \quad (59-1)$$

$$\Theta_{\text{III}1} = \frac{a_{s1} L_1^2}{\sigma_{\text{eff}1} z_{\text{int}1}} \left(1 + \frac{\sigma_{\text{eff}1}}{\kappa_{\text{eff}1}} \right) \quad (59-2)$$

$$\lambda_{\text{II}1} (\Theta_{\text{II}1}, \Theta_{\text{III}1}) = \frac{1}{2} \left(\bar{s}_1 + \Theta_{\text{II}1} + \Theta_{\text{III}1} + \sqrt{\bar{s}_1^2 + 2\bar{s}_1 (\Theta_{\text{II}1} - \Theta_{\text{III}1}) + (\Theta_{\text{II}1} + \Theta_{\text{III}1})^2} \right) \quad (59-3)$$

$$\lambda_{\text{III}1} (\Theta_{\text{II}1}, \Theta_{\text{III}1}) = \frac{1}{2} \left(\bar{s}_1 + \Theta_{\text{II}1} + \Theta_{\text{III}1} - \sqrt{\bar{s}_1^2 + 2\bar{s}_1 (\Theta_{\text{II}1} - \Theta_{\text{III}1}) + (\Theta_{\text{II}1} + \Theta_{\text{III}1})^2} \right) \quad (59-4)$$

$$\frac{\dot{\xi}_1 (\lambda_{\text{II}1}, \lambda_{\text{III}1}, \Theta_{\text{II}1}, \Theta_{\text{III}1}, \lambda_{\text{II}2}, \lambda_{\text{III}2}, \Theta_{\text{II}2}, \Theta_{\text{III}2})}{I} = \frac{\Lambda_{\text{II}1} + \frac{\Lambda_{\text{II}2}}{\lambda_{\text{II}2}} \Lambda_{\text{III}3}}{\Lambda_{\text{II}1} - \frac{1}{\lambda_{\text{II}2}} \Lambda_{\text{III}3}^2} \quad (59-5)$$

where

$$\Lambda_{\text{II}} (\lambda_{\text{II}1}, \lambda_{\text{III}1}, \Theta_{\text{II}1}, \Theta_{\text{III}1}) = - \frac{L_1^3 a_{s1} (1 - t_0^+)}{D_{\text{e,eff}1} \sigma_{\text{eff}1} (\lambda_{\text{II}1} - \lambda_{\text{III}1}) F z_{\text{int}1}} \left[\frac{1}{\sqrt{\lambda_{\text{II}1}} \sinh(\sqrt{\lambda_{\text{II}1}})} - \frac{1}{\sqrt{\lambda_{\text{III}1}} \sinh(\sqrt{\lambda_{\text{III}1}})} \right. \\ \left. + \frac{\sigma_{\text{eff}1}}{\kappa_{\text{eff}1}} \left(\frac{1}{\sqrt{\lambda_{\text{II}1}} \tanh(\sqrt{\lambda_{\text{II}1}})} - \frac{1}{\sqrt{\lambda_{\text{III}1}} \tanh(\sqrt{\lambda_{\text{III}1}})} \right) \right] \quad (60-1)$$

$$\Lambda_{\text{II}1} (\lambda_{\text{II}1}, \lambda_{\text{III}1}, \Theta_{\text{II}1}, \Theta_{\text{III}1}) = \frac{L_1}{D_{\text{e,eff}1} (\lambda_{\text{II}1} - \lambda_{\text{III}1})} \left[\frac{\bar{s}_1 + \Theta_{\text{II}1} - \lambda_{\text{II}1}}{\sqrt{\lambda_{\text{II}1}} \tanh(\sqrt{\lambda_{\text{II}1}})} - \frac{\bar{s}_1 + \Theta_{\text{II}1} - \lambda_{\text{II}1}}{\sqrt{\lambda_{\text{III}1}} \tanh(\sqrt{\lambda_{\text{III}1}})} \right] \\ + \Lambda_{\text{III}3} \cosh(\sqrt{\bar{s}_3}) \quad (60-2)$$

$$\Lambda_{\text{II}2} (\lambda_{\text{II}2}, \lambda_{\text{III}2}, \Theta_{\text{II}2}, \Theta_{\text{III}2}) = - \frac{L_2^3 a_{s2} (1 - t_0^+)}{D_{\text{e,eff}2} \sigma_{\text{eff}2} (\lambda_{\text{II}2} - \lambda_{\text{III}2}) F z_{\text{int}2}} \left[\frac{1}{\sqrt{\lambda_{\text{II}2}} \sinh(\sqrt{\lambda_{\text{II}2}})} - \frac{1}{\sqrt{\lambda_{\text{III}2}} \sinh(\sqrt{\lambda_{\text{III}2}})} \right. \\ \left. + \frac{\sigma_{\text{eff}2}}{\kappa_{\text{eff}2}} \left(\frac{1}{\sqrt{\lambda_{\text{II}2}} \tanh(\sqrt{\lambda_{\text{II}2}})} - \frac{1}{\sqrt{\lambda_{\text{III}2}} \tanh(\sqrt{\lambda_{\text{III}2}})} \right) \right] \quad (60-3)$$

$$\Lambda_{\text{II}2} (\lambda_{\text{II}2}, \lambda_{\text{III}2}, \Theta_{\text{II}2}, \Theta_{\text{III}2}) = \frac{L_2}{D_{\text{e,eff}2} (\lambda_{\text{II}2} - \lambda_{\text{III}2})} \left[\frac{\bar{s}_2 + \Theta_{\text{II}2} - \lambda_{\text{II}2}}{\sqrt{\lambda_{\text{II}2}} \tanh(\sqrt{\lambda_{\text{II}2}})} - \frac{\bar{s}_2 + \Theta_{\text{II}2} - \lambda_{\text{II}2}}{\sqrt{\lambda_{\text{III}2}} \tanh(\sqrt{\lambda_{\text{III}2}})} \right] \\ + \Lambda_{\text{III}3} \cosh(\sqrt{\bar{s}_3}) \quad (60-4)$$

$$\Lambda_{\text{III}3} = \frac{L_3}{D_{\text{e,eff}3} \sqrt{\bar{s}_3} \sinh(\sqrt{\bar{s}_3})} \quad (60-5)$$

$$\text{In Eq. (57-2) for } Z_2(s), \text{ the independent variable is the Laplace variable } s, \text{ and the undetermined coefficients } \Theta_{\text{II}2}, \Theta_{\text{III}2}, \lambda_{\text{II}2} \text{ and } \lambda_{\text{III}2} \text{ and } \dot{\xi}_2, \Gamma_{\text{II}2}, B_{\text{II}2}, B_{\text{III}2}, B_{\text{IV}2} \text{ can be defined as}$$

$$\Gamma_{\text{II}2} \left(\lambda_{\text{II}2}, \lambda_{\text{III}2}, \Theta_{\text{II}2}, \Theta_{\text{III}2}, \frac{\dot{\xi}_2}{I} \right) = B_{\text{II}2} \cosh(\sqrt{\lambda_{\text{II}2}}) + B_{\text{II}2} \sinh(\sqrt{\lambda_{\text{II}2}}) \quad (61-1)$$

$$\Gamma_{\text{III}2} \left(\lambda_{\text{II}2}, \lambda_{\text{III}2}, \Theta_{\text{II}2}, \Theta_{\text{III}2}, \frac{\dot{\xi}_2}{I} \right) = B_{\text{III}2} \cosh(\sqrt{\lambda_{\text{III}2}}) + B_{\text{IV}2} \sinh(\sqrt{\lambda_{\text{III}2}}) \quad (61-2)$$

$$B_{\text{II}2} \left(\lambda_{\text{II}2}, \lambda_{\text{III}2}, \Theta_{\text{II}2}, \Theta_{\text{III}2}, \frac{\dot{\xi}_2}{I} \right) = - \frac{\Theta_{\text{II}2}}{\sqrt{\lambda_{\text{II}2}} (\lambda_{\text{II}2} - \lambda_{\text{III}2}) \sinh(\sqrt{\lambda_{\text{II}2}})} \\ - \frac{B_{\text{II}2}}{\tanh(\sqrt{\lambda_{\text{II}2}})} \quad (61-3)$$

$$B_{\text{III}2} \left(\lambda_{\text{II}2}, \lambda_{\text{III}2}, \Theta_{\text{II}2}, \Theta_{\text{III}2}, \frac{\dot{\xi}_2}{I} \right) = \frac{\Theta_{\text{II}2}}{\sqrt{\lambda_{\text{II}2}} (\lambda_{\text{II}2} - \lambda_{\text{III}2}) \sinh(\sqrt{\lambda_{\text{II}2}})} \left[\frac{\sigma_{\text{eff}2}}{K_{\text{eff}2}} - \frac{Fz_{\text{int}2} \sigma_{\text{eff}2} (\bar{s}_2 + \Theta_{\text{II}2} - \lambda_{\text{II}2})}{L_2^2 a_{s2} (1 - t_0^+)} \frac{\dot{\xi}_2}{I} \right] \quad (61-4)$$

$$B_{\text{IV}2} \left(\lambda_{\text{II}2}, \lambda_{\text{III}2}, \Theta_{\text{II}2}, \Theta_{\text{III}2}, \frac{\dot{\xi}_2}{I} \right) = \frac{\Theta_{\text{II}2}}{\sqrt{\lambda_{\text{II}2}} (\lambda_{\text{II}2} - \lambda_{\text{III}2}) \sinh(\sqrt{\lambda_{\text{II}2}})} \\ - \frac{B_{\text{IV}2}}{\tanh(\sqrt{\lambda_{\text{II}2}})} \quad (61-5)$$

$$B_{IV2} \left(\lambda_{I2}, \lambda_{II2}, \Theta_{I2}, \Theta_{II2}, \frac{\dot{\zeta}_2}{I} \right) = -\frac{\Theta_{I2}}{\sqrt{\lambda_{II2}}(\lambda_{I2} - \lambda_{II2})} \left[\frac{\sigma_{eff2}}{K_{eff2}} - \frac{Fz_{int2}\sigma_{eff2}(\bar{s}_2 + \Theta_{I2} - \lambda_{I2})}{L_2^2 a_{s2}(1 - t_0^+)} \frac{\dot{\zeta}_2}{I} \right] \quad (61-6)$$

where

$$\Theta_{I2} = -\frac{\kappa_{D,eff2}(1 - t_0^+)a_{s2}L_2^2}{\kappa_{eff2}c_{e,0}FD_{e,eff2}z_{int2}} \quad (62-1)$$

$$\Theta_{II2} = \frac{a_{s2}L_2^2}{\sigma_{eff2}z_{int2}} \left(1 + \frac{\sigma_{eff2}}{K_{eff2}} \right) \quad (62-2)$$

$$\lambda_{I2}(\Theta_{I2}, \Theta_{II2}) = \frac{1}{2} \left(\bar{s}_2 + \Theta_{I2} + \Theta_{II2} + \sqrt{\bar{s}_2^2 + 2\bar{s}_2(\Theta_{I2} - \Theta_{II2}) + (\Theta_{I2} + \Theta_{II2})^2} \right) \quad (62-3)$$

$$\lambda_{II2}(\Theta_{I2}, \Theta_{II2}) = \frac{1}{2} \left(\bar{s}_2 + \Theta_{I2} + \Theta_{II2} - \sqrt{\bar{s}_2^2 + 2\bar{s}_2(\Theta_{I2} - \Theta_{II2}) + (\Theta_{I2} + \Theta_{II2})^2} \right) \quad (62-4)$$

$$\frac{\dot{\zeta}_2(\lambda_{I2}, \lambda_{II2}, \Theta_{I2}, \Theta_{II2}, \lambda_{I1}, \lambda_{II1}, \Theta_{I1}, \Theta_{II1})}{I} = \frac{\Lambda_{I2} + \frac{\Lambda_{II}}{\Lambda_{III}}\Lambda_{III3}}{\Lambda_{II2} - \frac{1}{\Lambda_{III}}\Lambda_{III3}^2} \quad (62-5)$$

In Eq. (57-3) for $Z_3(s)$, the independent variable is the Laplace variable s , and the undetermined coefficient Θ_{III3} can be defined as

$$\Theta_{III3} = -\frac{\kappa_{D,eff3}}{D_{e,eff3}c_{e,0}F} \quad (63)$$

In Eq. (57-4) for $Z_4(s)$, the independent variable is the Laplace variable s , and the undetermined coefficients Γ_{III3} , B_{I3} & B_{II3} , and H_{I1} , H_{II1} , H_{I2} & H_{II2} can be defined as

$$H_{I1} = -\frac{L_1}{\kappa_{eff1} + \sigma_{eff1}} \quad (64-1)$$

$$H_{II1} \left(\lambda_{I1}, \lambda_{II1}, \Theta_{I1}, \Theta_{II1}, \frac{\dot{\zeta}_1}{I}, \frac{\dot{\zeta}_2}{I} \right) = -\frac{L_1}{\sigma_{eff1}z_{int1}\Theta_{I1}} \left[\left(\bar{s}_1 - \lambda_{I1} \right) \Gamma_{I1} + \left(\bar{s}_1 - \lambda_{II1} \right) \Gamma_{II1} \right] + \frac{L_1^3 a_{s1}}{\sigma_{eff1}^2 z_{int1}\Theta_{I1}} \left(\frac{\bar{s}_1 - \lambda_{I1}}{\lambda_{I1}} \Gamma_{I1} + \frac{\bar{s}_1 - \lambda_{II1}}{\lambda_{II1}} \Gamma_{II1} \right) - H_{I1} + \frac{L_1}{\kappa_{eff3}} (1 + B_{I3} - \Gamma_{III3}) \quad (64-2)$$

$$H_{I2} = -\frac{L_2}{\kappa_{eff2} + \sigma_{eff2}} \quad (64-3)$$

$$H_{II2} \left(\lambda_{I2}, \lambda_{II2}, \Theta_{I2}, \Theta_{II2}, \frac{\dot{\zeta}_2}{I} \right) = -\frac{L_2}{\sigma_{eff2}z_{int2}\Theta_{I2}} \left[\left(\bar{s}_2 - \lambda_{I2} \right) B_{I2} + \left(\bar{s}_2 - \lambda_{II2} \right) B_{II2} \right] + \frac{L_2^3 a_{s2}}{\sigma_{eff2}^2 z_{int2}\Theta_{I2}} \left(\frac{\bar{s}_2 - \lambda_{I2}}{\lambda_{I2}} B_{I2} + \frac{\bar{s}_2 - \lambda_{II2}}{\lambda_{II2}} B_{II2} \right) \quad (64-4)$$

where

$$\Gamma_{III3} \left(\frac{\dot{\zeta}_1}{I}, \frac{\dot{\zeta}_2}{I} \right) = B_{I3} \cosh \left(\sqrt{\bar{s}_3} \right) + B_{II3} \sinh \left(\sqrt{\bar{s}_3} \right) \quad (65-1)$$

$$B_{I3} \left(\frac{\dot{\zeta}_1}{I}, \frac{\dot{\zeta}_2}{I} \right) = \frac{\Theta_{III3}F}{\sqrt{\bar{s}_3} \sinh \left(\sqrt{\bar{s}_3} \right)} \left[\frac{\dot{\zeta}_2}{I} - \frac{\dot{\zeta}_1}{I} \cosh \left(\sqrt{\bar{s}_3} \right) \right] \quad (65-2)$$

$$B_{II3} \left(\frac{\dot{\zeta}_1}{I} \right) = \frac{\Theta_{III3}F}{\sqrt{\bar{s}_3}} \frac{\dot{\zeta}_1}{I} \quad (65-3)$$

Up to now, the DFN impedance model has been fully deduced with the complex phasor method, the DFN-like impedance models under different physical scenes will be unified subsequently.

2.2. Unification of the DFN-like impedance models under different physical scenes

For the convenience of discussion for four different physical scenes, Scenes I and II refer to ignoring Li^+ concentration gradient in the pore electrolyte of the separator and the electrode, respectively, Scene III refers to ignoring the electronic resistance of active material in the electrode, and Scene IV refers to ignoring Li concentration gradient in the active particle of the electrode. This section unifies the DFN-like impedance models, including Model DFN and Models A–F, under different physical scenes, i.e., Scenes I–IV.

2.2.1. Degeneration from Model DFN to Model A & D

When $D_{e,eff3} \rightarrow \infty$, i.e. under the condition of Scene I, Model DFN can be degenerated into Model A. Thus, Model A can be obtained by letting $D_{e,eff3} \rightarrow \infty$ in Eqs. (57-1)–(57-4)

$$Z_{A\#1}(s) = \frac{L_1}{\kappa_{eff1} + \sigma_{eff1}} - \frac{L_1}{\sigma_{eff1}z_{int1}\Theta_{I1}} \left[\left(\bar{s}_1 - \lambda_{I1} \right) \Gamma_{I1} + \left(\bar{s}_1 - \lambda_{II1} \right) \Gamma_{II1} \right] + \frac{L_1^3 a_{s1}}{\sigma_{eff1}^2 z_{int1}\Theta_{I1}} \left[\frac{\bar{s}_1 - \lambda_{I1}}{\lambda_{I1}} (\Gamma_{I1} - B_{I1}) + \frac{\bar{s}_1 - \lambda_{II1}}{\lambda_{II1}} (\Gamma_{II1} - B_{II1}) \right] \quad (66-1)$$

$$Z_{A\#2}(s) = \frac{L_2}{\kappa_{eff2} + \sigma_{eff2}} + \frac{L_2}{\sigma_{eff2}z_{int2}\Theta_{I2}} \left[\left(\bar{s}_2 - \lambda_{I2} \right) B_{I2} + \left(\bar{s}_2 - \lambda_{II2} \right) B_{II2} \right] + \frac{L_2^3 a_{s2}}{\sigma_{eff2}^2 z_{int2}\Theta_{I2}} \left[\frac{\bar{s}_2 - \lambda_{I2}}{\lambda_{I2}} (\Gamma_{I2} - B_{I2}) + \frac{\bar{s}_2 - \lambda_{II2}}{\lambda_{II2}} (\Gamma_{II2} - B_{II2}) \right] \quad (66-2)$$

$$Z_{A\#3}(s) = \frac{L_3}{\kappa_{eff3}} \quad (66-3)$$

$$Z_{A\#4}(s) = \frac{L_2^3 a_{s2}}{\sigma_{eff2}^2 z_{int2}\Theta_{I2}} \left(\frac{\bar{s}_2 - \lambda_{I2}}{\lambda_{I2}} \Gamma_{I2} + \frac{\bar{s}_2 - \lambda_{II2}}{\lambda_{II2}} \Gamma_{II2} \right) - H_{I2} - H_{II2} - \frac{L_2^3 a_{s1}}{\sigma_{eff1}^2 z_{int1}\Theta_{I1}} \left(\frac{\bar{s}_1 - \lambda_{I1}}{\lambda_{I1}} B_{I1} + \frac{\bar{s}_1 - \lambda_{II1}}{\lambda_{II1}} B_{II1} \right) + H_{II1} \quad (66-4)$$

The coefficients in Eq. (66-1) for $Z_{A\#1}(s)$ are given as

$$\Gamma_{I1} \left(\lambda_{I1}, \lambda_{II1}, \Theta_{I1}, \Theta_{II1}, \frac{\dot{\zeta}_1}{I} \right) = B_{I1} \cosh \left(\sqrt{\lambda_{I1}} \right) + B_{II1} \sinh \left(\sqrt{\lambda_{I1}} \right) \quad (67-1)$$

$$\Gamma_{II1} \left(\lambda_{I1}, \lambda_{II1}, \Theta_{I1}, \Theta_{II1}, \frac{\dot{\zeta}_1}{I} \right) = B_{II1} \cosh \left(\sqrt{\lambda_{II1}} \right) + B_{IV1} \sinh \left(\sqrt{\lambda_{II1}} \right) \quad (67-2)$$

$$B_{I1} \left(\lambda_{I1}, \lambda_{II1}, \Theta_{I1}, \Theta_{II1}, \frac{\dot{\zeta}_1}{I} \right) = \frac{\Theta_{I1}}{\sqrt{\lambda_{II1}}(\lambda_{I1} - \lambda_{II1}) \sinh \left(\sqrt{\lambda_{I1}} \right)} \left[\cosh \left(\sqrt{\lambda_{I1}} \right) + \frac{\sigma_{eff1}}{\kappa_{eff1}} - \frac{Fz_{int1}\sigma_{eff1}(\bar{s}_1 + \Theta_{I1} - \lambda_{I1})}{L_1^2 a_{s1}(1 - t_0^+)} \frac{\dot{\zeta}_1}{I} \right] \quad (67-3)$$

$$B_{II1} \left(\lambda_{I1}, \lambda_{II1}, \Theta_{I1}, \Theta_{II1}, \frac{\dot{\zeta}_1}{I} \right) = -\frac{\Theta_{I1}}{\sqrt{\lambda_{II1}}(\lambda_{I1} - \lambda_{II1}) \sinh \left(\sqrt{\lambda_{II1}} \right)} \quad (67-4)$$

$$B_{III1} \left(\lambda_{I1}, \lambda_{II1}, \Theta_{I1}, \Theta_{II1}, \frac{\dot{\zeta}_1}{I} \right) = -\frac{\Theta_{I1}}{\sqrt{\lambda_{II1}}(\lambda_{I1} - \lambda_{II1}) \sinh \left(\sqrt{\lambda_{II1}} \right)} \left[\cosh \left(\sqrt{\lambda_{II1}} \right) + \frac{\sigma_{eff1}}{\kappa_{eff1}} - \frac{Fz_{int1}\sigma_{eff1}(\bar{s}_1 + \Theta_{I1} - \lambda_{I1})}{L_1^2 a_{s1}(1 - t_0^+)} \frac{\dot{\zeta}_1}{I} \right] \quad (67-5)$$

$$B_{IV1} \left(\lambda_{I1}, \lambda_{II1}, \Theta_{I1}, \Theta_{II1} \right) = \frac{\Theta_{I1}}{\sqrt{\lambda_{II1}}(\lambda_{I1} - \lambda_{II1})} \quad (67-6)$$

where

$$\Theta_{\text{I}1} = -\frac{\kappa_{\text{D},\text{eff}1}(1-t_0^+)a_{\text{s}1}L_1^2}{\kappa_{\text{eff}1}c_{\text{e},0}FD_{\text{e},\text{eff}1}Z_{\text{int}1}} \quad (68-1)$$

$$\Theta_{\text{II}1} = \frac{a_{\text{s}1}L_1^2}{\sigma_{\text{eff}1}Z_{\text{int}1}} \left(1 + \frac{\sigma_{\text{eff}1}}{\kappa_{\text{eff}1}} \right) \quad (68-2)$$

$$\lambda_{\text{I}1}(\Theta_{\text{I}2}, \Theta_{\text{II}2}) = \frac{1}{2} \left(\bar{s}_1 + \Theta_{\text{I}1} + \Theta_{\text{II}1} + \sqrt{\bar{s}_1^2 + 2\bar{s}_1(\Theta_{\text{I}1} - \Theta_{\text{II}1}) + (\Theta_{\text{I}1} + \Theta_{\text{II}1})^2} \right) \quad (68-3)$$

$$\lambda_{\text{II}1}(\Theta_{\text{I}2}, \Theta_{\text{II}2}) = \frac{1}{2} \left(\bar{s}_1 + \Theta_{\text{I}1} + \Theta_{\text{II}1} - \sqrt{\bar{s}_1^2 + 2\bar{s}_1(\Theta_{\text{I}1} - \Theta_{\text{II}1}) + (\Theta_{\text{I}1} + \Theta_{\text{II}1})^2} \right) \quad (68-4)$$

$$\frac{\dot{\zeta}_2(\lambda_{\text{I}1}, \lambda_{\text{II}1}, \Theta_{\text{I}1}, \Theta_{\text{II}1})}{\dot{I}} = \frac{\Lambda_{\text{I}1}}{\Lambda_{\text{II}1}} \quad (68-5)$$

where

$$\begin{aligned} \Lambda_{\text{I}1}(\lambda_{\text{I}1}, \lambda_{\text{II}1}, \Theta_{\text{I}1}, \Theta_{\text{II}1}) &= -\frac{L_1^2 a_{\text{s}1}(1-t_0^+)}{\sigma_{\text{eff}1} F Z_{\text{int}1}} \left[\frac{1}{\sqrt{\lambda_{\text{II}1}} \sinh(\sqrt{\lambda_{\text{II}1}})} - \frac{1}{\sqrt{\lambda_{\text{I}1}} \sinh(\sqrt{\lambda_{\text{I}1}})} \right] \\ &\quad + \frac{\sigma_{\text{eff}1}}{\kappa_{\text{eff}1}} \left(\frac{1}{\sqrt{\lambda_{\text{II}1}} \tanh(\sqrt{\lambda_{\text{II}1}})} - \frac{1}{\sqrt{\lambda_{\text{I}1}} \tanh(\sqrt{\lambda_{\text{I}1}})} \right) \end{aligned} \quad (69-1)$$

$$\Lambda_{\text{II}1}(\lambda_{\text{I}1}, \lambda_{\text{II}1}, \Theta_{\text{I}1}, \Theta_{\text{II}1}) = \frac{\bar{s}_1 + \Theta_{\text{I}1} - \lambda_{\text{II}1}}{\sqrt{\lambda_{\text{II}1}} \tanh(\sqrt{\lambda_{\text{II}1}})} - \frac{\bar{s}_1 + \Theta_{\text{I}1} - \lambda_{\text{I}1}}{\sqrt{\lambda_{\text{I}1}} \tanh(\sqrt{\lambda_{\text{I}1}})} \quad (69-2)$$

The coefficients in Eq. (66-2) for $Z_{\text{A}\#2}(s)$ are given as

$$\Gamma_{\text{I}2} \left(\lambda_{\text{I}2}, \lambda_{\text{II}2}, \Theta_{\text{I}2}, \Theta_{\text{II}2}, \frac{\dot{\zeta}_2}{\dot{I}} \right) = B_{\text{I}2} \cosh(\sqrt{\lambda_{\text{I}2}}) + B_{\text{II}2} \sinh(\sqrt{\lambda_{\text{I}2}}) \quad (70-1)$$

$$\Gamma_{\text{II}2} \left(\lambda_{\text{I}2}, \lambda_{\text{II}2}, \Theta_{\text{I}2}, \Theta_{\text{II}2}, \frac{\dot{\zeta}_2}{\dot{I}} \right) = B_{\text{III}2} \cosh(\sqrt{\lambda_{\text{II}2}}) + B_{\text{IV}2} \sinh(\sqrt{\lambda_{\text{II}2}}) \quad (70-2)$$

$$\begin{aligned} B_{\text{I}2} \left(\lambda_{\text{I}2}, \lambda_{\text{II}2}, \Theta_{\text{I}2}, \Theta_{\text{II}2}, \frac{\dot{\zeta}_2}{\dot{I}} \right) &= -\frac{\Theta_{\text{I}2}}{\sqrt{\lambda_{\text{I}2}}(\lambda_{\text{I}2} - \lambda_{\text{II}2}) \sinh(\sqrt{\lambda_{\text{I}2}})} \\ &\quad - \frac{B_{\text{II}2}}{\tanh(\sqrt{\lambda_{\text{I}2}})} \end{aligned} \quad (70-3)$$

$$B_{\text{II}2} \left(\lambda_{\text{I}2}, \lambda_{\text{II}2}, \Theta_{\text{I}2}, \Theta_{\text{II}2}, \frac{\dot{\zeta}_2}{\dot{I}} \right) = \frac{\Theta_{\text{I}2}}{\sqrt{\lambda_{\text{I}2}}(\lambda_{\text{I}2} - \lambda_{\text{II}2})} \left[\frac{\sigma_{\text{eff}2}}{\kappa_{\text{eff}2}} - \frac{F Z_{\text{int}2} \sigma_{\text{eff}2} (\bar{s}_2 + \Theta_{\text{I}2} - \lambda_{\text{II}2}) \dot{\zeta}_2}{L_2^2 a_{\text{s}2} (1-t_0^+)} \right] \quad (70-4)$$

$$\begin{aligned} B_{\text{III}2} \left(\lambda_{\text{I}2}, \lambda_{\text{II}2}, \Theta_{\text{I}2}, \Theta_{\text{II}2}, \frac{\dot{\zeta}_2}{\dot{I}} \right) &= \frac{\Theta_{\text{I}2}}{\sqrt{\lambda_{\text{II}2}}(\lambda_{\text{I}2} - \lambda_{\text{II}2}) \sinh(\sqrt{\lambda_{\text{II}2}})} \\ &\quad - \frac{B_{\text{IV}2}}{\tanh(\sqrt{\lambda_{\text{II}2}})} \end{aligned} \quad (70-5)$$

$$B_{\text{IV}2} \left(\lambda_{\text{I}2}, \lambda_{\text{II}2}, \Theta_{\text{I}2}, \Theta_{\text{II}2}, \frac{\dot{\zeta}_2}{\dot{I}} \right) = -\frac{\Theta_{\text{I}2}}{\sqrt{\lambda_{\text{II}2}}(\lambda_{\text{I}2} - \lambda_{\text{II}2})} \left[\frac{\sigma_{\text{eff}2}}{\kappa_{\text{eff}2}} - \frac{F Z_{\text{int}2} \sigma_{\text{eff}2} (\bar{s}_2 + \Theta_{\text{I}2} - \lambda_{\text{I}2}) \dot{\zeta}_2}{L_2^2 a_{\text{s}2} (1-t_0^+)} \right] \quad (70-6)$$

where

$$\Theta_{\text{I}2} = -\frac{\kappa_{\text{D},\text{eff}2}(1-t_0^+)a_{\text{s}2}L_2^2}{\kappa_{\text{eff}2}c_{\text{e},0}FD_{\text{e},\text{eff}2}Z_{\text{int}2}} \quad (71-1)$$

$$\Theta_{\text{II}2} = \frac{a_{\text{s}2}L_2^2}{\sigma_{\text{eff}2}Z_{\text{int}2}} \left(1 + \frac{\sigma_{\text{eff}2}}{\kappa_{\text{eff}2}} \right) \quad (71-2)$$

$$\lambda_{\text{I}2}(\Theta_{\text{I}2}, \Theta_{\text{II}2}) = \frac{1}{2} \left(\bar{s}_2 + \Theta_{\text{I}2} + \Theta_{\text{II}2} + \sqrt{\bar{s}_2^2 + 2\bar{s}_2(\Theta_{\text{I}2} - \Theta_{\text{II}2}) + (\Theta_{\text{I}2} + \Theta_{\text{II}2})^2} \right) \quad (71-3)$$

$$\lambda_{\text{II}2}(\Theta_{\text{I}2}, \Theta_{\text{II}2}) = \frac{1}{2} \left(\bar{s}_2 + \Theta_{\text{I}2} + \Theta_{\text{II}2} - \sqrt{\bar{s}_2^2 + 2\bar{s}_2(\Theta_{\text{I}2} - \Theta_{\text{II}2}) + (\Theta_{\text{I}2} + \Theta_{\text{II}2})^2} \right) \quad (71-4)$$

$$\frac{\dot{\zeta}_2(\lambda_{\text{I}2}, \lambda_{\text{II}2}, \Theta_{\text{I}2}, \Theta_{\text{II}2})}{\dot{I}} = \frac{\Lambda_{\text{I}2}}{\Lambda_{\text{II}2}} \quad (71-5)$$

where

$$\begin{aligned} \Lambda_{\text{I}2}(\lambda_{\text{I}2}, \lambda_{\text{II}2}, \Theta_{\text{I}2}, \Theta_{\text{II}2}) &= -\frac{L_2^2 a_{\text{s}2}(1-t_0^+)}{\sigma_{\text{eff}1} F Z_{\text{int}2}} \left[\frac{1}{\sqrt{\lambda_{\text{II}2}} \sinh(\sqrt{\lambda_{\text{II}2}})} - \frac{1}{\sqrt{\lambda_{\text{I}2}} \sinh(\sqrt{\lambda_{\text{I}2}})} \right] \\ &\quad + \frac{\sigma_{\text{eff}2}}{\kappa_{\text{eff}2}} \left(\frac{1}{\sqrt{\lambda_{\text{II}2}} \tanh(\sqrt{\lambda_{\text{II}2}})} - \frac{1}{\sqrt{\lambda_{\text{I}2}} \tanh(\sqrt{\lambda_{\text{I}2}})} \right) \end{aligned} \quad (72-1)$$

$$\Lambda_{\text{II}2}(\lambda_{\text{I}2}, \lambda_{\text{II}2}, \Theta_{\text{I}2}, \Theta_{\text{II}2}) = \frac{\bar{s}_2 + \Theta_{\text{I}2} - \lambda_{\text{II}2}}{\sqrt{\lambda_{\text{I}2}} \tanh(\sqrt{\lambda_{\text{I}2}})} - \frac{\bar{s}_2 + \Theta_{\text{I}2} - \lambda_{\text{I}2}}{\sqrt{\lambda_{\text{II}2}} \tanh(\sqrt{\lambda_{\text{II}2}})} \quad (72-2)$$

The coefficients in Eq. (66-4) for $Z_{\text{A}\#4}(s)$ are given as

$$H_{\text{I}1} = -\frac{L_1}{\kappa_{\text{eff}1} + \sigma_{\text{eff}1}} \quad (73-1)$$

$$\begin{aligned} H_{\text{II}1} \left(\lambda_{\text{I}1}, \lambda_{\text{II}1}, \Theta_{\text{I}1}, \Theta_{\text{II}1}, \frac{\dot{\zeta}_1}{\dot{I}} \right) &= -\frac{L_1}{\sigma_{\text{eff}1} \Theta_{\text{I}1}} \left[(\bar{s}_1 - \lambda_{\text{I}1}) \Gamma_{\text{I}1} + (\bar{s}_1 - \lambda_{\text{II}1}) \Gamma_{\text{II}1} \right] \\ &\quad + \frac{L_1^3 a_{\text{s}1}}{\sigma_{\text{eff}1}^2 Z_{\text{int}1} \Theta_{\text{I}1}} \left(\frac{\bar{s}_1 - \lambda_{\text{I}1}}{\lambda_{\text{I}1}} \Gamma_{\text{I}1} + \frac{\bar{s}_1 - \lambda_{\text{II}1}}{\lambda_{\text{II}1}} \Gamma_{\text{II}1} \right) - H_{\text{I}1} + \frac{L_3}{\kappa_{\text{eff}3}} \end{aligned} \quad (73-2)$$

$$H_{\text{I}2} = -\frac{L_2}{\kappa_{\text{eff}2} + \sigma_{\text{eff}2}} \quad (73-3)$$

$$\begin{aligned} H_{\text{II}2} \left(\lambda_{\text{I}2}, \lambda_{\text{II}2}, \Theta_{\text{I}2}, \Theta_{\text{II}2}, \frac{\dot{\zeta}_2}{\dot{I}} \right) &= -\frac{L_2}{\sigma_{\text{eff}2} \Theta_{\text{I}2}} \left[(\bar{s}_2 - \lambda_{\text{I}2}) B_{\text{I}2} + (\bar{s}_2 - \lambda_{\text{II}2}) B_{\text{II}2} \right] \\ &\quad + \frac{L_2^3 a_{\text{s}2}}{\sigma_{\text{eff}2}^2 Z_{\text{int}2} \Theta_{\text{I}2}} \left(\frac{\bar{s}_2 - \lambda_{\text{I}2}}{\lambda_{\text{I}2}} B_{\text{I}2} + \frac{\bar{s}_2 - \lambda_{\text{II}2}}{\lambda_{\text{II}2}} B_{\text{II}2} \right) \end{aligned} \quad (73-4)$$

In addition, Model A can be degenerated into Model D under the condition of Scene IV. The detailed degeneration from Model DFN to Model A and from Model A to Model D please refers to [Supporting Information](#). A detailed discussion for Mode D please refers to Reference [58].

2.2.2. Degeneration from Model A to Model B & E

When $D_{\text{e},\text{eff}} \rightarrow \infty$, i.e. under the condition of Scene II, Model A can be degenerated into Model B. Thus, Model B can be directly obtained by letting $D_{\text{e},\text{eff}} \rightarrow \infty$ in Eqs. (66-1)–(66-4)

$$Z_{\text{B}\#1}(s) = \frac{L_1}{\kappa_{\text{eff}1} + \sigma_{\text{eff}1}} \left[1 + \frac{2 + \left(\frac{\kappa_{\text{eff}1}}{\sigma_{\text{eff}1}} + \frac{\sigma_{\text{eff}1}}{\kappa_{\text{eff}1}} \right) \cosh(\sqrt{\Theta_{\text{I}1}})}{\sqrt{\Theta_{\text{I}1}} \sinh(\sqrt{\Theta_{\text{I}1}})} \right] \quad (74-1)$$

$$Z_{\text{B}\#2}(s) = \frac{L_2}{\kappa_{\text{eff}2} + \sigma_{\text{eff}2}} \left[1 + \frac{2 + \left(\frac{\kappa_{\text{eff}2}}{\sigma_{\text{eff}2}} + \frac{\sigma_{\text{eff}2}}{\kappa_{\text{eff}2}} \right) \cosh(\sqrt{\Theta_{\text{II}2}})}{\sqrt{\Theta_{\text{II}2}} \sinh(\sqrt{\Theta_{\text{II}2}})} \right] \quad (74-2)$$

$$Z_{\text{B}\#3}(s) = \frac{L_3}{\kappa_{\text{eff}3}} \quad (74-3)$$

$$\begin{aligned} Z_{B\#4}(s) &= \frac{L_2}{\sigma_{\text{eff}2} + \kappa_{\text{eff}2}} \frac{\kappa_{\text{eff}2}}{\sigma_{\text{eff}2}} \Gamma_{\text{II}2} - H_{\text{II}2} - H_{\text{II}2} \\ &\quad - \frac{L_1}{\sigma_{\text{eff}1} + \kappa_{\text{eff}1}} \frac{\kappa_{\text{eff}1}}{\sigma_{\text{eff}1}} B_{\text{III}1} + H_{\text{III}1} \end{aligned} \quad (74-4)$$

The coefficients in Eqs. (74-1) and (74-2) for $Z_{B\#1}(s)$ and $Z_{B\#2}(s)$ are given as

$$\Theta_{\text{II}1} = \frac{a_{s1} L_1^2}{\sigma_{\text{eff}1} z_{\text{int}1}} \left(1 + \frac{\sigma_{\text{eff}1}}{\kappa_{\text{eff}1}} \right) \quad (75-1)$$

$$\Theta_{\text{II}2} = \frac{a_{s2} L_2^2}{\sigma_{\text{eff}2} z_{\text{int}2}} \left(1 + \frac{\sigma_{\text{eff}2}}{\kappa_{\text{eff}2}} \right) \quad (75-2)$$

The coefficients in Eq. (74-4) for $Z_{B\#4}(s)$ are given as

$$H_{\text{II}1} = -\frac{L_1}{\kappa_{\text{eff}1} + \sigma_{\text{eff}1}} \quad (76-1)$$

$$H_{\text{II}1}(\Theta_{\text{II}1}) = -\frac{L_1}{\sigma_{\text{eff}1} + \kappa_{\text{eff}1}} \Gamma_{\text{II}1} - H_{\text{II}1} + \frac{L_3}{\kappa_{\text{eff}3}} \quad (76-2)$$

$$H_{\text{II}2} = -\frac{L_2}{\kappa_{\text{eff}2} + \sigma_{\text{eff}2}} \quad (76-3)$$

$$H_{\text{II}2}(\Theta_{\text{II}2}) = -\frac{L_2}{\sigma_{\text{eff}2} + \kappa_{\text{eff}2}} B_{\text{III}2} \quad (76-4)$$

$$\Gamma_{\text{II}1}(\Theta_{\text{II}1}) = B_{\text{III}1} \cosh(\sqrt{\Theta_{\text{II}1}}) + B_{\text{IV}1} \sinh(\sqrt{\Theta_{\text{II}1}}) \quad (76-5)$$

$$\Gamma_{\text{II}2}(\Theta_{\text{II}2}) = B_{\text{III}2} \cosh(\sqrt{\Theta_{\text{II}2}}) + B_{\text{IV}2} \sinh(\sqrt{\Theta_{\text{II}2}}) \quad (76-6)$$

where

$$B_{\text{III}1}(\Theta_{\text{II}1}) = -\frac{1}{\sqrt{\Theta_{\text{II}1}} \sinh(\sqrt{\Theta_{\text{II}1}})} \left[\cosh(\sqrt{\Theta_{\text{II}1}}) + \frac{\sigma_{\text{eff}1}}{\kappa_{\text{eff}1}} \right] \quad (77-1)$$

$$B_{\text{IV}1}(\Theta_{\text{II}1}) = \frac{1}{\sqrt{\Theta_{\text{II}1}}} \quad (77-2)$$

$$B_{\text{III}2}(\Theta_{\text{II}2}) = \frac{1}{\sqrt{\Theta_{\text{II}2}} \sinh(\sqrt{\Theta_{\text{II}2}})} \left[\frac{\sigma_{\text{eff}2}}{\kappa_{\text{eff}2}} \cosh(\sqrt{\Theta_{\text{II}2}}) + 1 \right] \quad (77-3)$$

$$B_{\text{IV}2}(\Theta_{\text{II}2}) = -\frac{1}{\sqrt{\Theta_{\text{II}2}}} \frac{\sigma_{\text{eff}2}}{\kappa_{\text{eff}2}} \quad (77-4)$$

In addition, Model B can be degenerated into Model E under the condition of Scene IV. The detailed degeneration from Model A to Model B and from Model B to Model E please refers to [Supporting Information](#). A detailed discussion for Mode D please refers to References [45,46,124].

2.2.3. Degeneration from Model B to Model C & F

When $\sigma_{\text{eff}} \rightarrow \infty$, i.e. under the condition of Scene III, Model B can be degenerated into Model C. Thus, Model C can be directly obtained by letting $\sigma_{\text{eff}} \rightarrow \infty$ in Eqs. (74-1)–(74-4)

$$Z_{C\#1}(s) = \frac{L_1}{\kappa_{\text{eff}1}} \frac{\coth(\sqrt{\Theta_{\text{II}1}})}{\sqrt{\Theta_{\text{II}1}}} \quad (78-1)$$

$$Z_{C\#2}(s) = \frac{L_2}{\kappa_{\text{eff}2}} \frac{\coth(\sqrt{\Theta_{\text{II}2}})}{\sqrt{\Theta_{\text{II}2}}} \quad (78-2)$$

$$Z_{C\#3}(s) = \frac{L_3}{\kappa_{\text{eff}3}} \quad (78-3)$$

$$Z_{C\#4}(s) = -H_{\text{II}2} + H_{\text{II}1} \quad (78-4)$$

The coefficients in Eqs. (78-1) and (78-2) for $Z_{C\#1}(s)$ and $Z_{C\#2}(s)$ are given as

$$\Theta_{\text{II}1} = \frac{a_{s1} L_1^2}{\kappa_{\text{eff}1} z_{\text{int}1}} \quad (79-1)$$

$$\Theta_{\text{II}2} = \frac{a_{s2} L_2^2}{\kappa_{\text{eff}2} z_{\text{int}2}} \quad (79-2)$$

The coefficients in Eq. (78-4) for $Z_{C\#4}(s)$ are given as

$$H_{\text{II}1}(\Theta_{\text{II}1}) = -\frac{L_1}{\kappa_{\text{eff}1}} \Gamma_{\text{II}1} + \frac{L_3}{\kappa_{\text{eff}3}} \quad (80-1)$$

$$H_{\text{II}2}(\Theta_{\text{II}2}) = -\frac{L_2}{\kappa_{\text{eff}2}} B_{\text{III}2} \quad (80-2)$$

where

$$\Gamma_{\text{II}1}(\Theta_{\text{II}1}) = -\frac{1}{\sqrt{\Theta_{\text{II}1}} \tanh(\sqrt{\Theta_{\text{II}1}})} \quad (81-1)$$

$$B_{\text{III}2}(\Theta_{\text{II}2}) = \frac{1}{\sqrt{\Theta_{\text{II}2}} \tanh(\sqrt{\Theta_{\text{II}2}})} \quad (81-2)$$

In addition, Model C can be degenerated into Model F under the condition of Scene IV. The detailed degeneration from Model B to Model C and from Model C to Model F please refers to [Supporting Information](#). A detailed discussion for Mode F please refers to References [42,43].

[Fig. 4](#) shows that the DFN-like impedance models are unified under different physical scenes of Sences I–IV for LIBs.

Based on the unified impedance model, the solid/electrolyte/full diffusion impedance $Z_{\text{Ds}1}/Z_{\text{De}1}/Z_{\text{D}1}$ for the negative electrode in the low frequency region can be estimated as [125]

$$Z_{\text{Ds}1}(s) \stackrel{\text{def}}{=} Z_{B\#1}(s) - Z_{E\#1}(s) \quad (82-1)$$

$$Z_{\text{De}1}(s) \stackrel{\text{def}}{=} Z_1(s) - Z_{B\#1}(s) \quad (82-2)$$

$$Z_{\text{D}1}(s) \stackrel{\text{def}}{=} Z_{\text{Ds}1}(s) + Z_{\text{De}1}(s) = Z_1(s) - Z_{E\#1}(s) \quad (82-3)$$

Taking the negative electrode as an example, [Fig. 5\(a\)](#) shows Nyquist plots of Model DFN and Models A–F, and [Fig. 5\(b\)](#) shows the solid/electrolyte/full diffusion impedance. It is easy to understand how does the physical scene affects charge transfer reactions with impedance characteristics. In addition, the impedance spectra can also be interpreted with ECMs as shown in [Fig. 5\(c or d\)](#).

The above summarizes the discrepancies between the DFN-like impedance models under different physical scenes. There also exists a discrepancy between the DFN-like impedance models from the TLM. Recently, Moškon et al. [126,127] proposed the 3D TLM to simulate the actual network for the porous electrode, which could capture transport/reaction steps similar to the DFN-like impedance models. Compared to the conventional TLM, the current TLM mainly involves three points [126–128]: (i) the charged species diffusion in the pore electrolyte; (ii) the species diffusion in the active particle; (iii) both the solid diffusion and electrolyte diffusion being directly coupled to the charge transfer reaction. The correlation between the updated TLM and the DFN-like impedance models will be discussed in our next work.

2.3. EIS-Toolbox@LIB based on the unified impedance model

This section introduces EIS-Toolbox@LIB based on the unified impedance model under different physical scenes.

2.3.1. What can EIS-Toolbox@LIB do?

EIS-Toolbox@LIB can be used to calculate the core variables for LIBs, such as electrolyte concentration c_e , electrolyte potential ϕ_e , solid phase concentration c_s , solid phase potential ϕ_s , and the flux j transferred between the electrolyte and the solid phase. Furthermore, EIS-Toolbox@LIB can be used to calculate impedance spectra at multiple scales for LIBs under different physical scenes. These results have been summarized in Table 2.

2.3.2. How is EIS-Toolbox@LIB implemented?

The EIS-Toolbox@LIB toolbox is developed in Matlab and is freely available for download in [Supporting Information](#). In the present work, graphite is chosen as the negative electrode and

LiCoO_2 as the positive electrode, respectively. All default parameter values required by EIS-Toolbox@LIB simulation are listed in Table 3.

Actually, some of these parameters, such as $D_{s1}, D_{s2}, k_1, k_2, D_e, \kappa$, and ρ_{sei} are closely independent of the operating temperature via the Arrhenius equation $\alpha = \alpha_0 \times \exp[-E_a/R \times (1/T - 1/T_0)]$ [69,129,130]. Herein, α represents the temperature dependent parameter, E_a is the activation energy, and α_0 is the value at the reference temperature T_0 and its default value is listed in Table 3. In addition, the open circuit potentials of the negative and positive electrodes at different temperatures are $U_{ocp1} = U_{ocp1,0} + (T - T_0)(\partial U_{ocp1}/\partial T)|_{T_0}$ and $U_{ocp2} = U_{ocp2,0} + (T - T_0)(\partial U_{ocp2}/\partial T)|_{T_0}$, respectively. Unless otherwise specified, $T = T_0$ is used for the present simulation.

In addition, D_e and κ of the binary electrolyte are related via the Nernst-Einstein equation $D_e = 2RT/(F^2 c_{e,0}) \times (1 + d\ln f_\pm/d\ln c_e) \times t_+^0(1 - t_+^0) \times \kappa$ [73]. For

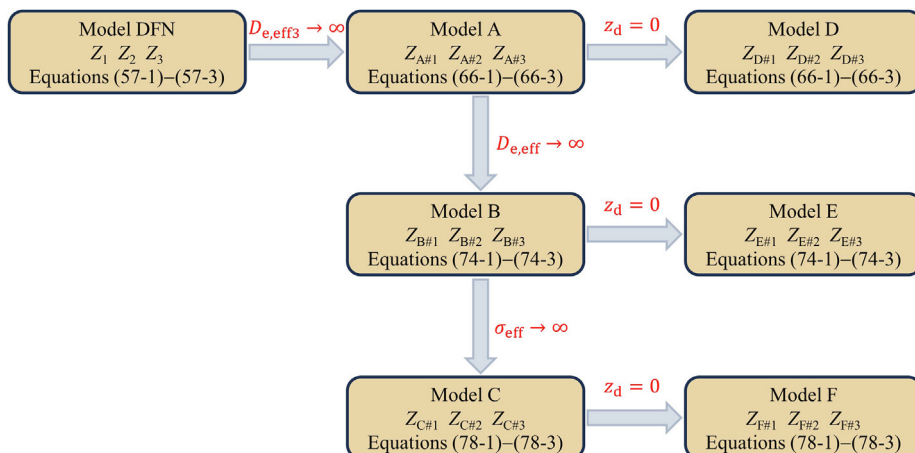


Fig. 4. The DFN-like impedance models are unified under different physical scenes for LIBs.

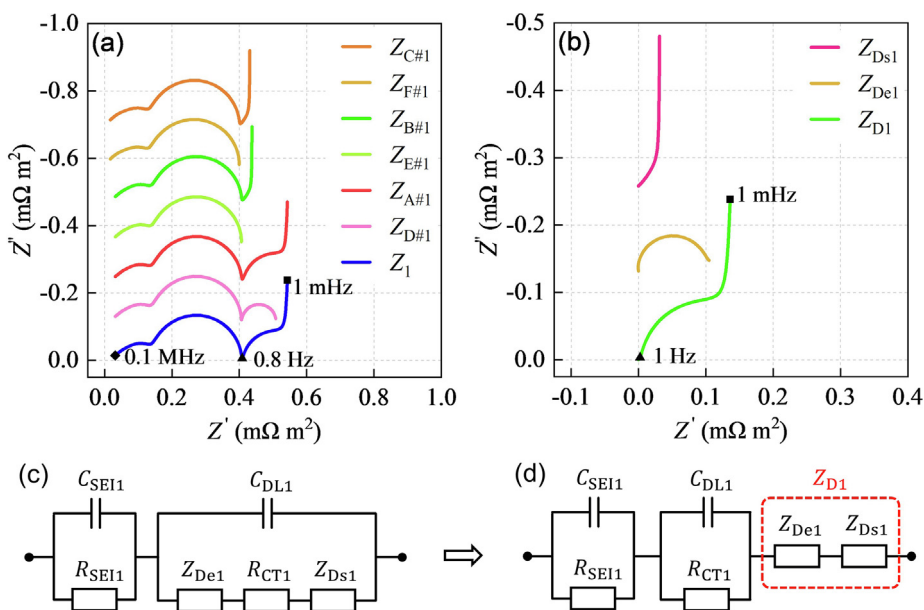


Fig. 5. Nyquist plots and equivalent circuits of the DFN-like impedance models for the negative electrode. (a) Nyquist plots of Model DFN and Models A–F. (b) Nyquist plots of the solid/electrolyte/full diffusion impedance. (c) Equivalent circuit of the Model DFN. (d) Simplification of the circuit model in (c). If necessary, the simulated impedance spectra shift along the imaginary axis in order to avoid Nyquist plots overlapping.

simplifying simulation in the present work, D_e , κ , and t_+^0 will not satisfy the Nernst-Einstein relation when D_e and T change.

In detail, EIS-Toolbox@LIB mainly consists of 11 sub-functions, i.e., EIS.m, Extract_Re_Im.m, Model_A_D_calculate.m, Model_B_E_-calculate.m, Model_C_F_calculate.m, Model_DFN_calculate.m, Model_Diffusion_calculate.m, Model_Particle_calculate.m, Parameter_initialize.m, Parameter_update.m, and Sensitivity_calculate.m. For the detailed definition and implementation please refer to [Supporting Information](#). With these sub-functions in EIS-Toolbox@LIB, it is convenient for researchers to analyze the competitive mechanisms of charge transfer reactions in LIBs with respect to parameters of the active particle, the electrode/separator matrix,

Table 2
EIS-Toolbox@LIB based on the unified impedance model.

Calculation	Description
Z_1, Z_2, Z_3	Model DFN has no extra simplifications
Z_d, Z_F, Z_{int}	The single particle model has three scales
$Z_{A\#1}, Z_{A\#2}, Z_{A\#3}$	Model A ignores the diffusion impedance of the pore electrolyte in the separator based on Model DFN
$Z_{B\#1}, Z_{B\#2}, Z_{B\#3}$	Model B ignores the diffusion impedance of the pore electrolyte in the electrode based on Model A
$Z_{C\#1}, Z_{C\#2}, Z_{C\#3}$	Model C ignores the electronic resistance of the solid phase in the electrode based on Model B
$Z_{D\#1}, Z_{D\#2}, Z_{D\#3}$	Model D ignores the diffusion impedance of the solid phase in the electrode based on Model A
$Z_{E\#1}, Z_{E\#2}, Z_{E\#3}$	Model E ignores the diffusion impedance of the solid phase in the electrode based on Model B
$Z_{F\#1}, Z_{F\#2}, Z_{F\#3}$	Model F ignores the diffusion impedance of the solid phase in the electrode based on Model C
Z_{Ds}, Z_{De}	The solid and electrolyte diffusion impedance

Table 3
Default parameters and $SOC_0 = 100\%$ used for the present simulation [129,130].

Type	Active particle	Electrode matrix	Separator/electrolyte
Geometry	$r_{s1} = 2 \times 10^{-6} \text{ m}$ $r_{s2} = 2 \times 10^{-6} \text{ m}$	$\epsilon_{e1} = 0.485; \epsilon_{e2} = 0.385$ $\epsilon_{s1} = 0.4824; \epsilon_{s2} = 0.59$ $\epsilon_{f1} = 0.0326; \epsilon_{f2} = 0.025$ $L_1 = 88 \times 10^{-6} \text{ m}$ $L_2 = 80 \times 10^{-6} \text{ m}$ $C_{dl1} = 0.1 \text{ F m}^{-2}$ $C_{dl2} = 0.1 \text{ F m}^{-2}$	$\epsilon_{e3} = 0.724$ $L_3 = 25 \times 10^{-6} \text{ m}$ $c_{e,0} = 1000 \text{ mol m}^{-3}$
Kinetics	$k_{1,0} = 5.031 \times 10^{-11} \text{ mol}/(\text{m}^2 \text{ s})/(\text{mol}/\text{m}^3)^{1+\alpha a1}$ $k_{2,0} = 2.334 \times 10^{-11} \text{ mol}/(\text{m}^2 \text{ s})/(\text{mol}/\text{m}^3)^{1+\alpha a2}$ $E_{k1} = 39.57 \times 10^3 \text{ J mol}^{-1}; E_{k2} = 37.48 \times 10^3 \text{ J mol}^{-1}$ $\delta_{sei1} = 0.04 \times 10^{-6} \text{ m}; \rho_{sei1,0} = 1.40 \times 10^5 \Omega \text{ m}$ $E_{psei1} = 33.26 \times 10^3 \text{ J mol}^{-1}; \epsilon_{sei1} = 3.92 \times 10^{-10} \text{ F m}^{-1}$ $R_{sei2} = 0 \Omega \text{ m}^2; C_{sei2} = 0 \text{ F m}^{-2}$		
Transport	$D_{s1,0} = 1.2 \times 10^{-14} \text{ m}^2 \text{ s}^{-1}$ $D_{s2,0} = 1.0 \times 10^{-14} \text{ m}^2 \text{ s}^{-1}$ $E_{Ds1} = 42.77 \times 10^3 \text{ J mol}^{-1}$ $E_{Ds2} = 18.55 \times 10^3 \text{ J mol}^{-1}$	$\alpha_{a1} = \alpha_{a2} = 0.5$ $\alpha_{c1} = \alpha_{c2} = 0.5$ $brug_1 = brug_2 = 1.5$ $\sigma_1 = 10 \text{ S m}^{-1}$ $\sigma_2 = 3.8 \text{ S m}^{-1}$	$brug_3 = 1.5; \kappa_0 = 1.20 \text{ S m}^{-1}$ $D_{e,0} = 3.22 \times 10^{-10} \text{ m}^2 \text{ s}^{-1}$ $\partial f_e / \partial \ln c_e = 1.13; t_+^0 = 0.38$ $E_K = 34.70 \times 10^3 \text{ J mol}^{-1}$ $E_{De} = 37.04 \times 10^3 \text{ J mol}^{-1}$
Thermo-dynamics	$\theta_{1,100\%} = 0.85510; \theta_{2,100\%} = 0.49950$ $\theta_{1,0\%} = 0.01429; \theta_{2,0\%} = 0.99174$ $c_{s1,max} = 30555 \text{ mol m}^{-3}; c_{s2,max} = 51554 \text{ mol m}^{-3}$ $F = 96487 \text{ C mol}^{-1}; R = 8.314 \text{ J mol}^{-1} \text{ K}^{-1}; T_0 = 298.15 \text{ K}$		
Constant	For the negative electrode, the open-circuit potential is defined as $U_{ocp1,0} = 0.7222 + 0.1387\theta_1 + 0.0290\theta_1^{0.5} - \frac{0.0172}{\theta_1} + \frac{0.0019}{\theta_1^{0.5}} + 0.2808\exp(0.90-150\theta_1) - 0.7984\exp(0.4465\theta_1-0.4108)$ The entropy change of the negative electrode is $\left. \frac{\partial U_{ocp1}}{\partial T} \right _{T_0} = \frac{0.001 \left(0.005269056 + 3.299265709\theta_1 - 91.79325798\theta_1^2 + 1004.911008\theta_1^3 - 5812.278127\theta_1^4 \right.}{1 - 48.09287227\theta_1 + 1017.234804\theta_1^2 - 10481.80419\theta_1^3 + 59431.3\theta_1^4} \\ \left. + 19329.7549\theta_1^5 - 37147.8947\theta_1^6 + 38379.18127\theta_1^7 - 16515.05308\theta_1^8 \right) \\ - 195881.6488\theta_1^9 + 374577.3152\theta_1^6 - 385821.1607\theta_1^7 + 165705.8597\theta_1^8$ For the positive electrode, the open-circuit potential is defined as $U_{ocp2,0} = -4.656 + 88.669\theta_2^2 - 401.119\theta_2^4 + 342.909\theta_2^6 - 462.471\theta_2^8 + 433.434\theta_2^{10}$ The entropy change of the positive electrode is $\left. \frac{\partial U_{ocp2}}{\partial T} \right _{T_0} = -0.001 \left(\frac{0.199521039 - 0.928373822\theta_2 + 1.364550689000000\theta_2^2 - 0.611544893999998\theta_2^3}{1 - 5.661479886999997\theta_2 + 11.47636191\theta_2^2 - 9.82431213599998\theta_2^3 + 3.048755063\theta_2^4} \right)$ where $\theta_1 = c_{s1}/c_{s1,max}$ and $\theta_2 = c_{s2}/c_{s2,max}$		

the pore electrolyte, and the operating temperature under different physical scenes.

3. Unveil the competitive mechanisms of charge transfer reactions in LIBs

In the present work, charge transfer reactions collectively refer to charge transport through the SEI film, mass diffusion/charge conductance in the solid/electrolyte bulk, and charge transfer reaction at the solid/electrolyte interface. This section aims at revealing the competitive mechanisms of charge transfer reactions, based on the unified impedance model under different physical scenes for LIBs.

For example, it is inevitable that battery capacitance decreases and internal resistance increases after cyclic aging [131]. In order to reveal the aging mechanisms, such as SEI layer growth, lithium plating, particle fracture, and loss of active material, two questions need to be answered: one is what you need to know [132], and the other is how to model the aging [133]. As known, charge transfer reactions are directly related to energy density, cycling life, charging rate, and operating safety for LIBs. As a result, EIS plays a critical role in revealing the competitive mechanisms of charge transfer reactions after cyclic aging [98,134,135], especially in identifying the aging mechanisms [136,137].

3.1. Fundamentals of the unified impedance model for LIBs

3.1.1. Typical characteristics of the unified impedance model

Firstly, different contributions to the impedance for LIBs can be summarized [138–141] as follows: (i) the ohmic resistance is

attributed to the ionic migration in the pore electrolyte, the electronic conductance across the active material, and the contact between the current collector and the electrode. (ii) the interfacial resistance is attributed to the charge transfer reaction at the interface of solid/electrolyte and the migration through the SEI film. (iii) the diffusion impedance is attributed to the charge diffusion in the pore electrolyte and active particle material.

Based on the unified impedance model derived in Section 2, Fig. 6 shows Nyquist plots of Model DFN and Models A–C as well

as Bode plots of solid/electrolyte diffusion impedance for the negative electrode, the positive electrode, the separator, and the full cell, respectively. Herein, R_{DS1}/Z_{DS1} denotes the solid-state diffusion resistance/impedance, respectively, which are scaled up from the component z_{d1} of the single particle, as shown in Fig. 2(d); R_{De1}/Z_{De1} denotes the diffusion resistance/impedance in the pore electrolyte, respectively; R_{CT1} denotes the charge transfer resistance, which is scaled up from R_{ct1} at the interface of the single particle and the sei film; R_{SEI1} denotes the migration resistance through

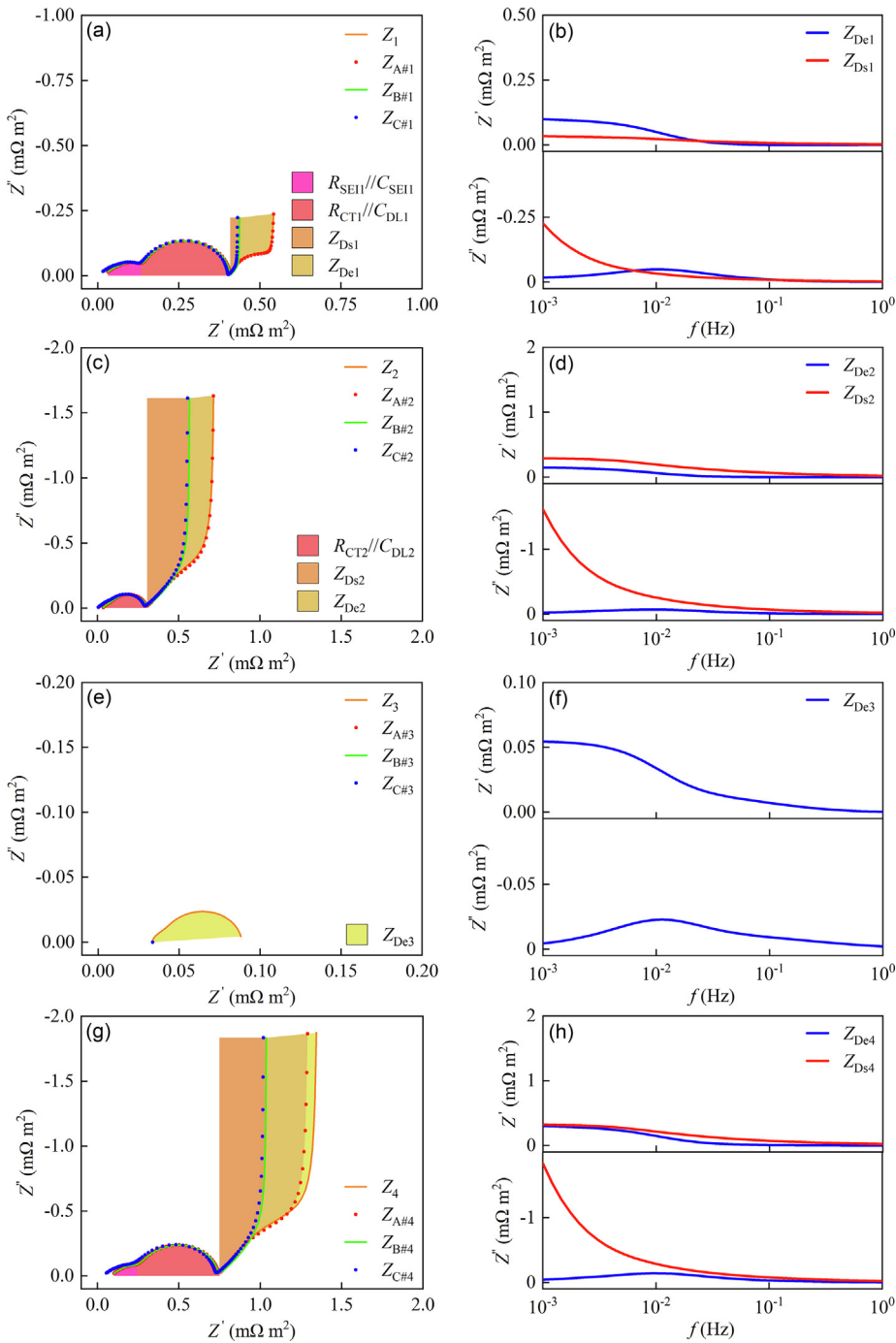


Fig. 6. Typical characteristics of the unified impedance model for LIBs. Nyquist plots for Model DFN and Models A–C in (a, c, e, and g). Bode plots for the solid/electrolyte diffusion impedance in (b, d, f, and h), corresponding to the negative electrode, the positive electrode, the separator, and the full cell, respectively. Default parameters for simulation are listed in Table 3.

the SEI film, which is scaled up from $R_{\text{sei}1}$ at the sei film of the single particle.

Fig. 6 shows the impedance characteristics of the unified impedance model. The impedance characteristics can be concluded as follows:

- (i) There is no obvious difference between Z_1/Z_2 for Model DFN and $Z_{\text{A}\#1}/Z_{\text{A}\#2}$ for Model A except at the transition region, suggesting Li⁺ concentration gradient in the separator has weakly effect on the porous electrode.

(ii) The diffusion impedance $Z_{\text{De}3}$ in the pore electrolyte of the separator is not much but very significant because it makes EIS analysis more complicated [142–144]. In addition, $Z_{\text{A}\#3}$ for Model A is the same as both $Z_{\text{B}\#3}$ for Model B and $Z_{\text{C}\#3}$ for Model C in the separator.

- (iii) The solid/electrolyte diffusion impedance can be approximately calculated based on the unified impedance model [125]. Moreover, $Z_{\text{Ds}1}/Z_{\text{Ds}2}$ and $Z_{\text{De}1}/Z_{\text{De}2}/Z_{\text{De}3}$ can be roughly emulated by finite length Warburg elements under transmissive and reflective BCs [58,145], respectively.

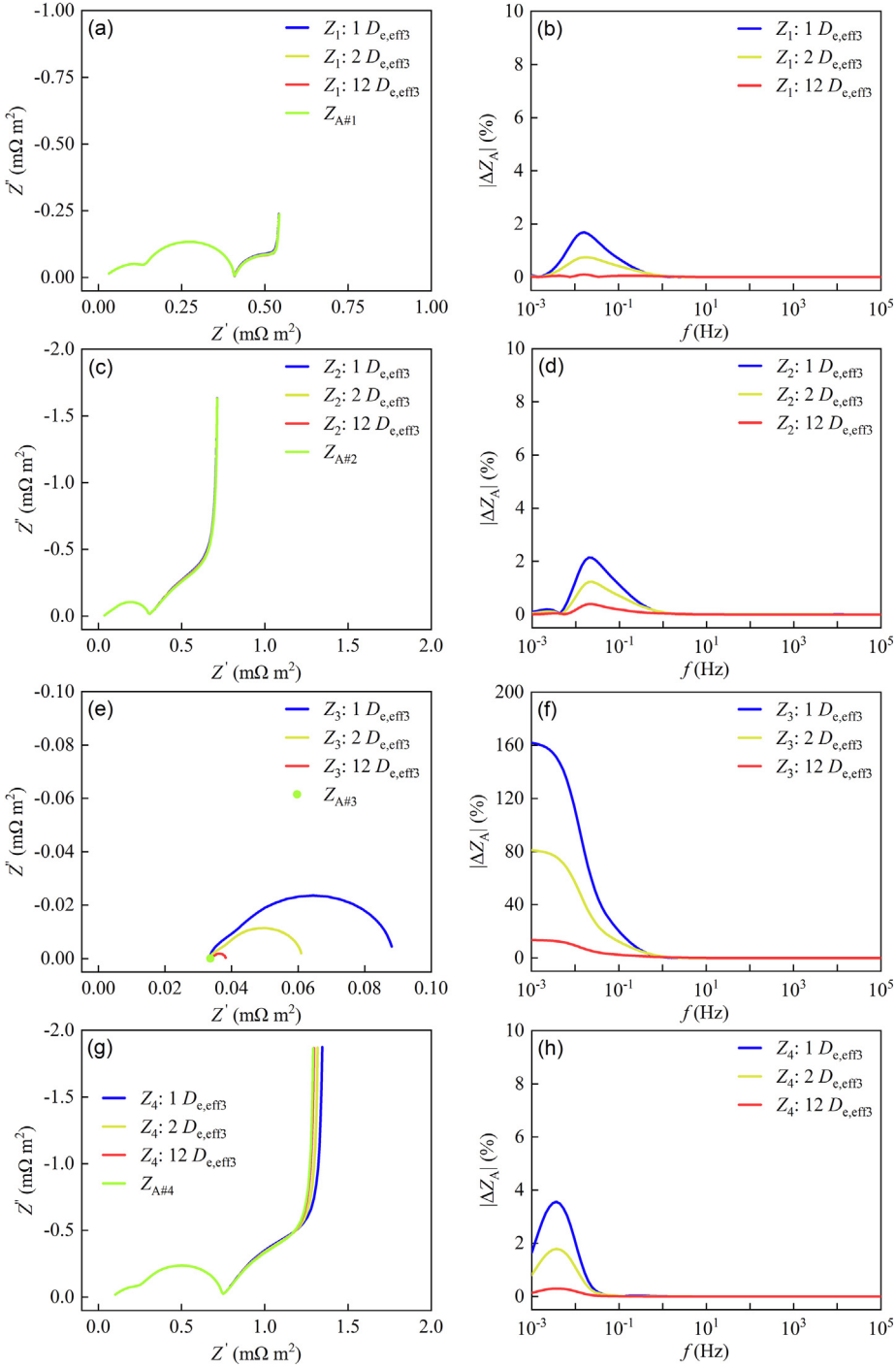


Fig. 7. Degeneration and relative differences for Model DFN toward Model A with increasing $D_{\text{eff}3}$ in the separator. (a, b) The negative electrode. (c, d) The positive electrode. (e, f) The separator. (g, h) The full cell. Default parameters for simulation are listed in Table 3.

The finite length Warburg impedance element under reflective and transmissive BCs are defined as following [146], respectively:

$$Z_{W0}(s) = R_{W0} \frac{\coth(\sqrt{s\tau_{W0}})}{\sqrt{s\tau_{W0}}} \quad (83-1)$$

$$R_{W0} = \frac{RT\delta_s}{z^2 F^2 c_{s,0} D_s} \quad (83-2)$$

$$\tau_{W0} = \frac{\delta_s^2}{D_s} \quad (83-3)$$

$$Z_{Ws}(s) = R_{Ws} \frac{\tanh(\sqrt{s\tau_{Ws}})}{\sqrt{s\tau_{Ws}}} \quad (84-1)$$

$$R_{Ws} = \frac{RT\delta_e}{z^2 F^2 c_{e,0} D_e} \quad (84-2)$$

$$\tau_{Ws} = \frac{\delta_e^2}{D_e} \quad (84-3)$$

where τ_{W0}/τ_{Ws} and δ_s/δ_e are the characteristic time constant and equivalent path length of solid/electrolyte diffusion impedance in the porous electrode, respectively.

3.1.2. Limiting situations of the unified impedance model

Below are two kinds of limiting situations which will be discussed for the unified impedance model. One is under different physical scenes, and the other is at high and low frequencies.

(1) Limiting situations under different physical scenes

Section 2.2 defines four different physical scenes, i.e., Scenes I, II, III, and IV, under which seven kinds of impedance models, i.e., the DFN-like impedance models, are theoretically unified for LIBs. The below shows a quantitative numerical calculation, which will be conducted to demonstrate the unified impedance model with emphasis on Model DFN and Models A–C for LIBs.

Fig. 7 shows the degeneration and relative differences for Model DFN toward Model A with increasing $D_{e,eff}$ in the separator. Below, $|\Delta Z_{A\#n}| \stackrel{\text{def}}{=} |(Z_n - Z_{A\#n})/Z_{A\#n}| \times 100\%$, $n = 1, 2, 3, 4$, and conclusions can be made:

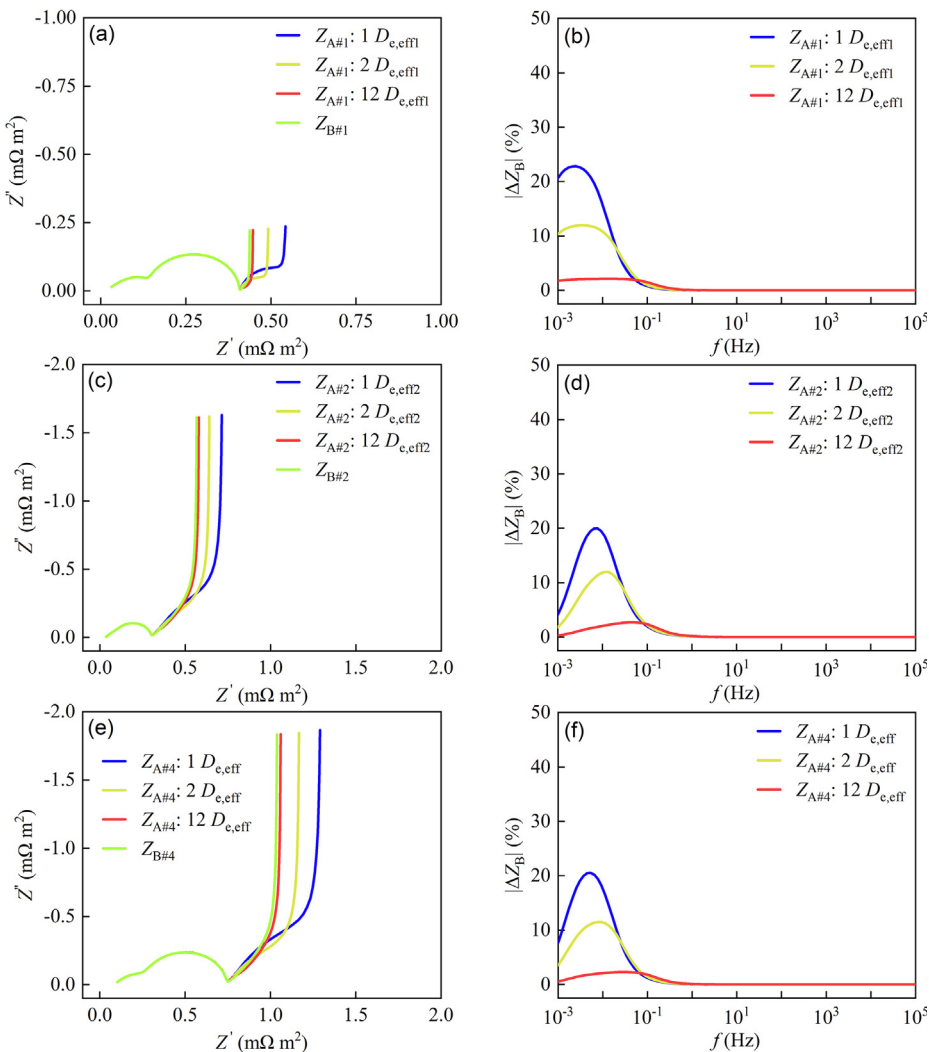


Fig. 8. Degeneration and relative differences for Model A toward Model B with increasing $D_{e,eff}$ in the whole electrode. (a, b) The negative electrode. (c, d) The positive electrode. (e, f) The full cell. Default parameters for simulation are listed in Table 3.

- (i) As $D_{e,\text{eff}3}$ increases to 2 times, Z_1 and Z_2 almost keep constant. In detail, the maximum relative difference in the electrode impedance for Model DFN toward Model A is 1.2%, meaning that the coupling effect between the electrode and the separator is not so strong.
- (ii) As $D_{e,\text{eff}3}$ increases to 12 times, Z_3 sharply decreases. In detail, the maximum relative difference in the separator impedance for Model DFN toward Model A decreases from 162% to 13%. This difference will also be transferred to Z_4 .
- (iii) In engineering, if $D_{e,\text{eff}3} > 10 \times D_{e,T3}$ and $D_{e,T3} \stackrel{\text{def}}{=} -\kappa_{D,\text{eff}3}/(c_{e,0}F)$ holds, Model DFN can be degenerated into Model A for LIBs. In this case, Z_3 is degenerated into a pure resistance, and Model DFN can be regarded as the equivalent to Model A.

Fig. 8 shows the degeneration and relative differences for Model A toward Model B with increasing $D_{e,\text{eff}}$ in the electrode. Herein, $|\Delta Z_{B\#n}| \% \stackrel{\text{def}}{=} |(Z_{A\#n} - Z_{B\#n})/Z_{B\#n}| \times 100\%$, $n = 1, 2, 4$, and conclusions can be made:

- (i) As $D_{e,\text{eff}}$ increases to 2 times, $Z_{A\#1}$ and $Z_{A\#2}$ at low frequencies gradually decrease, however, it keeps almost constant at middle/high frequencies. This evolution trend demonstrates that the electrolyte diffusion impedance mainly spans the low frequency region.
- (ii) As $D_{e,\text{eff}}$ increases to 12 times, the maximum relative difference in the electrode impedance for Model A toward Model B decreases from 23% to 2.7%, meaning that Z_{De1}/Z_{De2} does not dominate the electrode polarization, which is different from the separator.
- (iii) In engineering, if $D_{e,\text{eff}} > 10 \times D_{e,T}$ and $D_{e,T} \stackrel{\text{def}}{=} -\kappa_{D,\text{eff}}/(c_{e,0}F)$ holds, Model A can be degenerated into Model B for LIBs. In this case, the electrolyte diffusion impedance in the electrode is approximately zero, and Model A can be regarded as the equivalent to Model B.

Fig. 9 shows the degeneration and relative differences for Model B toward Model C with increasing σ_{eff} in the electrode. Herein, $|\Delta Z_{C\#n}| \% \stackrel{\text{def}}{=} |(Z_{B\#n} - Z_{C\#n})/Z_{C\#n}| \times 100\%$, $n = 1, 2, 4$, and conclusions can be made

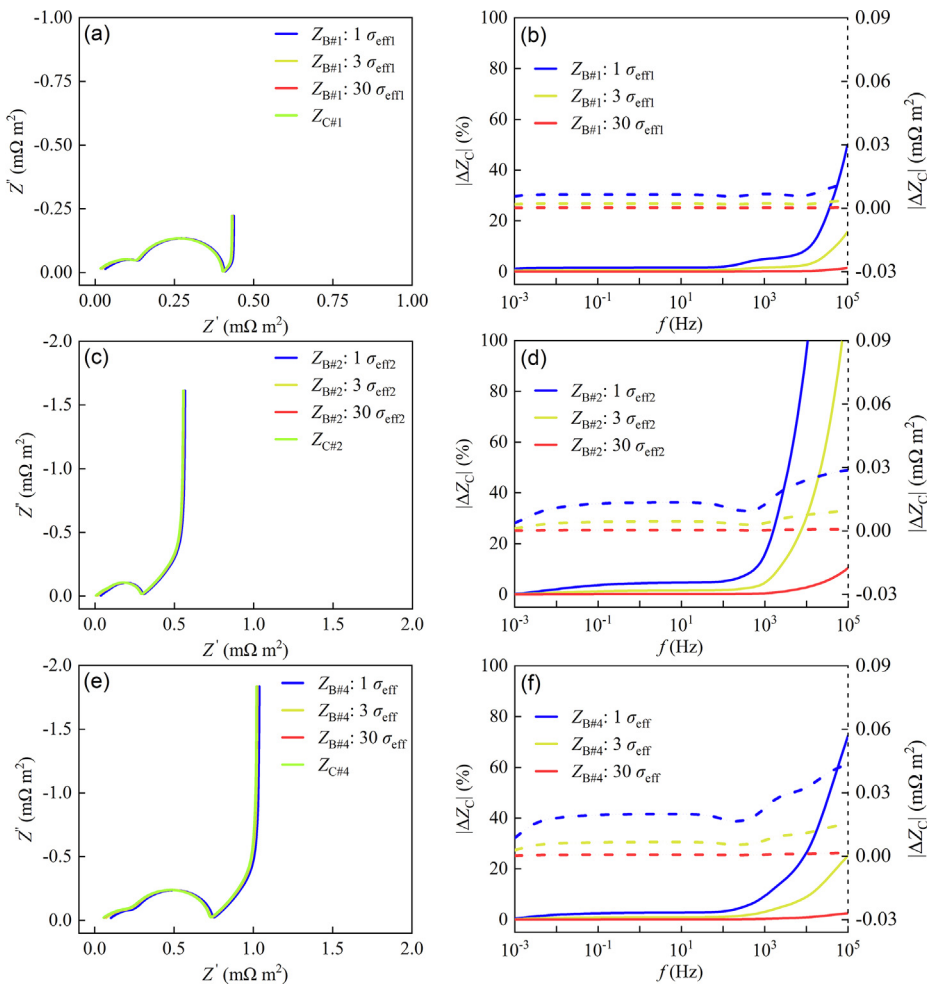


Fig. 9. Degeneration and relative differences for Model B toward Model C with increasing σ_{eff} in the whole electrode. (a, b) The negative electrode. (c, d) The positive electrode. (e, f) The full cell. Default parameters for simulation are listed in [Table 3](#).

- (i) As σ_{eff} increases to 3 times, $Z_{B\#1}$ and $Z_{B\#2}$ decrease over the whole frequency range, however, the decrease at high frequencies is slightly bigger than at low frequencies. This evolution trend demonstrates that the Nyquist plot roughly shifts toward the left with increasing σ_{eff} .
- (ii) As σ_{eff} increases to 30 times, the maximum relative difference in the electrode impedance for Model B toward Model C decreases from 364% to 10%. The large relative difference at high frequencies is attributed to the low impedance value compared to that at low frequencies.
- (iii) In engineering, if $\sigma_{\text{eff}} > 10^2 - 10^3 \times \kappa_{\text{eff}}$ holds, Model B will be degenerated into Model C for LIBs. In this case, the electronic resistance in the active material might be ignored, and Model B can be regarded as the equivalent to Model C.

(2) Limiting situations at high and low frequencies

Frequency might be the most critical parameter during the EIS diagnosis. The below is the limiting situations of the unified impe-

dance model at high and low frequencies, which will be discussed [52,54] with emphasis on Model B and Model C for LIBs.

(I) At the high frequency limit

If $\omega \rightarrow \infty$, Eq. (23-3) will tend to

$$z_{\text{int}1}(j\omega)|_{\omega \rightarrow \infty} = \frac{1}{j\omega C_{\text{sei}1} + \frac{1}{R_{\text{sei}1} + j\omega C_{\text{dl}1}}} \quad (85-1)$$

If the sei film is ignored, Eq. (85-1) can be rewritten as

$$z_{\text{int}1}(j\omega)|_{\omega \rightarrow \infty} = \frac{1}{j\omega C_{\text{dl}1}} \quad (85-2)$$

In this situation, $z_{\text{int}1}(j\omega)$ exhibits a pure capacitance behavior.

If the electrolyte diffusion impedance in Model DFN is ignored, under the high frequency limiting condition, Eq. (74-1) will tend to

Table 4
Characteristic time constants (s) for LIBs under 12 different parameters.

Par	τ_{d1} (cal)	τ_{ds1} (fit)	τ_{de1} (fit)	τ_{de3} (fit)	τ_{ct1} (cal)	τ_{ct1} (fit)	τ_{sei1} (cal)	τ_{sei1} (fit)
0.6 D_{s1}	61.73	69.06	47.84	39.25	1.56×10^{-3}	1.61×10^{-3}	5.50×10^{-5}	3.24×10^{-5}
1.0 D_{s1}	37.04	43.57	47.84	39.25	1.56×10^{-3}	1.61×10^{-3}	5.50×10^{-5}	3.24×10^{-5}
1.8 D_{s1}	20.58	25.30	47.84	39.25	1.56×10^{-3}	1.61×10^{-3}	5.50×10^{-5}	3.24×10^{-5}
3.2 D_{s1}	11.57	14.77	47.84	39.25	1.56×10^{-3}	1.61×10^{-3}	5.50×10^{-5}	3.24×10^{-5}
1.0 r_{s1}	37.04	43.57	47.84	39.25	1.56×10^{-3}	1.61×10^{-3}	5.50×10^{-5}	3.24×10^{-5}
1.5 r_{s1}	83.33	95.16	47.63	39.25	1.56×10^{-3}	1.64×10^{-3}	5.50×10^{-5}	3.66×10^{-5}
2.0 r_{s1}	148.15	168.5	47.61	39.25	1.56×10^{-3}	1.66×10^{-3}	5.50×10^{-5}	3.99×10^{-5}
2.5 r_{s1}	231.48	258.9	47.61	39.25	1.56×10^{-3}	1.68×10^{-3}	5.50×10^{-5}	4.23×10^{-5}
0.6 k_1	37.04	43.46	47.41	39.25	2.59×10^{-3}	2.72×10^{-3}	5.50×10^{-5}	3.31×10^{-5}
1.0 k_1	37.04	43.57	47.84	39.25	1.56×10^{-3}	1.61×10^{-3}	5.50×10^{-5}	3.24×10^{-5}
1.8 k_1	37.04	43.88	48.98	39.25	8.65×10^{-4}	8.67×10^{-4}	5.50×10^{-5}	3.11×10^{-5}
3.2 k_1	37.04	44.45	50.73	39.25	4.86×10^{-4}	4.09×10^{-4}	5.50×10^{-5}	2.37×10^{-5}
0.5 ρ_{sei1}	37.04	43.57	48.14	39.25	1.56×10^{-3}	1.58×10^{-3}	2.75×10^{-5}	1.55×10^{-5}
1.0 ρ_{sei1}	37.04	43.57	47.84	39.25	1.56×10^{-3}	1.61×10^{-3}	5.50×10^{-5}	3.24×10^{-5}
2.0 ρ_{sei1}	37.04	43.57	47.53	39.25	1.56×10^{-3}	1.60×10^{-3}	1.10×10^{-4}	7.46×10^{-5}
4.0 ρ_{sei1}	37.04	43.57	47.34	39.25	1.56×10^{-3}	1.48×10^{-3}	2.20×10^{-4}	1.49×10^{-4}
0.8 L_1	37.04	43.48	30.31	39.25	1.56×10^{-3}	1.65×10^{-3}	5.50×10^{-5}	3.70×10^{-5}
1.0 L_1	37.04	43.57	47.84	39.25	1.56×10^{-3}	1.61×10^{-3}	5.50×10^{-5}	3.24×10^{-5}
1.2 L_1	37.04	43.72	69.70	39.25	1.56×10^{-3}	1.57×10^{-3}	5.50×10^{-5}	2.99×10^{-5}
1.4 L_1	37.04	43.92	97.26	39.25	1.56×10^{-3}	1.53×10^{-3}	5.50×10^{-5}	2.87×10^{-5}
0.8 L_3	37.04	43.57	47.84	25.68	1.56×10^{-3}	1.61×10^{-3}	5.50×10^{-5}	3.24×10^{-5}
1.0 L_3	37.04	43.57	47.84	39.25	1.56×10^{-3}	1.61×10^{-3}	5.50×10^{-5}	3.24×10^{-5}
1.2 L_3	37.04	43.57	47.84	54.82	1.56×10^{-3}	1.61×10^{-3}	5.50×10^{-5}	3.24×10^{-5}
1.4 L_3	37.04	43.57	47.84	71.87	1.56×10^{-3}	1.61×10^{-3}	5.50×10^{-5}	3.24×10^{-5}
0.8 ε_{e1}	37.04	43.83	53.26	39.25	1.56×10^{-3}	1.54×10^{-3}	5.50×10^{-5}	2.82×10^{-5}
0.9 ε_{e1}	37.04	43.67	50.34	39.25	1.56×10^{-3}	1.58×10^{-3}	5.50×10^{-5}	2.99×10^{-5}
1.0 ε_{e1}	37.04	43.57	47.84	39.25	1.56×10^{-3}	1.61×10^{-3}	5.50×10^{-5}	3.24×10^{-5}
1.1 ε_{e1}	37.04	43.51	45.67	39.25	1.56×10^{-3}	1.64×10^{-3}	5.50×10^{-5}	3.55×10^{-5}
0.8 ε_{e3}	37.04	43.57	47.84	41.14	1.56×10^{-3}	1.61×10^{-3}	5.50×10^{-5}	3.24×10^{-5}
0.9 ε_{e3}	37.04	43.57	47.84	40.24	1.56×10^{-3}	1.61×10^{-3}	5.50×10^{-5}	3.24×10^{-5}
1.0 ε_{e3}	37.04	43.57	47.84	39.25	1.56×10^{-3}	1.61×10^{-3}	5.50×10^{-5}	3.24×10^{-5}
1.1 ε_{e3}	37.04	43.57	47.84	38.23	1.56×10^{-3}	1.61×10^{-3}	5.50×10^{-5}	3.24×10^{-5}
0.6 σ_1	37.04	43.57	47.84	39.25	1.56×10^{-3}	1.63×10^{-3}	5.50×10^{-5}	3.43×10^{-5}
1.0 σ_1	37.04	43.57	47.84	39.25	1.56×10^{-3}	1.61×10^{-3}	5.50×10^{-5}	3.24×10^{-5}
1.8 σ_1	37.04	43.57	47.84	39.25	1.56×10^{-3}	1.60×10^{-3}	5.50×10^{-5}	3.10×10^{-5}
3.2 σ_1	37.04	43.57	47.84	39.25	1.56×10^{-3}	1.59×10^{-3}	5.50×10^{-5}	3.01×10^{-5}
0.6 D_e	37.04	43.57	80.20	64.83	1.56×10^{-3}	1.61×10^{-3}	5.50×10^{-5}	3.24×10^{-5}
1.0 D_e	37.04	43.57	47.84	39.25	1.56×10^{-3}	1.61×10^{-3}	5.50×10^{-5}	3.24×10^{-5}
1.8 D_e	37.04	43.57	26.69	21.73	1.56×10^{-3}	1.61×10^{-3}	5.50×10^{-5}	3.24×10^{-5}
3.2 D_e	37.04	43.57	14.96	12.14	1.56×10^{-3}	1.61×10^{-3}	5.50×10^{-5}	3.24×10^{-5}
0.7 κ	37.04	43.57	69.63	54.24	1.56×10^{-3}	1.56×10^{-3}	5.50×10^{-5}	2.91×10^{-5}
1.0 κ	37.04	43.57	47.84	39.25	1.56×10^{-3}	1.61×10^{-3}	5.50×10^{-5}	3.24×10^{-5}
1.3 κ	37.04	43.57	36.69	30.69	1.56×10^{-3}	1.64×10^{-3}	5.50×10^{-5}	3.58×10^{-5}
1.6 κ	37.04	43.57	29.62	25.17	1.56×10^{-3}	1.66×10^{-3}	5.50×10^{-5}	3.87×10^{-5}
0.8 t_0^+	37.04	43.57	52.67	43.14	1.56×10^{-3}	1.61×10^{-3}	5.50×10^{-5}	3.24×10^{-5}
1.0 t_0^+	37.04	43.57	47.84	39.25	1.56×10^{-3}	1.61×10^{-3}	5.50×10^{-5}	3.24×10^{-5}
1.2 t_0^+	37.04	43.57	45.91	37.65	1.56×10^{-3}	1.61×10^{-3}	5.50×10^{-5}	3.24×10^{-5}
1.4 t_0^+	37.04	43.57	46.21	37.85	1.56×10^{-3}	1.61×10^{-3}	5.50×10^{-5}	3.24×10^{-5}

$$\begin{aligned} Z_{B\#1}(j\omega)|_{\omega \rightarrow \infty} &= \frac{L_1}{K_{\text{eff}1} + \sigma_{\text{eff}1}} \\ &+ \frac{\kappa_{\text{eff}1}^2 + \sigma_{\text{eff}1}^2}{(\kappa_{\text{eff}1} \sigma_{\text{eff}1})^{0.5} (\kappa_{\text{eff}1} + \sigma_{\text{eff}1})^{1.5}} \sqrt{\frac{z_{\text{int}1}(j\omega)|_{\omega \rightarrow \infty}}{a_{s1}}} \end{aligned} \quad (85-3)$$

Furthermore, if the electronic conductance resistance in the active material is further ignored, under the high frequency limiting condition, Eq. (78-1) will tend to

$$Z_{C\#1}(j\omega)|_{\omega \rightarrow \infty} = \sqrt{\frac{z_{\text{int}1}(j\omega)|_{\omega \rightarrow \infty}}{a_{s1} \kappa_{\text{eff}1}}} \quad (85-4)$$

In this situation, $Z_{B\#1}(j\omega)$ and $Z_{C\#1}(j\omega)$ exhibit a semi-infinite diffusion Warburg behavior.

(II) At the low frequency limit

Firstly, Taylor series expansion is introduced for tanh function

$$\tanh(x)|_{x \rightarrow 0} = x - \frac{x^3}{3} + \frac{2x^5}{15} \dots \quad (86-1)$$

Then, under the low frequency limiting condition, Eq. (18-2) can be expressed as [122]

$$\frac{1}{Y_{s1}(j\omega)|_{\omega \rightarrow 0}} = \frac{1}{5} + 3 \frac{D_{s1}}{j\omega r_{s1}^2} \quad (86-2)$$

Thus, when $\omega \rightarrow 0$, Eq. (23-3) will tend to

$$z_{\text{int}1}(j\omega)|_{\omega \rightarrow 0} = R_{ct1} + R_{sei1} + \frac{1}{5} R_{\text{diff}1} - \frac{3}{j\omega r_{s1} F} \frac{\partial U_{\text{ocp}1}}{\partial c_{ss1}}|_{c_{s1,0}} \quad (86-3)$$

Table 5
Polarization resistances ($\Omega \text{ m}^2$) for LIBs under 12 different parameters.

Par	R _{d1(cal)}	R _{Ds1(fit)}	R _{De1(fit)}	R _{De3(fit)}	R _{ct1(cal)}	R _{ct1(fit)}	R _{sei1(cal)}	R _{sei1(fit)}
0.6 D _{s1}	9.44×10^{-4}	1.01×10^{-4}	9.96×10^{-5}	5.21×10^{-5}	1.56×10^{-2}	2.67×10^{-4}	5.50×10^{-3}	9.09×10^{-5}
1.0 D _{s1}	5.66×10^{-4}	6.26×10^{-5}	9.96×10^{-5}	5.21×10^{-5}	1.56×10^{-2}	2.67×10^{-4}	5.50×10^{-3}	9.09×10^{-5}
1.8 D _{s1}	3.15×10^{-4}	3.60×10^{-5}	9.96×10^{-5}	5.21×10^{-5}	1.56×10^{-2}	2.67×10^{-4}	5.50×10^{-3}	9.09×10^{-5}
3.2 D _{s1}	1.77×10^{-4}	2.09×10^{-5}	9.96×10^{-5}	5.21×10^{-5}	1.56×10^{-2}	2.67×10^{-4}	5.50×10^{-3}	9.09×10^{-5}
1.0 r _{s1}	5.66×10^{-4}	6.26×10^{-5}	9.96×10^{-5}	5.21×10^{-5}	1.56×10^{-2}	2.67×10^{-4}	5.50×10^{-3}	9.09×10^{-5}
1.5 r _{s1}	8.49×10^{-4}	1.38×10^{-4}	1.02×10^{-4}	5.21×10^{-5}	1.56×10^{-2}	3.96×10^{-4}	5.50×10^{-3}	1.22×10^{-4}
2.0 r _{s1}	1.13×10^{-3}	2.42×10^{-4}	1.04×10^{-4}	5.21×10^{-5}	1.56×10^{-2}	5.26×10^{-4}	5.50×10^{-3}	1.54×10^{-4}
2.5 r _{s1}	1.42×10^{-3}	3.73×10^{-4}	1.06×10^{-4}	5.21×10^{-5}	1.56×10^{-2}	6.55×10^{-4}	5.50×10^{-3}	1.88×10^{-4}
0.6 k ₁	5.66×10^{-4}	6.23×10^{-5}	1.03×10^{-4}	5.21×10^{-5}	2.59×10^{-2}	4.28×10^{-4}	5.50×10^{-3}	9.21×10^{-5}
1.0 k ₁	5.66×10^{-4}	6.26×10^{-5}	9.96×10^{-5}	5.21×10^{-5}	1.56×10^{-2}	2.67×10^{-4}	5.50×10^{-3}	9.09×10^{-5}
1.8 k ₁	5.66×10^{-4}	6.33×10^{-5}	9.63×10^{-5}	5.21×10^{-5}	8.65×10^{-3}	1.61×10^{-4}	5.50×10^{-3}	8.87×10^{-5}
3.2 k ₁	5.66×10^{-4}	6.44×10^{-5}	9.38×10^{-5}	5.21×10^{-5}	4.86×10^{-3}	1.10×10^{-4}	5.50×10^{-3}	8.26×10^{-5}
0.5 ρ _{sei1}	5.66×10^{-4}	6.26×10^{-5}	9.85×10^{-5}	5.21×10^{-5}	1.56×10^{-2}	2.60×10^{-4}	2.75×10^{-3}	6.16×10^{-5}
1.0 ρ _{sei1}	5.66×10^{-4}	6.26×10^{-5}	9.96×10^{-5}	5.21×10^{-5}	1.56×10^{-2}	2.67×10^{-4}	5.50×10^{-3}	9.09×10^{-5}
2.0 ρ _{sei1}	5.66×10^{-4}	6.26×10^{-5}	1.01×10^{-4}	5.21×10^{-5}	1.56×10^{-2}	2.86×10^{-4}	1.10×10^{-2}	1.48×10^{-4}
4.0 ρ _{sei1}	5.66×10^{-4}	6.26×10^{-5}	1.04×10^{-4}	5.21×10^{-5}	1.56×10^{-2}	3.45×10^{-4}	2.20×10^{-2}	2.54×10^{-4}
0.8 L ₁	5.66×10^{-4}	7.79×10^{-5}	8.47×10^{-5}	5.21×10^{-5}	1.56×10^{-2}	3.30×10^{-4}	5.50×10^{-3}	1.00×10^{-4}
1.0 L ₁	5.66×10^{-4}	6.26×10^{-5}	9.96×10^{-5}	5.21×10^{-5}	1.56×10^{-2}	2.67×10^{-4}	5.50×10^{-3}	9.09×10^{-5}
1.2 L ₁	5.66×10^{-4}	5.26×10^{-5}	1.15×10^{-4}	5.21×10^{-5}	1.56×10^{-2}	2.27×10^{-4}	5.50×10^{-3}	8.74×10^{-5}
1.4 L ₁	5.66×10^{-4}	4.57×10^{-5}	1.26×10^{-4}	5.21×10^{-5}	1.56×10^{-2}	1.99×10^{-4}	5.50×10^{-3}	8.60×10^{-5}
0.8 L ₃	5.66×10^{-4}	6.26×10^{-5}	9.96×10^{-5}	4.25×10^{-5}	1.56×10^{-2}	2.67×10^{-4}	5.50×10^{-3}	9.09×10^{-5}
1.0 L ₃	5.66×10^{-4}	6.26×10^{-5}	9.96×10^{-5}	5.21×10^{-5}	1.56×10^{-2}	2.67×10^{-4}	5.50×10^{-3}	9.09×10^{-5}
1.2 L ₃	5.66×10^{-4}	6.26×10^{-5}	9.96×10^{-5}	6.13×10^{-5}	1.56×10^{-2}	2.67×10^{-4}	5.50×10^{-3}	9.09×10^{-5}
1.4 L ₃	5.66×10^{-4}	6.26×10^{-5}	9.96×10^{-5}	7.01×10^{-5}	1.56×10^{-2}	2.67×10^{-4}	5.50×10^{-3}	9.09×10^{-5}
0.8 ε _{e1}	5.66×10^{-4}	5.35×10^{-5}	1.29×10^{-4}	5.21×10^{-5}	1.56×10^{-2}	2.32×10^{-4}	5.50×10^{-3}	9.71×10^{-5}
0.9 ε _{e1}	5.66×10^{-4}	5.75×10^{-5}	1.13×10^{-4}	5.21×10^{-5}	1.56×10^{-2}	2.47×10^{-4}	5.50×10^{-3}	9.27×10^{-5}
1.0 ε _{e1}	5.66×10^{-4}	6.26×10^{-5}	9.96×10^{-5}	5.21×10^{-5}	1.56×10^{-2}	2.67×10^{-4}	5.50×10^{-3}	9.09×10^{-5}
1.1 ε _{e1}	5.66×10^{-4}	6.89×10^{-5}	8.89×10^{-5}	5.21×10^{-5}	1.56×10^{-2}	2.93×10^{-4}	5.50×10^{-3}	9.22×10^{-5}
0.8 ε _{e3}	5.66×10^{-4}	6.26×10^{-5}	9.96×10^{-5}	7.29×10^{-5}	1.56×10^{-2}	2.67×10^{-4}	5.50×10^{-3}	9.09×10^{-5}
0.9 ε _{e3}	5.66×10^{-4}	6.26×10^{-5}	9.96×10^{-5}	6.11×10^{-5}	1.56×10^{-2}	2.67×10^{-4}	5.50×10^{-3}	9.09×10^{-5}
1.0 ε _{e3}	5.66×10^{-4}	6.26×10^{-5}	9.96×10^{-5}	5.21×10^{-5}	1.56×10^{-2}	2.67×10^{-4}	5.50×10^{-3}	9.09×10^{-5}
1.1 ε _{e3}	5.66×10^{-4}	6.26×10^{-5}	9.96×10^{-5}	4.51×10^{-5}	1.56×10^{-2}	2.67×10^{-4}	5.50×10^{-3}	9.09×10^{-5}
0.6 σ ₁	5.66×10^{-4}	6.26×10^{-5}	9.96×10^{-5}	5.21×10^{-5}	1.56×10^{-2}	2.66×10^{-4}	5.50×10^{-3}	8.83×10^{-5}
1.0 σ ₁	5.66×10^{-4}	6.26×10^{-5}	9.96×10^{-5}	5.21×10^{-5}	1.56×10^{-2}	2.67×10^{-4}	5.50×10^{-3}	9.09×10^{-5}
1.8 σ ₁	5.66×10^{-4}	6.26×10^{-5}	9.96×10^{-5}	5.21×10^{-5}	1.56×10^{-2}	2.68×10^{-4}	5.50×10^{-3}	9.30×10^{-5}
3.2 σ ₁	5.66×10^{-4}	6.26×10^{-5}	9.96×10^{-5}	5.21×10^{-5}	1.56×10^{-2}	2.68×10^{-4}	5.50×10^{-3}	9.42×10^{-5}
0.6 D _e	5.66×10^{-4}	6.26×10^{-5}	1.60×10^{-4}	8.28×10^{-5}	1.56×10^{-2}	2.67×10^{-4}	5.50×10^{-3}	9.09×10^{-5}
1.0 D _e	5.66×10^{-4}	6.26×10^{-5}	9.96×10^{-5}	5.21×10^{-5}	1.56×10^{-2}	2.67×10^{-4}	5.50×10^{-3}	9.09×10^{-5}
1.8 D _e	5.66×10^{-4}	6.26×10^{-5}	5.82×10^{-5}	2.99×10^{-5}	1.56×10^{-2}	2.67×10^{-4}	5.50×10^{-3}	9.09×10^{-5}
3.2 D _e	5.66×10^{-4}	6.26×10^{-5}	3.24×10^{-5}	1.71×10^{-5}	1.56×10^{-2}	2.67×10^{-4}	5.50×10^{-3}	9.09×10^{-5}
0.7 κ	5.66×10^{-4}	6.26×10^{-5}	1.34×10^{-4}	7.30×10^{-5}	1.56×10^{-2}	2.72×10^{-4}	5.50×10^{-3}	1.07×10^{-4}
1.0 κ	5.66×10^{-4}	6.26×10^{-5}	9.96×10^{-5}	5.21×10^{-5}	1.56×10^{-2}	2.67×10^{-4}	5.50×10^{-3}	9.09×10^{-5}
1.3 κ	5.66×10^{-4}	6.26×10^{-5}	7.95×10^{-5}	4.06×10^{-5}	1.56×10^{-2}	2.65×10^{-4}	5.50×10^{-3}	8.30×10^{-5}
1.6 κ	5.66×10^{-4}	6.26×10^{-5}	6.51×10^{-5}	3.32×10^{-5}	1.56×10^{-2}	2.64×10^{-4}	5.50×10^{-3}	7.86×10^{-5}
0.8 t ₊ ⁰	5.66×10^{-4}	6.26×10^{-5}	1.36×10^{-4}	7.23×10^{-5}	1.56×10^{-2}	2.67×10^{-4}	5.50×10^{-3}	9.09×10^{-5}
1.0 t ₊ ⁰	5.66×10^{-4}	6.26×10^{-5}	9.96×10^{-5}	5.21×10^{-5}	1.56×10^{-2}	2.67×10^{-4}	5.50×10^{-3}	9.09×10^{-5}
1.2 t ₊ ⁰	5.66×10^{-4}	6.26×10^{-5}	7.42×10^{-5}	3.83×10^{-5}	1.56×10^{-2}	2.67×10^{-4}	5.50×10^{-3}	9.09×10^{-5}
1.4 t ₊ ⁰	5.66×10^{-4}	6.26×10^{-5}	5.53×10^{-5}	2.83×10^{-5}	1.56×10^{-2}	2.67×10^{-4}	5.50×10^{-3}	9.09×10^{-5}

If the electrolyte diffusion impedance in Model DFN is ignored, under the low frequency limiting condition, Eq. (74-1) will tend to

$$Z_{B\#1}(j\omega)|_{\omega=0} = \frac{L_1}{\kappa_{\text{eff}1} + \sigma_{\text{eff}1}} \left(1 + \frac{\kappa_{\text{eff}1}^2 + \sigma_{\text{eff}1}^2}{3\sigma_{\text{eff}1}\kappa_{\text{eff}1}} \right) + \frac{1}{a_{s1}L_1} z_{\text{int}1}(j\omega)|_{\omega=0} \quad (86-4)$$

Furthermore, if the electronic conductance resistance in the active material is further ignored, under the low frequency limiting condition, Eq. (78-1) will tend to

$$Z_{C\#1}(j\omega)|_{\omega=0} = \frac{L_1}{3\kappa_{\text{eff}1}} + \frac{1}{a_{s1}L_1} z_{\text{int}1}(j\omega)|_{\omega=0} \quad (86-5)$$

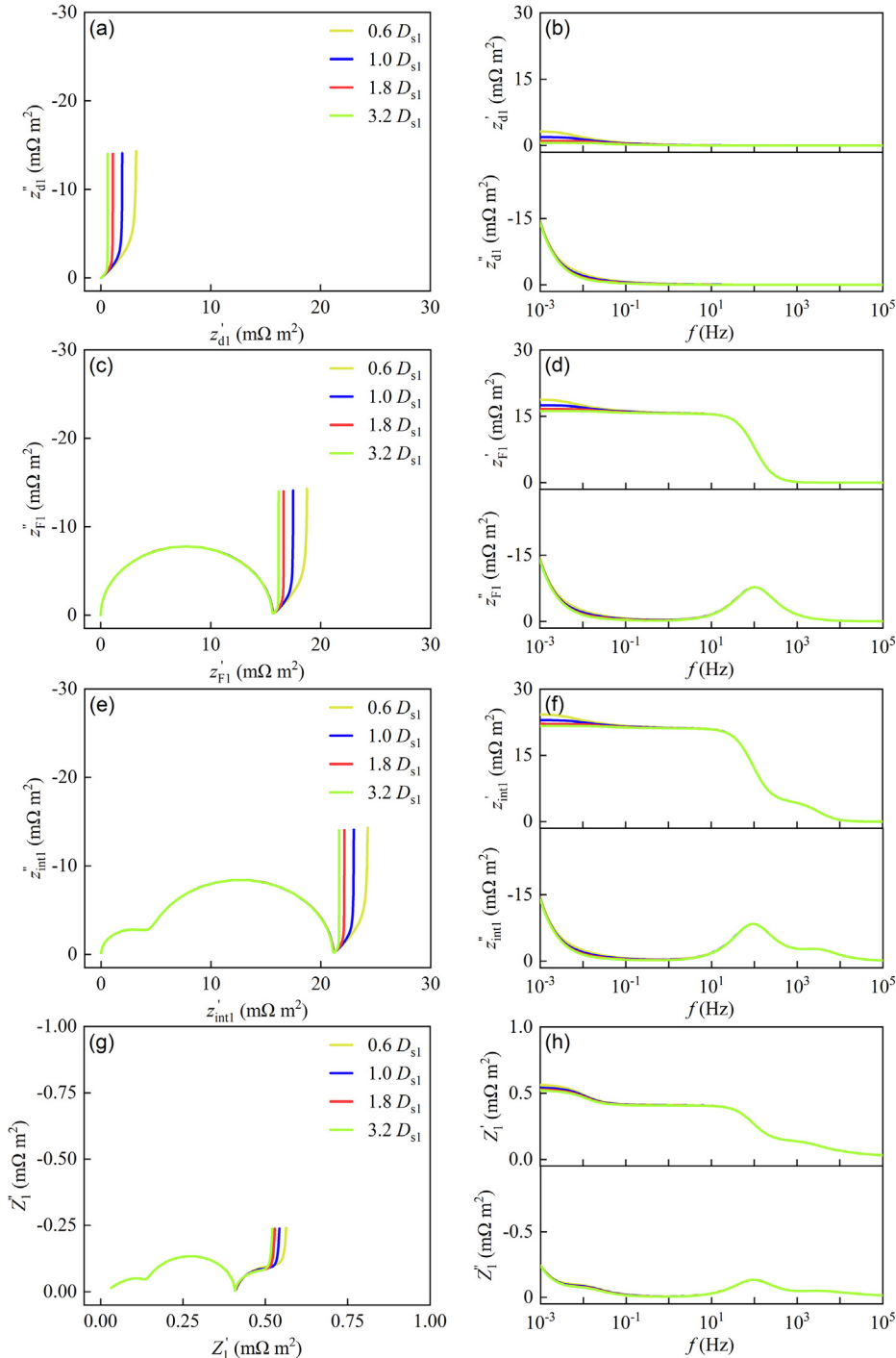


Fig. 10. Competitive effect of charge transfer reactions from the particle to the negative electrode based on the unified impedance model with respect to D_{s1} . Nyquist and Bode plots of (a, b), (c, d), (e, f), and (g, h) for z_{dl} , z_{F1} , z_{int1} , and Z_1 , respectively. Default parameters for simulation are listed in Table 3.

In this situation, $z_{\text{int1}}(j\omega)$, $Z_{\text{B}\#1}(j\omega)$, and $Z_{\text{C}\#1}(j\omega)$ exhibit a vertical line.

Both typical characteristics and limiting situations of the unified impedance model have been discussed for LIBs. Now it is ready to unveil the competitive mechanisms of charge transfer reactions in LIBs by combining with a deeper sensitivity analysis of impedance characteristics under different physical scenes [69].

3.2. Competitive mechanisms of charge transfer reactions in LIBs

The competitive mechanisms of charge transfer reactions are mainly reflected by the polarization resistance and characteristic frequency of different physicochemical processes at multiple scales with respect to various core parameters. Impedance spectra can be easily calculated with the developed EIS-Toolbox@LIB based on the unified impedance under different physical scenes.

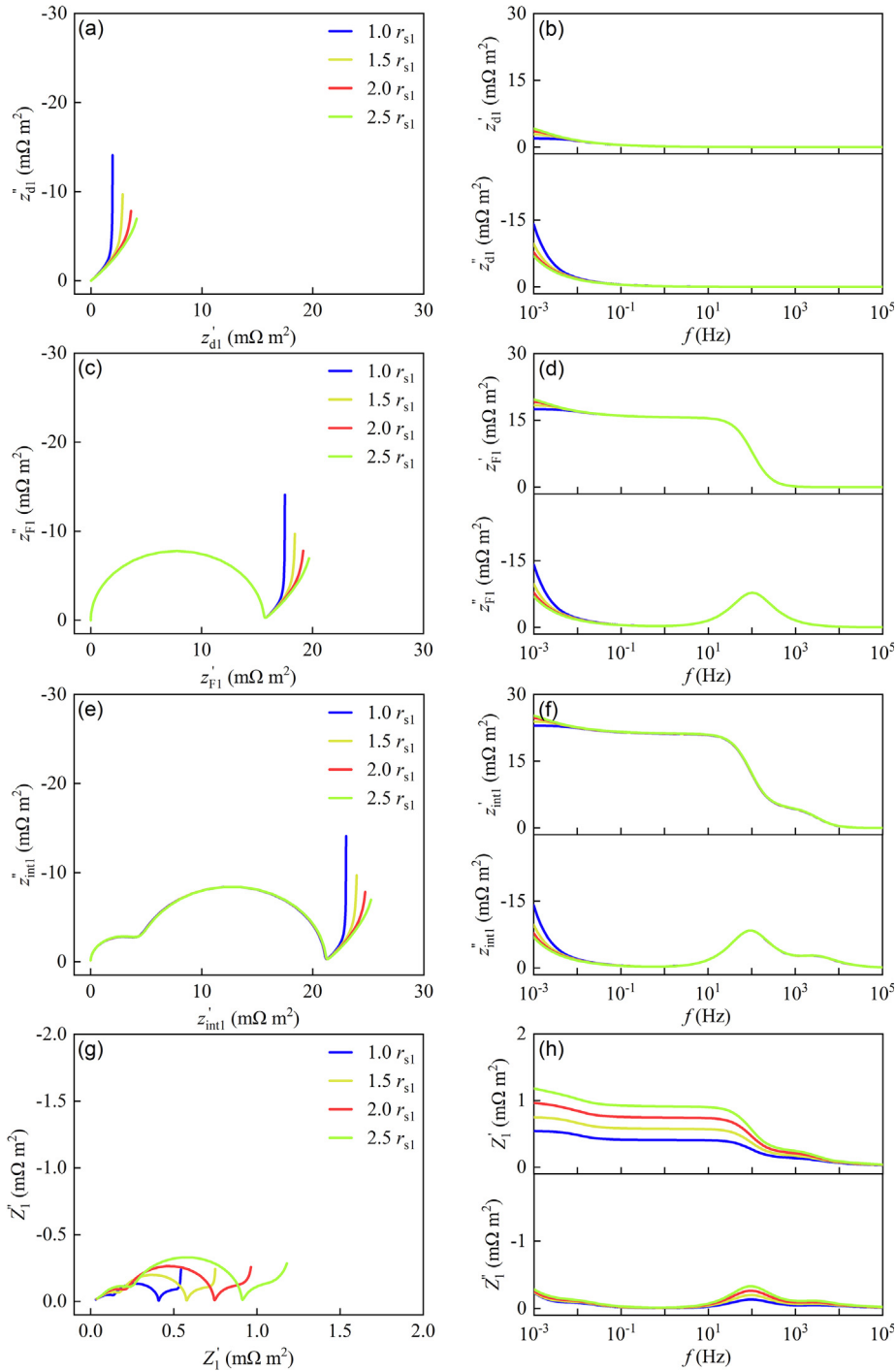


Fig. 11. Competitive effect of charge transfer reactions from the particle to the negative electrode based on the unified impedance model with respect to r_{s1} . Nyquist and Bode plots of (a, b), (c, d), (e, f), and (g, h) for $z_{\text{d}1}$, $z_{\text{F}1}$, z_{int1} , and Z_1 , respectively. Default parameters for simulation are listed in Table 3.

In order to better unveil the competitive mechanisms of charge transfer reactions, the simulated impedance spectra based on the unified impedance model is interpreted in terms of the ECM, as shown in Fig. 5(d). Hence, $Z_{W0}(s)$ as defined in Eqs. (83-1)–(83-3) is used in theoretical calculation or fitting analysis for the solid diffusion in the electrode. As a result, characteristic time constants at the particle and electrode scales can be theoretically calculated in terms of $\tau_d = (r_s/3)^2/D_s$ and $\tau_{Ds} \approx \tau_d$ [147], respectively. Similarly, $Z_{Ws}(s)$ as defined in Eqs. (84-1)–(84-3) is used in theoretical calculation or fitting analysis for the electrolyte diffusion in the elec-

trode/separator. As a result, the characteristic time constant at the electrode scale can be theoretically calculated in terms of $\tau_{De} = L^2/D_{e,eff}$. At the particle scale, characteristic time constants of interfacial electrochemical reaction and charge transport through the sei film can be calculated in terms of $\tau_{ct} = R_{ct} \times C_{dl}$ and $\tau_{sei} = R_{sei} \times C_{sei}$ [145], respectively. In a word, characteristic time constants and polarization resistances for various processes can be fitted or calculated, as listed in Tables 4 and 5.

For the convenience of the discussion, parameters to be studied for LIBs are classified into four sorts: (i) the active particle involves

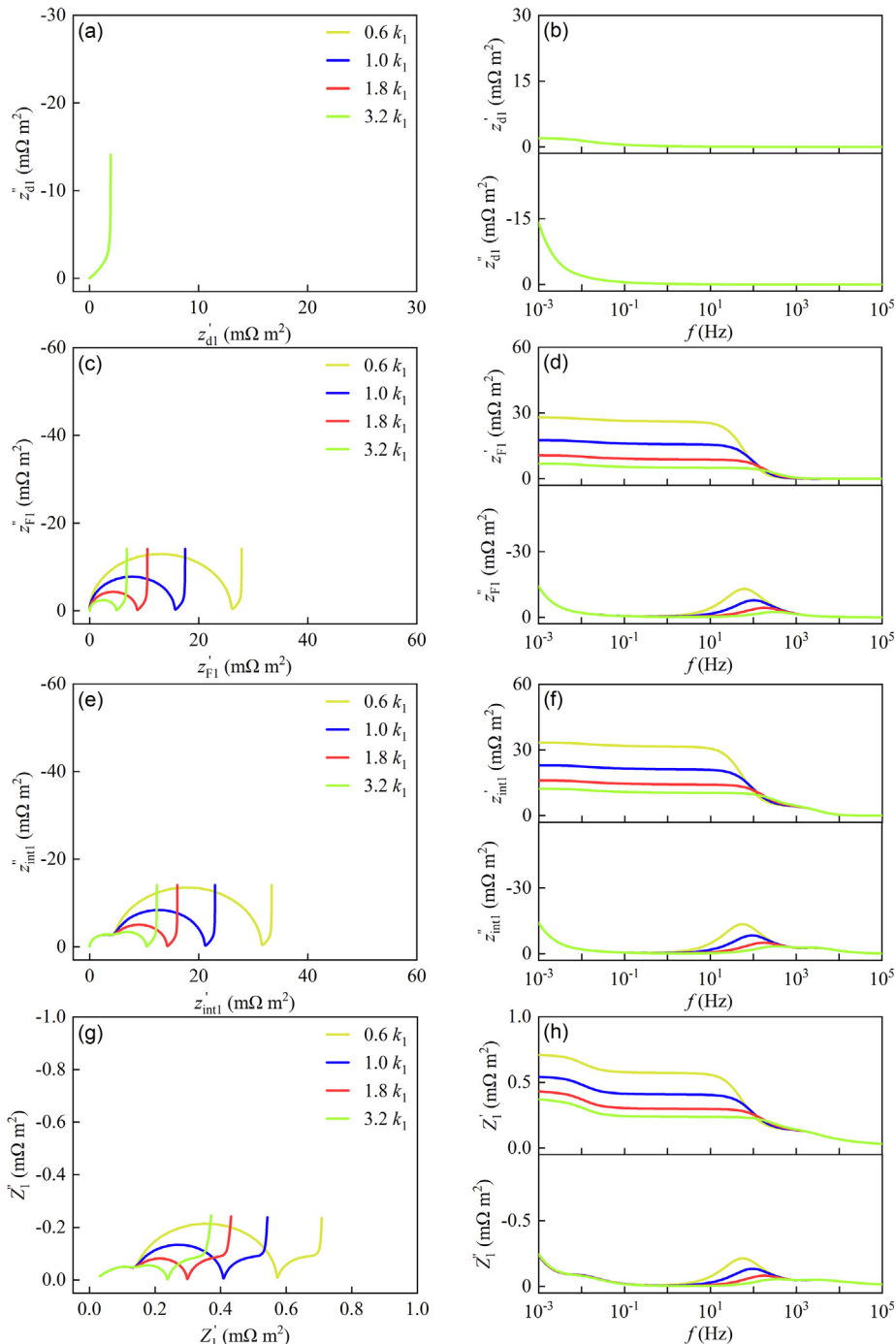


Fig. 12. Competitive effect of charge transfer reactions from the particle to the negative electrode based on the unified impedance model with respect to k_1 . Nyquist and Bode plots of (a, b), (c, d), (e, f), and (g, h) for z_{dl} , z_{F1} , z_{intl} , and Z_1 , respectively. Default parameters for simulation are listed in Table 3.

solid diffusivity D_{s1} , particle radius r_{s1} , rate constant k_1 , and sei resistivity ρ_{sei1} ; (ii) the electrode/separator matrix involves thickness $L_1/L_2/L_3$, porosity $\varepsilon_{e1}/\varepsilon_{e2}/\varepsilon_{e3}$, and electronic conductivity σ_1/σ_2 ; (iii) the pore electrolyte involves electrolyte diffusion coefficient D_e , ionic conductivity κ , and ion transference number t_+^0 ; (iv) the operating temperature T .

Physical parameters are identified for LIBs with impedance-based diagnosis [82]. No doubt, these parameters have a close relationship with cycling degradation. A furthermore analysis of the competitive mechanisms of charge transfer reactions, similar to field-effect transistor [148], will also be beneficial to revealing the aging mechanisms for LIBs [149–151].

3.2.1. Effect of active particle parameters

(1) Solid diffusivity

Fig. 10 and **Tables 4 and 5** show the competitive effect of charge transfer reactions from the particle to the electrode with respect to D_{s1} [50,51]. The following conclusions can be made:

- (i) At the particle scale, impedance response processes of charge transport through sei film, charge transfer reaction at the solid/electrolyte interface, and solid diffusion located at high frequency, middle frequency, and low frequency regions, respectively, have no obvious overlap.
- (ii) As D_{s1} increases to m times, τ_{d1} decreases to $1/m$ times, and the polarization processes at middle to high frequencies from the particle to the electrode is not affected at all. In addition, τ_{Ds1} is almost equal to τ_{d1} . Scaling up from the particle to the electrode does not affect τ_{Ds1} but R_{Ds1} for the solid diffusion.
- (iii) At the electrode scale, the electrolyte diffusion is not affected by D_{s1} but is overlapped with the solid diffusion severely, which makes it difficult to distinguish them. In addition, it is greatly compressed during scaling up from R_{ct1}/R_{sei1} to R_{CT1}/R_{SEI1} .

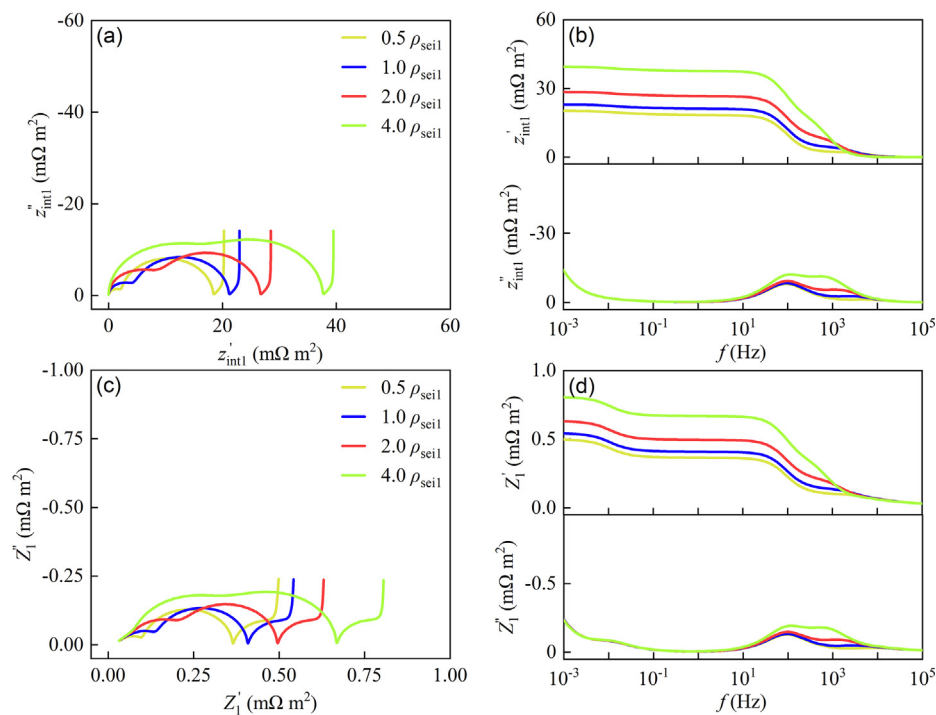


Fig. 13. Competitive effect of charge transfer reactions from the particle to the negative electrode based on the unified impedance model with respect to ρ_{sei1} . Nyquist and Bode plots of (a, b) and (c, d) for z'_{int1} and Z'_1 , respectively. Default parameters for simulation are listed in **Table 3**.

(2) Particle radius

Fig. 11 and **Tables 4 and 5** show the competitive effect of charge transfer reactions from the particle to the electrode with respect to r_{s1} [152,153]. The following conclusions can be made:

- (iv) As r_{s1} increases to m times, τ_{d1} increases to m^2 times, and neither R_{sei1} nor R_{ct1} at the particle scale is affected, however R_{SEI1} and R_{CT1} at the electrode scale increase to m times approximately. Scaled up from the particle to the electrode, R_{SEI1} and R_{CT1} are compressed. In addition, the low frequency diffusion region becomes wider, suggesting a bigger r_{s1} might achieve a slower charge capability.
- (v) At the particle scale, r_{s1} affects neither τ_{sei1} nor τ_{ct1} at middle to high frequencies but τ_{d1} at low frequencies. At the electrode scale, r_{s1} affects charge transfer reactions from low to high frequencies except τ_{De1}/R_{De1} .

In short, charge transfer reactions not only depend on battery parameters themselves but also on the scale at which it is located, which results in the complexity of interpreting the EIS data for LIBs.

(3) Rate constant

Fig. 12 and **Tables 4 and 5** show the competitive effect of charge transfer reactions from the particle to the electrode with respect to k_1 [51]. The following conclusions can be made:

As k_1 increases to m times, both τ_{ct1}/τ_{CT1} and R_{ct1}/R_{CT1} decrease to $1/m$ times, and other polarization resistances and characteristic time constants from the particle to the electrode, for instance, both $\tau_{d1}/\tau_{Ds1}/\tau_{De1}/\tau_{Ds3}/\tau_{sei1}/\tau_{SEI1}$ and $R_{d1}/R_{Ds1}/R_{De1}/R_{De3}/R_{sei1}/R_{SEI1}$ are not affected by the change of k_1 at all. It can be said that the influence of k_1 is mainly on the solid/electrolyte interface, and its impact on the frequency response is also limited to the mid-frequency range.

(4) Resistivity of sei

Fig. 13 and **Tables 4 and 5** show the competitive effect of charge transfer reactions from the particle to the electrode with respect to ρ_{sei1} [121,154,155]. The following conclusions can be made:

As ρ_{sei1} increases to m times, both τ_{sei1}/τ_{SEI1} and R_{sei1}/R_{SEI1} increase to m times, and other polarization resistances and characteristic time constants from the particle to the electrode are not affected by ρ_{sei1} . The influence of ρ_{sei1} is mainly concentrated on the charge transport through the sei/SEI film, and its impact on

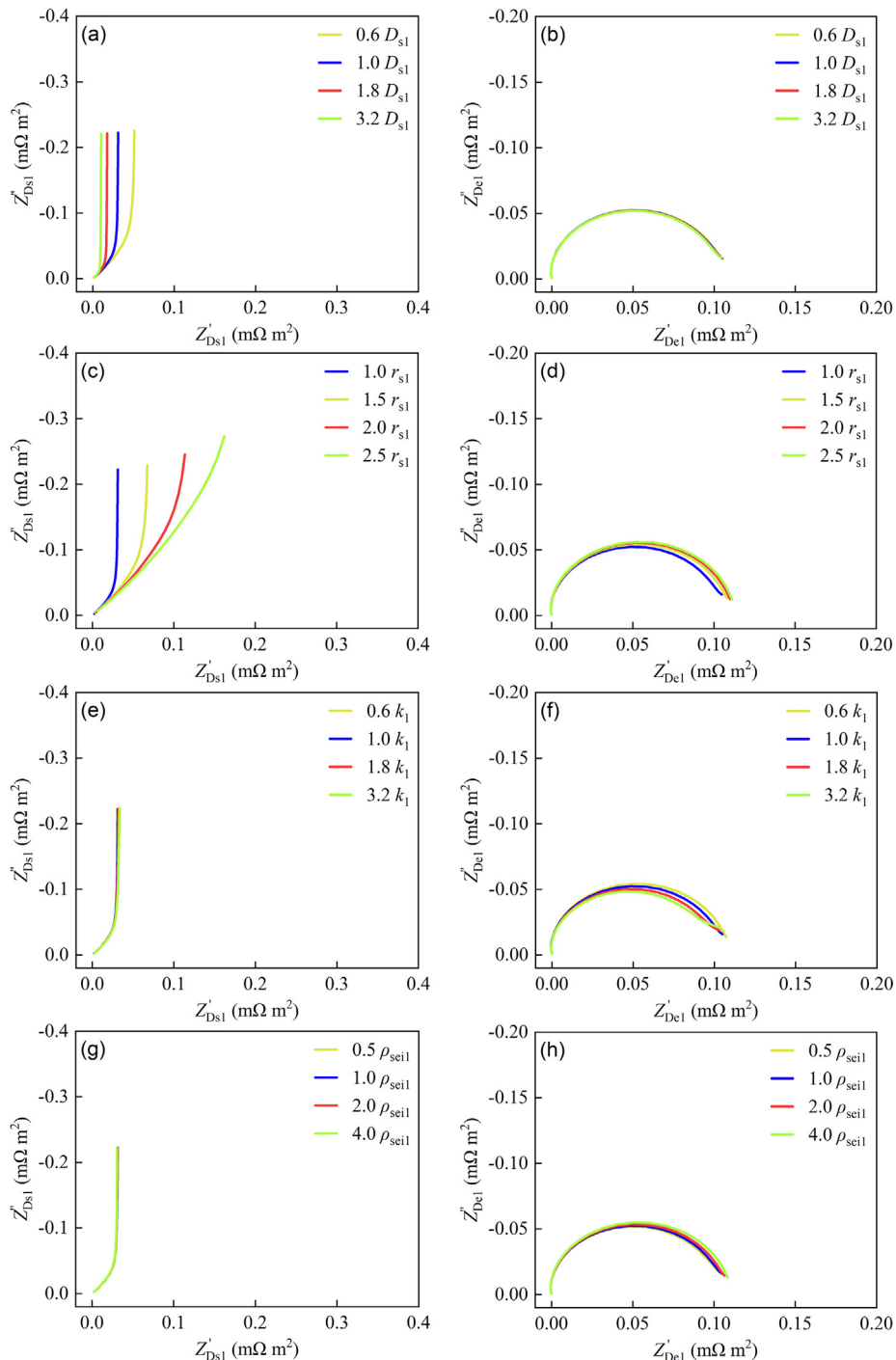


Fig. 14. Competitive effect of the solid/electrolyte diffusion in the negative electrode based on the unified impedance model with respect to D_{s1} , r_{s1} , k_1 , and ρ_{sei1} . Nyquist plots of (a, c, e, g) and (b, d, f, h) for Z'_{Ds1} and Z'_{De1} , respectively. Default parameters for simulation are listed in **Table 3**.

the frequency response is just limited to the high frequency range.

Based on data from Figs. 10–13, the solid/electrolyte diffusion impedance at the electrode scale can be calculated approximately with respect to active particle parameters, as shown in Fig. 14. The following conclusions can be made: (i) D_{s1} does not affect the electrolyte diffusion but the solid diffusion; (ii) r_{s1} affects the solid diffusion a little more than the electrolyte diffusion; (iii) k_1 and ρ_{sei1} affect the solid/electrolyte diffusion very weakly or even the effect can be ignored. The above conclusions are also suitable for the positive electrode.

3.2.2. Effect of electrode/separator matrix parameters

(1) Electrode/sePARATOR thicknesses

Fig. 15 and Tables 4 and 5 show the competitive effect of charge transfer reactions in the electrode/separator with respect to $L_1/L_2/L_3$ [57,95,153,156]. The following conclusions can be made:

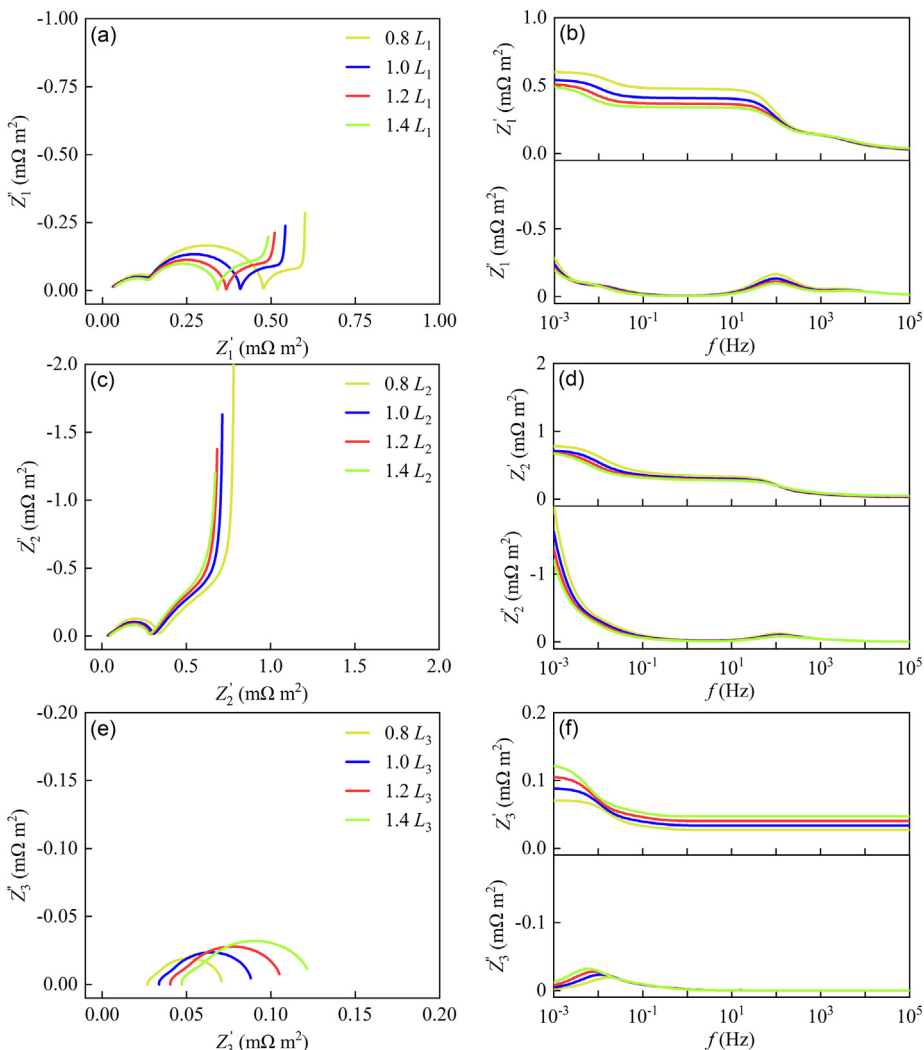


Fig. 15. Competitive effect of charge transfer reactions in the electrode/separator based on the unified impedance model with respect to $L_1/L_2/L_3$. Nyquist and Bode plots of (a, b), (c, d), and (e, f) for Z_1 , Z_2 , and Z_3 , respectively. Default parameters for simulation are listed in Table 3.

(i) As L_1 increases to m times, τ_{d1} keeps constant and τ_{ds1} approximately keeps constant; however, τ_{de1} increases to m^2 times and R_{de1} increases to m times roughly. Other polarization resistances and characteristic time constants from the particle to the electrode, for instance, both $\tau_{ct1}/\tau_{ct1}/\tau_{sei1}/\tau_{sei1}$ and $R_{ct1}/R_{ct1}/R_{sei1}/R_{sei1}$ are not affected by the change of L_1 . As L_3 increases to m times, τ_{de3} increases to m^2 times and R_{de3} increases to m times. In addition, the ohmic resistance of the separator is proportional to L_3 .

(ii) Generally speaking, the influence of L_1/L_2 is mainly on the solid/electrolyte diffusion from the particle to the electrode, and its impact on the frequency response is just limited to the low frequency range. In contrast, the influence of L_3 on the negative/positive electrode usually can be ignored, however, its influence on charge transfer reactions sometimes is substantial and cannot be ignored.

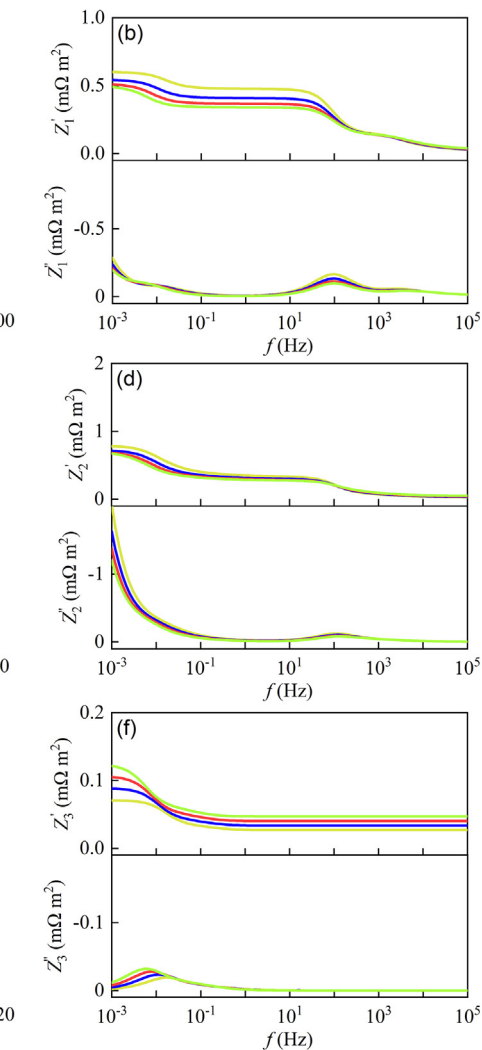


Fig. 15. Competitive effect of charge transfer reactions in the electrode/separator based on the unified impedance model with respect to $L_1/L_2/L_3$. Nyquist and Bode plots of (a, b), (c, d), and (e, f) for Z_1 , Z_2 , and Z_3 , respectively. Default parameters for simulation are listed in Table 3.

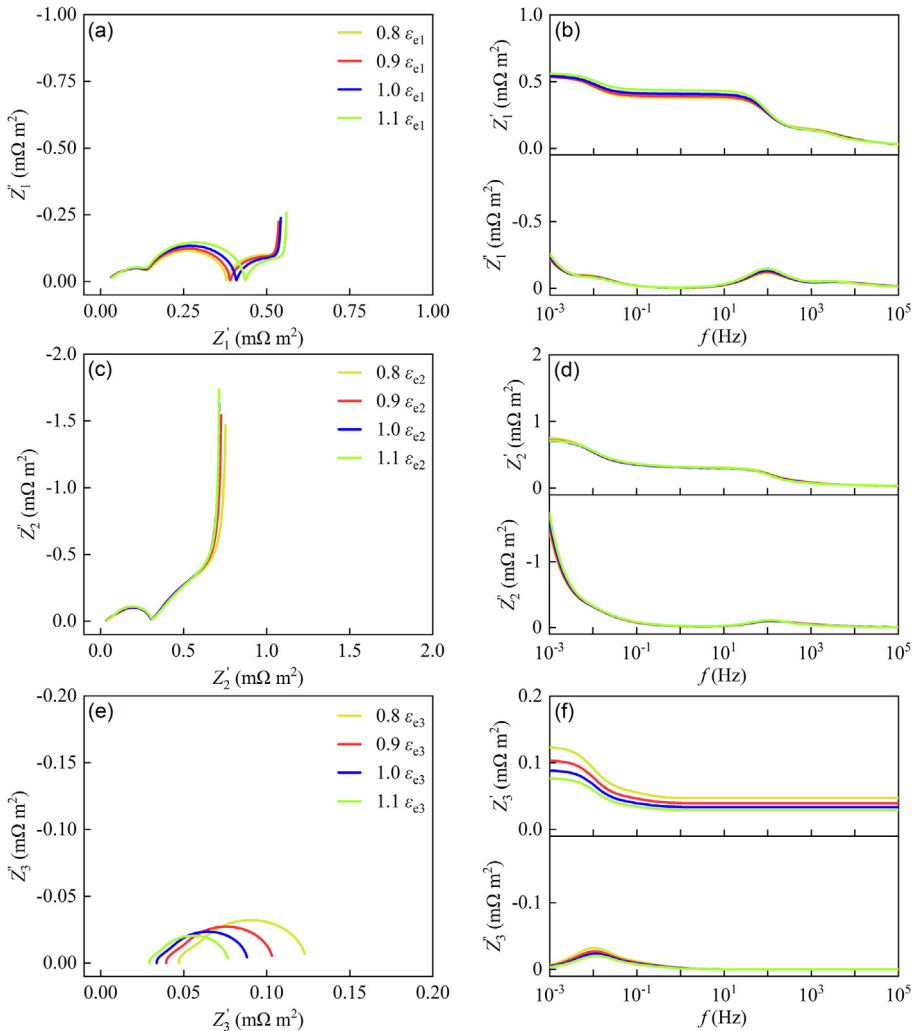


Fig. 16. Competitive effect of charge transfer reactions for the electrode/separator based on the unified impedance model with respect to $\varepsilon_{e1}/\varepsilon_{e2}/\varepsilon_{e3}$. Nyquist and Bode plots of (a, b), (c, d), and (e, f) for Z_1 , Z_2 , and Z_3 , respectively. Default parameters for simulation are listed in Table 3.

The above results show that the thickness of electrode/separator plays a critical role in mitigating the polarization loss and capacity fade for LIBs [57,128,157], which are well in agreement with experimental results reported previously [131].

(2) Electrode/separator porosity

Fig. 16 and Tables 4 and 5 show the competitive effect of charge transfer reactions in the electrode/separator with respect to $\varepsilon_{e1}/\varepsilon_{e2}/\varepsilon_{e3}$ [152,153]. The following conclusions can be made:

- As ε_{e1} increases to m times, both $\tau_{d1}/\tau_{ct1}/\tau_{sei1}$ and $R_{d1}/R_{ct1}/R_{sei1}$ keep constant; however, both τ_{De1} and R_{De1} decrease to $1/m^{brug1}$ times roughly. This is still an open question and it needs to be calibrated due to the high sensitivity of electrode microstructure to the porosity. So does ε_{e2} for Z_2 .

- As ε_{e3} increases to m times, τ_{De3} almost keeps constant; however, R_{De3} and R_{O3} decrease to $1/m^{brug3}$ times precisely. The precision and relationship for τ_{De3} and R_{De3} are different from those for τ_{De1}/τ_{De2} and R_{De1}/R_{De2} because the separator is simpler than electrodes in both composition and microstructure.

The pore electrolyte offers an ionic path for Li^+ into or out of all active particles. Hence, the porosity plays a critical role in the solid/electrolyte diffusion [158,159]. The effect of the porosity on the solid/electrolyte diffusion is highly nonlinear and sensitive, and thus more attention needs to be paid to it in order to optimize the design for porous electrodes [153].

(3) Electrode electronic conductivity

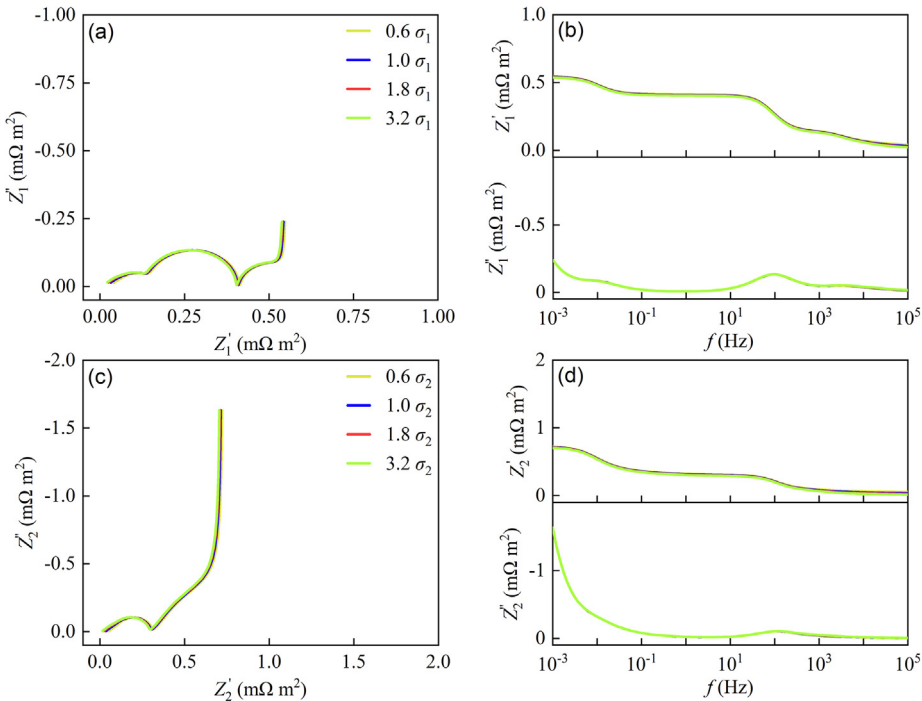


Fig. 17. Competitive effect of charge transfer reactions for the negative/positive electrodes based on the unified impedance model with respect to σ_1/σ_2 . Nyquist and Bode plots of (a, b) and (c, d) for Z_1 and Z_2 , respectively. Default parameters for simulation are listed in Table 3.

Fig. 17 and Tables 4 and 5 show the competitive effect of charge transfer reactions in electrodes with respect to σ_1/σ_2 [51]. The following conclusions can be made:

The ohmic item of Eq. (57)–(1) decreases with increasing σ_1 . Hence, various polarization processes keep constant except that Nyquist plots of Z_1 will shift slightly toward the left. So does σ_2 for Z_2 .

Based on data from Figs. 15–17, the solid/electrolyte diffusion impedance at the electrode scale can be calculated approximately with respect to electrode/separator matrix parameters, as shown in Fig. 18. The following conclusions can be made: (i) at the particle scale, electrode/separator matrix parameters do not affect various polarization processes; (ii) at the electrode scale, L_1 has a slight impact on the solid diffusion, but a serious impact on the electrolyte diffusion; (iii) at the electrode scale, ε_{e1} affects both the solid diffusion and the electrolyte diffusion, mainly focusing on the low frequency range; (iv) at the electrode scale, as σ_1 increases, the solid/electrolyte diffusion keeps constant and Nyquist plot shifts slightly to the left. The above conclusions are also suitable for the positive electrode.

3.2.3. Effect of pore electrolyte parameters

(1) Electrolyte diffusion coefficient

Fig. 19 and Tables 4 and 5 show the competitive effect of charge transfer reactions in LIBs with respect to D_e [51]. The following conclusions can be made:

- (i) At the particle scale, the change of D_e does not affect charge transport through sei film, charge transfer reaction at the solid/electrolyte interface, and solid diffusion at all, i.e., as D_e changes, both $\tau_{d1}/\tau_{d2}/\tau_{ct1}/\tau_{ct2}/\tau_{sei1}/\tau_{sei2}$ and $R_{d1}/R_{d2}/R_{ct1}/R_{ct2}/R_{sei1}/R_{sei2}$ keep constant. The above conclusions are also true at the electrode scale.

- (ii) At the electrode/separator scale, as D_e increases to m times, $\tau_{de1}/\tau_{de2}/\tau_{de3}$ and $R_{de1}/R_{de2}/R_{de3}$ decrease to $1/m$ times; however, both $\tau_{ds1}/\tau_{ds2}/\tau_{ct1}/\tau_{ct2}/\tau_{sei1}/\tau_{sei2}$ and $R_{ds1}/R_{ds2}/R_{ct1}/R_{ct2}/R_{sei1}/R_{sei2}$ approximately keep constant, and ohmic resistances for electrodes and the separator approximately keep constant as well.

(2) Ionic conductivity

Fig. 20 and Tables 4 and 5 show the competitive effect of charge transfer reactions in LIBs with respect to κ [120]. The following conclusions can be made:

- (i) At the particle scale, the change of κ does not affect charge transport through sei film, charge transfer reaction at the solid/electrolyte interface, and solid diffusion at all, i.e., as κ changes, both $\tau_{d1}/\tau_{d2}/\tau_{ct1}/\tau_{ct2}/\tau_{sei1}/\tau_{sei2}$ and $R_{d1}/R_{d2}/R_{ct1}/R_{ct2}/R_{sei1}/R_{sei2}$ keep constant. The above conclusions are also applied to τ_{ds1}/τ_{ds2} and R_{ds1}/R_{ds2} at the electrode scale.
- (ii) At the electrode/separator scale, as κ increases from 0.7κ to 1.6κ (herein $m = 1.6/0.7 \approx 2.3$ times), both $\tau_{ct1}/\tau_{ct2}/\tau_{sei1}/\tau_{sei2}$ and $R_{ct1}/R_{ct2}/R_{sei1}/R_{sei2}$ change below 30%; at the same time, both $\tau_{de1}/\tau_{de2}/\tau_{de3}$ and $R_{de1}/R_{de2}/R_{de3}$ decrease to $1/m$ times via the Nernst-Einstein relation; in addition, ohmic resistances for electrodes almost keep constant. However, the ohmic resistance for the separator decreases dramatically, which results in a big shift of its Nyquist plot to the left.

The above difference originates from the differences in composition and microstructure between the electrode and the separator.

(3) Ion transference number

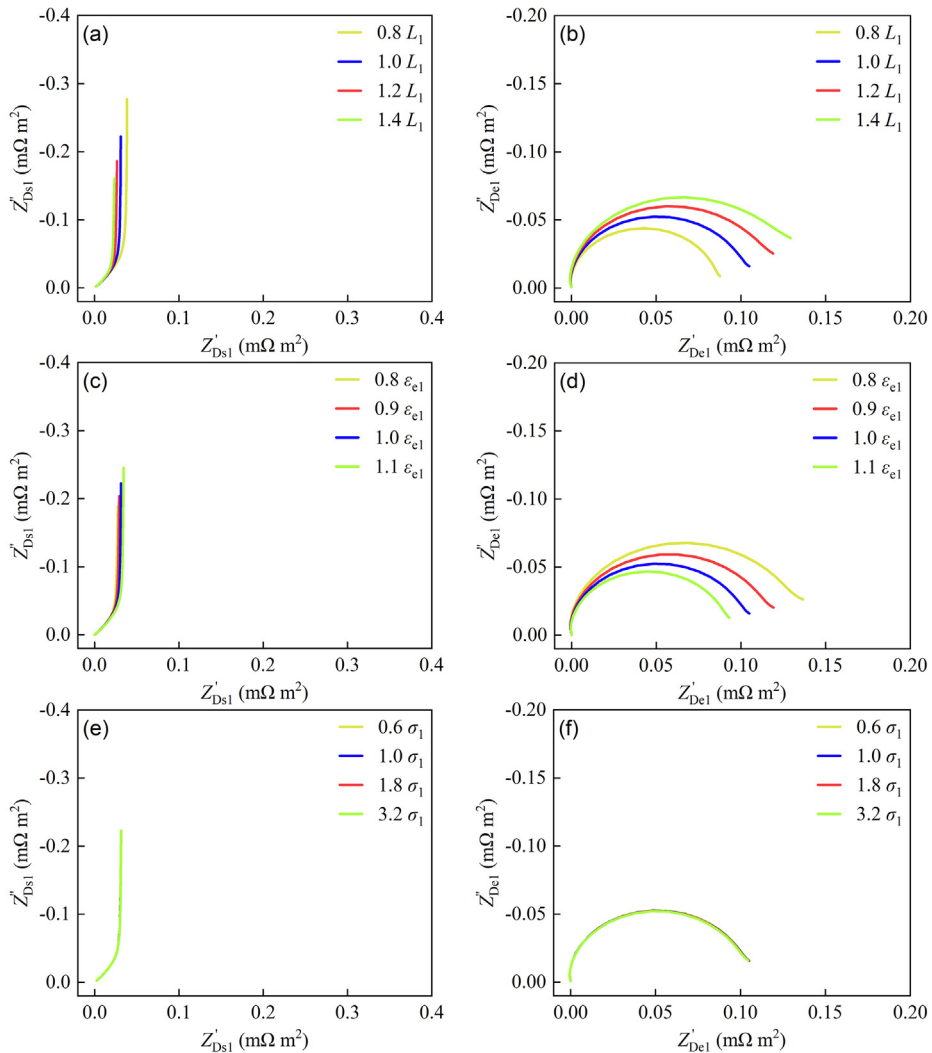


Fig. 18. Competitive effect of the solid/electrolyte diffusion in the negative electrode based on the unified impedance model with respect to L_1 , ε_{e1} , and σ_1 . Nyquist plots of (a, c, e) and (b, d, f) for Z'_{DS1} and Z'_{De1} , respectively. Default parameters for simulation are listed in Table 3.

Fig. 21 and Tables 4 and 5 show the competitive effect of charge transfer reactions in LIBs with respect to t_+^0 [51]. The following conclusions can be made:

(i) At the particle scale, the change of t_+^0 does not affect charge transport through the sei film, charge transfer reaction at the solid/electrolyte interface, solid diffusion, and ohmic polarization from the particle to the electrode, i.e., characteristic time constants and polarization resistances corresponding to above processes basically keep constant.

(ii) At the electrode/separator scale, as t_+^0 increases to m times, τ_{De1}/τ_{De3} is approximately inversely proportional to $(1 - mt_+^0) \times (mt_+^0)$, and R_{De1}/R_{De3} is approximately proportional to $(1 - mt_+^0)/(mt_+^0)$ via the Nernst-Einstein relation.

Obviously, t_+^0 mainly affects the electrolyte diffusion, and a higher t_+^0 benefits reducing the polarization loss and speeding up the kinetics for the electrolyte diffusion.

Based on data from Figs. 19–21, the solid/electrolyte diffusion impedance at the electrode/separator scale can be calculated

approximately with respect to pore electrolyte parameters, as shown in Fig. 22. The following conclusions can be made: (i) the changes of pore electrolyte parameters including D_e , κ , and t_+^0 basically do not affect the solid diffusion from the particle to the electrode, but just affect the electrolyte diffusion in the electrode and the separator; (ii) the increases of pore electrolyte parameters including D_e , κ , and t_+^0 not only reduce the polarization loss but also speed up the kinetic rate for the electrolyte diffusion processes in both the electrode and the separator. The above conclusions are also suitable for the positive electrode.

3.2.4. Effect of the operating temperature

Till now, the competitive mechanisms of charge transfer reactions have been numerically analyzed with respect to parameters of the active particle, the electrode/separator matrix, and the pore electrolyte. Under different operating temperatures of 15, 25, 35, and 45 °C, the impedance spectra for the particle to the negative electrode can be calculated, as shown in Fig. 23, for the separator as shown in Fig. 24, and for the solid/electrolyte diffusion in the

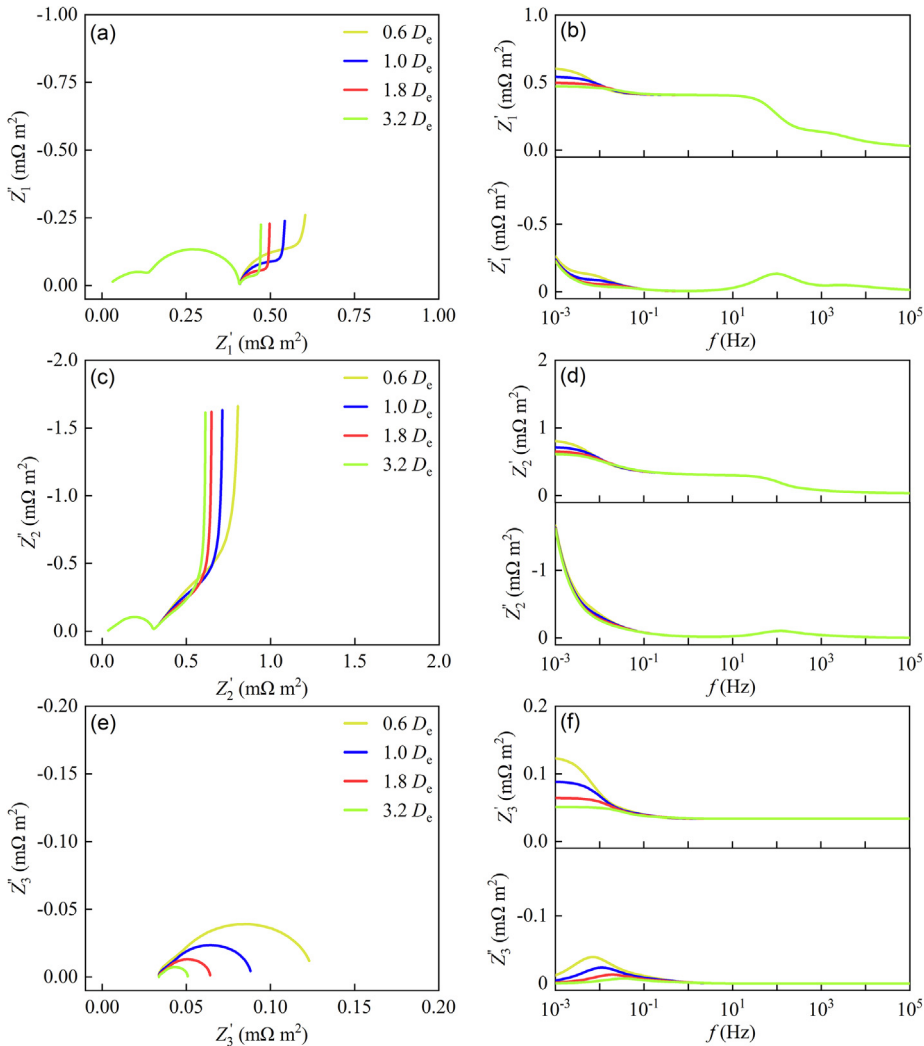


Fig. 19. Competitive effect of charge transfer reactions in LIBs based on the unified impedance model with respect to D_e . Nyquist and Bode plots of (a, b), (c, d), and (e, f) for Z_1 , Z_2 , and Z_3 , respectively. Default parameters for simulation are listed in Table 3.

negative electrode as shown in Fig. 25. In addition, characteristic time constants and polarization resistances shown in Table 6 can also be obtained with methods adopted for Tables 4 and 5.

Figs. 23–25 and Table 6 show the competitive effect of charge transfer reactions from the particle to the electrode/separator with respect to T [69,160]. The following conclusions can be made: (i) In detail, with increasing T from 15 to 45 °C, on the one hand, $\tau_{\text{sei}1}/\tau_{\text{SEI}1}$ and $R_{\text{sei}1}/R_{\text{SEI}1}$ increase 2–4 times dramatically; on the other hand, $\tau_{\text{d}1}/\tau_{\text{D}1}/\tau_{\text{De}1}/\tau_{\text{De}3}/\tau_{\text{ct}1}/\tau_{\text{CT}1}$ and $R_{\text{d}1}/R_{\text{D}1}/R_{\text{De}1}/R_{\text{De}3}/R_{\text{ct}1}/R_{\text{CT}1}$ decrease to 1/3–1/5 times. (ii) In short, with increasing T , kinetic parameters of $D_{\text{s}1}$, $D_{\text{s}2}$, k_1 , k_2 , D_e , κ , and $\rho_{\text{sei}1}$ will increase sharply according to the Arrhenius equation. In turn, the increase of these kinetic parameters will comprehensively and deeply affect charge transfer reactions in LIBs.

As a result, temperature is a global variable with high sensitivity, and its changes increase the complexity of analyzing the competitive mechanisms of charge transport reactions.

3.3. Sensitivity analysis

Based on the above competitive analysis of charge transfer reactions with respect to 11 parameters for LIBs at multiple scales, this section will analyze parameter sensitivity in order to gain a further insight into the competitive mechanisms of charge transfer reactions.

In the present work, the solid/electrolyte diffusion impedance from 1 Hz to 1 mHz is approximately calculated based on the unified impedance model. The sensitivity of the solid/electrolyte diffusion impedance to parameter set X can be evaluated according to their standard deviations. The change range of X is set to be 0.56, 0.75, 1.00, 1.33, and 1.78 times of its default value, and its relative sensitivity is defined as

$$\overline{Z_f} = \frac{\sum_{i=1}^N Z'_{f,i} + jZ''_{f,i}}{N} \quad (87a)$$

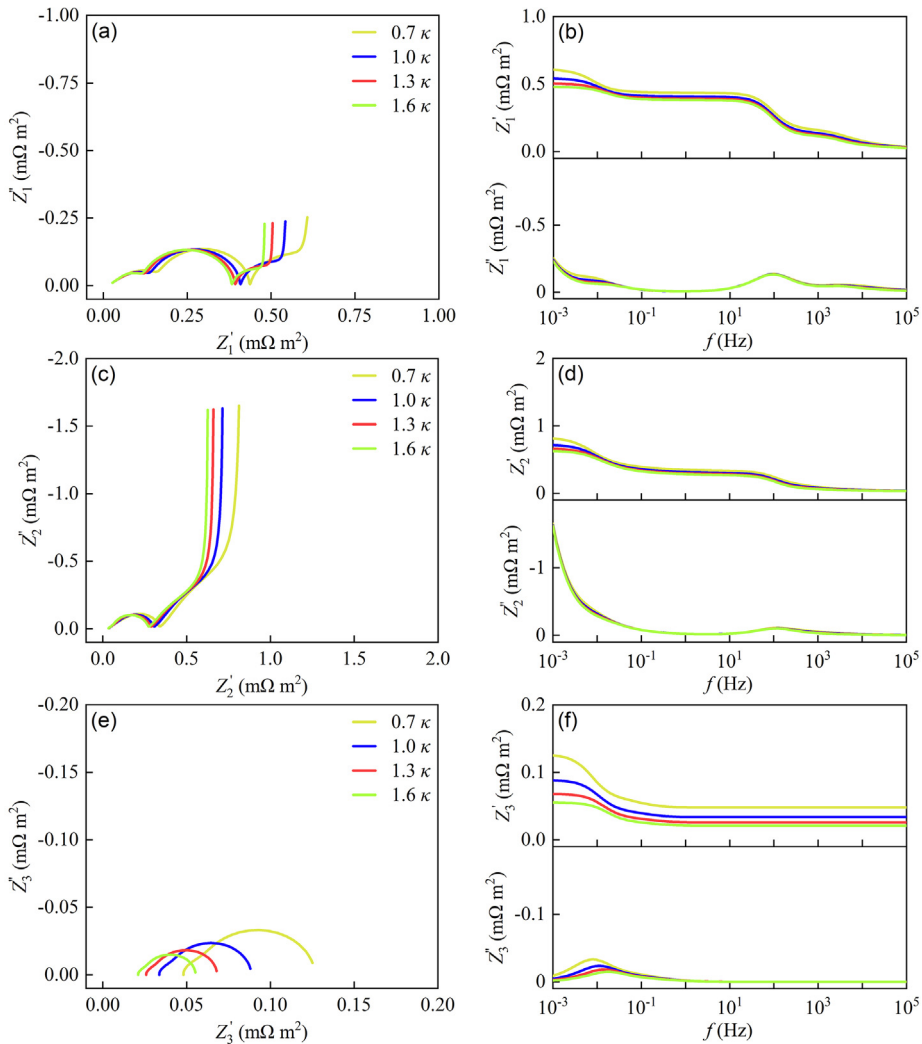


Fig. 20. Competitive effect of charge transfer reactions in LIBs based on the unified impedance model with respect to κ . Nyquist and Bode plots of (a, b), (c, d), and (e, f) for Z_1 , Z_2 , and Z_3 , respectively. Default parameters for simulation are listed in Table 3.

$$SZ_f = \sqrt{\frac{\sum_{i=1}^N |Z_{f,i} - \bar{Z}_f|^2}{N}} \quad (87b)$$

$$SZ\% = \frac{\sum_f SZ_f}{\sum_f |\bar{Z}_f|} \times 100\% \quad (87c)$$

where \bar{Z}_f is the average value of $Z_{f,i}$ at frequency f over the $i = 1-N$ ($N = 5$) time simulating results; $Z_{f,i}$ is the i th simulating result of the solid/electrolyte diffusion impedance; SZ_f is the standard derivation of $Z_{f,i}$ over M sampling frequency points ($M = 38$); and $SZ\%$ is the relative sensitivity of the solid/electrolyte diffusion impedances to parameter set X .

Fig. 26 shows the sensitive analysis of the solid/electrolyte diffusion impedance to parameter set X ($X = D_{s1}, r_{s1}, k_1, \rho_{sei1}, L_1, \varepsilon_{e1}$,

$\sigma_1, D_e, \kappa, t_+^0$, or T). Herein, D_{s1} denotes the Li solid phase diffusion coefficient in the negative electrode; r_{s1} denotes the particle radius in the negative electrode; k_1 denotes the rate constant for the negative electrode electrochemical reaction; ρ_{sei1} denotes the sei resistivity in the negative electrode; L_1 denotes the thickness of the negative electrode; ε_{e1} denotes the electrolyte phase volume fraction(porosity) in the negative electrode; σ_1 denotes the electronic conductivity of solid matrix in the negative electrode; D_e denotes the Li^+ diffusion coefficient in the electrolyte phase; κ denotes the ionic conductivity of electrolyte; t_+^0 denotes the transference number of Li^+ with respect to the velocity of solvent; and T denotes the operating temperature. All definitions similar to the above parameters also may refer to Supporting Information.

It can be seen from Fig. 26: (i) both the solid diffusion and the electrolyte diffusion have high sensitivities to L_1 , ε_{e1} , and T , among

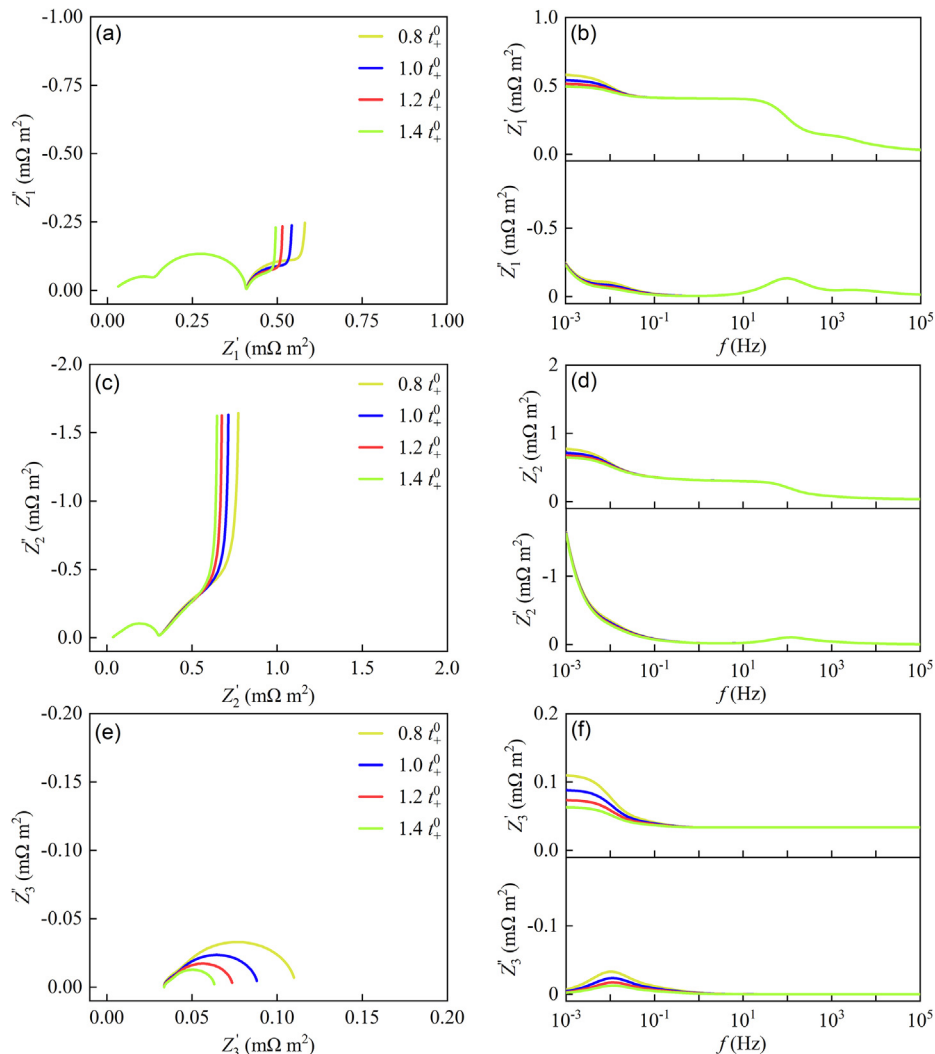


Fig. 21. Competitive effect of charge transfer reactions in LIBs based on the unified impedance model with respect to t_+^0 . Nyquist and Bode plots of (a, b), (c, d), and (e, f) for Z_1 , Z_2 , and Z_3 , respectively. Default parameters for simulation are listed in Table 3.

which, the sensitivity is the highest to ε_{e1} ; (ii) the solid diffusion has a high sensitivity to D_{s1} and r_{s1} ; however, the electrolyte diffusion has low or even no sensitivity to them; (iii) the electrolyte diffusion has a high sensitivity to D_e , κ , and t_+^0 ; however, the solid diffusion has low or even no sensitivity to them; and (iv) the solid/electrolyte diffusion have low or even no sensitivities to k_1 , ρ_{se1} , and σ_1 .

4. Conclusions

The present work aims at building a theory framework to mitigate the blindness and uncertainty in unveiling charge transfer

reactions with EIS analysis for LIBs. Concentrated on the above goals, the following progresses have been made:

- (1) Unifying the DFN-like impedance models for LIBs under different physical scenes. With this unified impedance model, it becomes simple for the readers to scientifically select a proper impedance model based on the actual physical scene and truly achieve the diagnostic purpose for the competitive mechanisms of charge transfer reactions.
- (2) Separating the solid/electrolyte diffusion impedance of the electrode for LIBs. Based on the separating method, the sensitivity of diffusion impedance to parameter set X ($X = D_{s1}$,

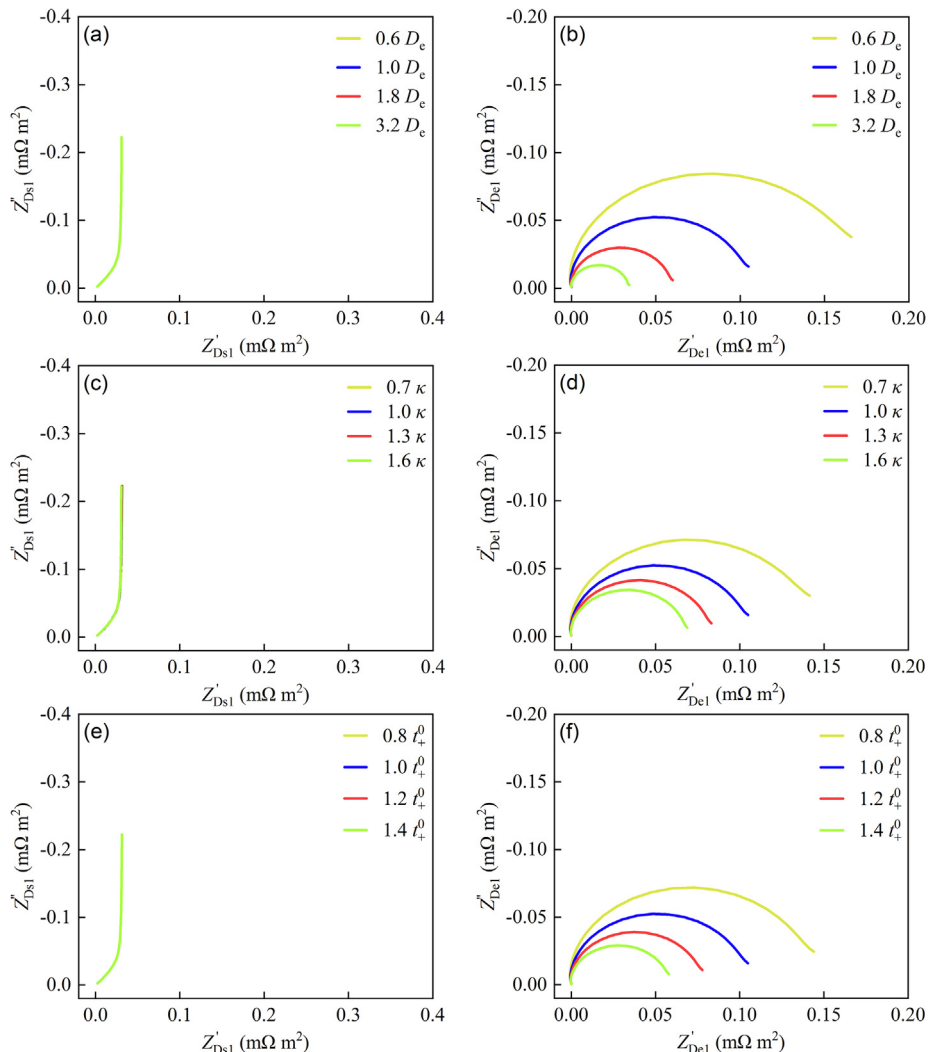


Fig. 22. Competitive effect of the solid/electrolyte diffusion in the negative electrode based on the unified impedance model with respect to D_e , κ , and t_+^0 . Nyquist plots of (a, c, e) and (b, d, f) for Z'_{Dsl} and Z'_{Del} , respectively. Default parameters for simulation are listed in Table 3.

r_{s1} , k_1 , ρ_{sei1} , L_1 , ε_{e1} , σ_1 , D_e , κ , t_+^0 , or T) can be calculated quantitatively, which provides fundamental information for battery parameter identification.

(3) Building up a theory framework to unveil the competitive mechanisms of charge transfer reactions in LIBs. Based on the built EIS-Toolbox@LIB for the unified impedance model, we believe the open source code might accelerate the spread of impedance diagnosis in the electrochemical energy storage and conversion field.

In summary, the above results should be beneficial to revealing charge transfer reactions, monitoring the battery status, identifying the electrode kinetics, and understanding the charge storage/transport mechanisms for LIBs and other electrochemical devices.

CRediT authorship contribution statement

Yuxuan Bai: Data curation, Writing – original draft, Visualization, Methodology, Software. **Qiu-An Huang:** Conceptualization, Writing – review & editing, Validation, Supervision. **Kai Wu:** Investigation, Formal analysis, Project administration. **Jiujun Zhang:** Funding acquisition, Resources.

Declaration of competing interest

The authors declare that they have no known competing financial interests or personal relationships that could have appeared to influence the work reported in this paper.

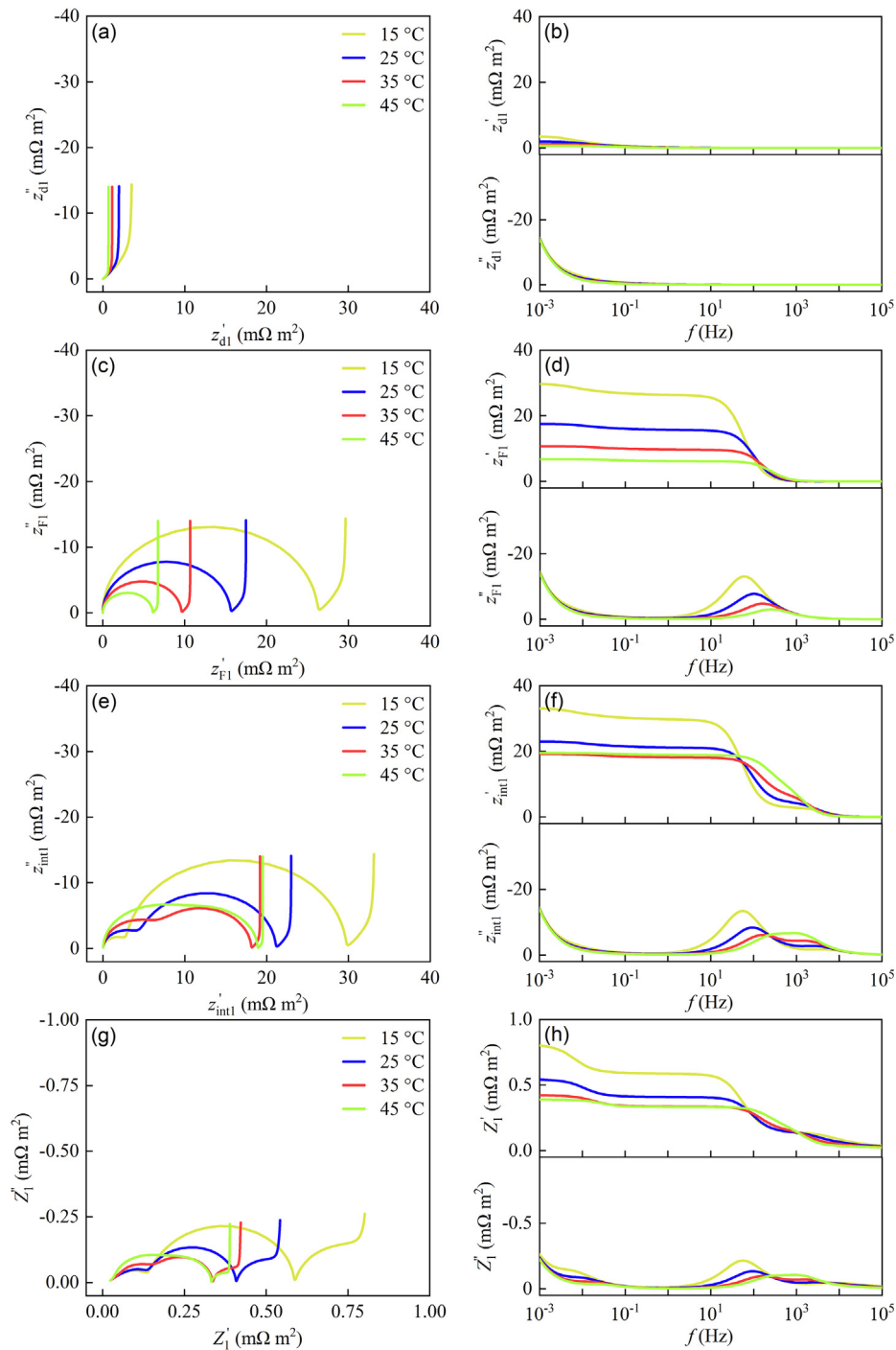


Fig. 23. Competitive effect of charge transfer reaction from the particle to the negative electrode based on the unified impedance model with respect to T . Nyquist and Bode plots of (a, b), (c, d), (e, f), and (g, h) for z_{dl} , z_{Fl} , z_{intl} , and Z_l , respectively. Default parameters for simulation are listed in Table 3.

Acknowledgments

We are grateful for the financial support from the National Science Foundation of China (22078190) and the National Key R & D Plan of China (2020YFB1505802).

Appendix A Supplementary data

EIS-Toolbox@LIB availability statement

The Matlab[®] source code for EIS-Toolbox@LIB is attached in the Supplementary data.

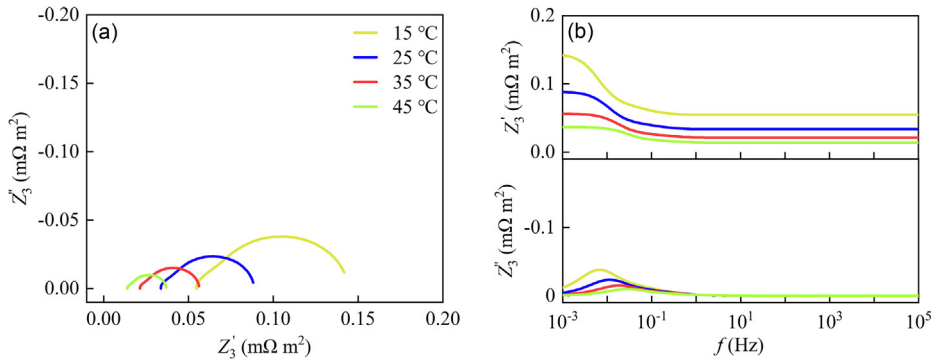


Fig. 24. Competitive effect of the ohmic behavior and the electrolyte diffusion for the separator based on the unified impedance model with respect to T . (a) Nyquist plot and (b) Bode plot for Z_3 . Default parameters for simulation are listed in Table 3.

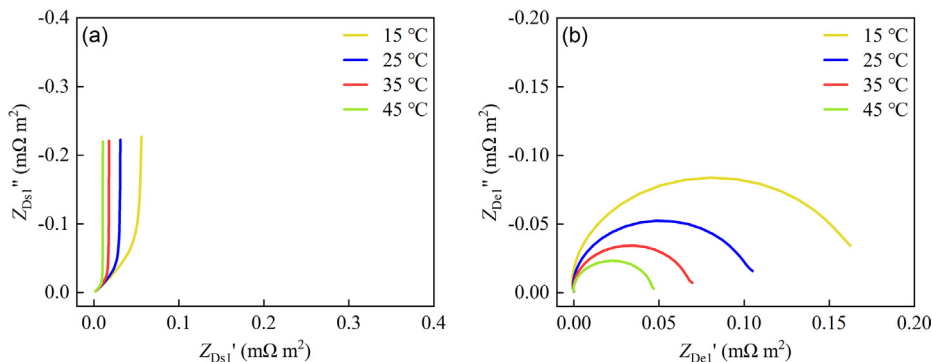


Fig. 25. Competitive effect of the solid/electrolyte diffusion in the negative electrode based on the unified impedance model with respect to T . Nyquist plots of (a) Z_{Ds1} and (b) Z_{De1} for the solid and electrolyte diffusion, respectively. Default parameters for simulation are listed in Table 3.

Table 6

Characteristic time constants (s) and polarization resistances (Ω m 2) for LIBs under different temperatures.

Temperature	τ_{d1} (cal)	τ_{Ds1} (fit)	τ_{De1} (fit)	τ_{De3} (fit)	τ_{ct1} (cal)	τ_{ct1} (fit)	τ_{se11} (cal)	τ_{se11} (fit)
15 °C	67.40	74.63	81.43	65.68	2.62×10^{-3}	2.54×10^{-3}	3.45×10^{-5}	1.63×10^{-5}
25 °C	37.04	43.57	47.84	39.25	1.56×10^{-3}	1.61×10^{-3}	5.50×10^{-5}	3.24×10^{-5}
35 °C	21.16	25.94	29.06	24.33	9.58×10^{-4}	9.44×10^{-4}	8.50×10^{-5}	5.41×10^{-5}
45 °C	12.52	15.88	18.29	15.57	6.09×10^{-4}	6.31×10^{-4}	1.28×10^{-4}	1.02×10^{-4}
Temperature	R_{d1} (cal)	R_{Ds1} (fit)	R_{De1} (fit)	R_{De3} (fit)	R_{ct1} (cal)	R_{ct1} (fit)	R_{se11} (cal)	R_{se11} (fit)
15 °C	9.96×10^{-4}	1.10×10^{-4}	1.60×10^{-4}	8.12×10^{-5}	2.62×10^{-2}	4.35×10^{-4}	3.45×10^{-3}	9.45×10^{-5}
25 °C	5.66×10^{-4}	6.26×10^{-5}	9.96×10^{-5}	5.21×10^{-5}	1.56×10^{-2}	2.67×10^{-4}	5.50×10^{-3}	9.09×10^{-5}
35 °C	3.34×10^{-4}	3.68×10^{-5}	6.55×10^{-5}	3.39×10^{-5}	9.58×10^{-3}	1.86×10^{-4}	8.50×10^{-3}	1.08×10^{-4}
45 °C	2.04×10^{-4}	2.24×10^{-5}	4.47×10^{-5}	2.25×10^{-5}	6.09×10^{-3}	1.51×10^{-4}	1.28×10^{-2}	1.48×10^{-4}

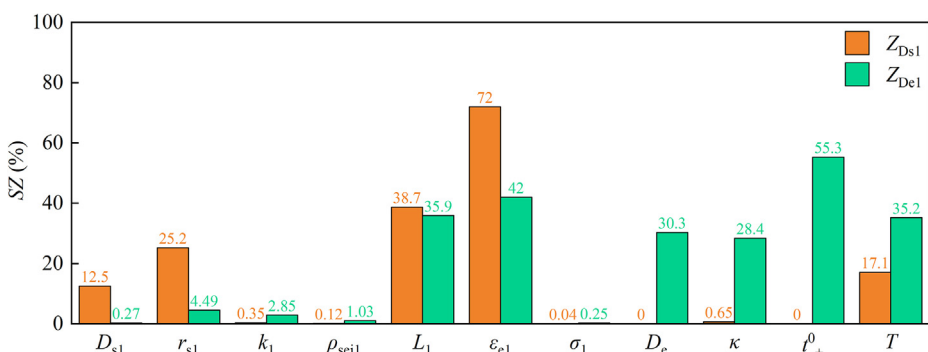


Fig. 26. Sensitive analysis of the solid/electrolyte diffusion to the parameter set X ($X = D_{s1}, r_{s1}, k_1, \rho_{se11}, L_1, \varepsilon_{e1}, \sigma_1, D_e, \kappa, t_+^0$, or T) based on the unified impedance model. Default parameters for simulation are listed in Table 3.

Supplementary data to this article can be found online at <https://doi.org/10.1016/j.jechem.2024.02.003>.

References

- [1] J. Xing, S. Bliznakov, L. Bonville, M. Oljaca, R. Maric, *Electrochim. Energy Rev.* 5 (2022) 14.
- [2] Y. Yu, Q. Zhang, J. Chen, S.-G. Sun, *Energy Fuels* 35 (2021) 10945–10948.
- [3] Y. Feng, L. Zhou, H. Ma, Z. Wu, Q. Zhao, H. Li, K. Zhang, J. Chen, *Energy Environ. Sci.* 15 (2022) 1711–1759.
- [4] S. Zhao, B. Wang, Z. Zhang, X. Zhang, S. He, H. Yu, *Electrochim. Energy Rev.* 5 (2022) 1–31.
- [5] F. Single, B. Horstmann, A. Latz, *J. Phys. Chem. C* 123 (2019) 27327–27343.
- [6] H. Qian, H. Ren, Y. Zhang, X. He, W. Li, J. Wang, J. Hu, H. Yang, H.M.K. Sari, Y. Chen, X. Li, *Electrochim. Energy Rev.* 5 (2022) 2.
- [7] S. Wang, J. Zhang, O. Gharbi, V. Vivier, M. Gao, M.E. Orazem, *Nat. Rev. Methods Primers.* 1 (2021) 41.
- [8] K. Ariyoshi, Z. Siroma, A. Mineshige, M. Takeno, T. Fukutsuka, T. Abe, S. Uchida, *Electrochim.* 90 (2022) 102007.
- [9] V. Vivier, M.E. Orazem, *Chem. Rev.* 122 (2022) 11131–11168.
- [10] Y.X. Yao, X. Chen, N. Yao, J.H. Gao, G. Xu, J.F. Ding, C.L. Song, W.L. Cai, C. Yan, Q. Zhang, *Angew. Chem. Int. Ed.* 62 (2023) e202214828.
- [11] S.S. Zhang, *InfoMat.* 2 (2020) 942–949.
- [12] H. Hamed, S. Yari, J. D'Haen, F.U. Renner, N. Reddy, A. Hardy, M. Safari, *Adv. Energy Mater.* 10 (2020) 2002492.
- [13] R. Tian, S.-H. Park, P.J. King, G. Cunningham, J. Coelho, V. Nicolosi, J.N. Coleman, *Nat. Commun.* 10 (2019) 1933.
- [14] C. Heubner, M. Schneider, A. Michaelis, *Adv. Energy Mater.* 10 (2020) 1902523.
- [15] T.R. Tanim, P.J. Weddle, Z. Yang, A.M. Colclasure, H. Charalambous, D.P. Finegan, Y. Lu, M. Preefer, S. Kim, J.M. Allen, F.L.E. Usseglio-Viretta, P.R. Chinnam, I. Bloom, E.J. Dufek, K. Smith, G. Chen, K.M. Wiaderek, J.N. Weker, Y. Ren, *Adv. Energy Mater.* 12 (2022) 2202795.
- [16] S. Tu, Z. Lu, M. Zheng, Z. Chen, X. Wang, Z. Cai, C. Chen, L. Wang, C. Li, Z.W. Seh, S. Zhang, J. Lu, Y. Sun, *Adv. Mater.* 34 (2022) 2202892.
- [17] A. Bhowmik, T. Vegge, *Joule* 4 (2020) 717–719.
- [18] P.M. Attia, A. Grover, N. Jin, K.A. Severson, T.M. Markov, Y.-H. Liao, M.H. Chen, B. Cheong, N. Perkins, Z. Yang, P.K. Herring, M. Aykol, S.J. Harris, R.D. Braatz, S. Ermon, W.C. Chueh, *Nature* 578 (2020) 397–402.
- [19] J. Wang, R. Zhao, Q.-A. Huang, J. Wang, Y. Fu, W. Li, Y. Bai, Y. Zhao, X. Li, J. Zhang, *J. Power Sources.* 561 (2023) 232737.
- [20] M. Bercicibar, *Nature*. 568 (2019) 325–326.
- [21] S.J. Moura, in: 2015 54th IEEE Conference on Decision and Control (CDC). (2015) 3906–3912.
- [22] S. Sarkar, S.Z. Halim, M.M. El-Halwagi, F.I. Khan, *J. Electrochim. Soc.* 169 (2022) 100501.
- [23] W. Li, Y. Fan, F. Ringbeck, D. Jöst, D.U. Sauer, *Appl. Energy.* 306 (2022) 118114.
- [24] M.R. Palacín, A. de Guibert, *Science.* 351 (2016) 1253292.
- [25] S. Ding, Y. Li, H. Dai, L. Wang, X. He, *Adv. Energy Mater.* (2023) 2301452.
- [26] M.D. Murbach, D.T. Schwartz, *J. Electrochim. Soc.* 165 (2018) A297–A304.
- [27] A.M. Bizeray, J.H. Kim, S.R. Duncan, D.A. Howey, *IEEE Trans. Control Syst. Technol.* 27 (2018) 1862–1877.
- [28] Y. Lu, C.-Z. Zhao, J.-Q. Huang, Q. Zhang, *Joule*. 6 (2022) 1172–1198.
- [29] Y. Che, X. Hu, R. Teodorescu, *Joule*. 7 (2023) 1405–1407.
- [30] C. Zhu, R.E. Usiskin, Y. Yu, J. Maier, *Science.* 358 (2017) eaao2808.
- [31] N.A. Chaturvedi, R. Klein, J. Christensen, J. Ahmed, A. Kojic, *IEEE Control Syst. Mag.* 30 (2010) 49–68.
- [32] T. Gao, Y. Han, D. Fragedakis, S. Das, T. Zhou, C.-N. Yeh, S. Xu, W.C. Chueh, J. Li, M.Z. Bazant, *Joule*. 5 (2021) 393–414.
- [33] H. Gao, Q. Yan, J. Holoubek, Y. Yin, W. Bao, H. Liu, A. Baskin, M. Li, G. Cai, W. Li, D. Tran, P. Liu, J. Luo, Y.S. Meng, Z. Chen, *Adv. Energy Mater.* 13 (2023) 2202906.
- [34] J. Hu, H. Guo, Y. Li, H. Wang, Z. Wang, W. Huang, L. Yang, H. Chen, Y. Lin, F. Pan, *Nano Energy.* 89 (2021) 106413.
- [35] Z. Deng, X. Lin, Z. Huang, J. Meng, Y. Zhong, G. Ma, Y. Zhou, Y. Shen, H. Ding, Y. Huang, *Adv. Energy Mater.* 11 (2020) 2000806.
- [36] Y. Li, Z. Gao, F. Hu, X. Lin, Y. Wei, J. Peng, J. Yang, Z. Li, Y. Huang, H. Ding, *Small Methods.* 4 (2020) 106413.
- [37] Q. Meng, S. Lou, B. Shen, X. Wan, X. Xiao, Y. Ma, H. Huo, G. Yin, *Electrochim. Energy Rev.* 5 (2022) 30.
- [38] A.A. Franco, A. Rucci, D. Brandell, C. Frayret, M. Gaberscek, P. Jankowski, P. Johansson, *Chem. Rev.* 119 (2019) 4569–4627.
- [39] Z. Deng, V. Kumar, F.T. Bölle, F. Caro, A.A. Franco, I.E. Castelli, P. Canepa, Z.W. Seh, *Energy Environ. Sci.* 15 (2022) 579–594.
- [40] J. Halme, P. Vahermaa, K. Miettunen, P. Lund, *Adv. Mater.* 22 (2010) E210–E234.
- [41] J.T.S. Irvine, D.C. Sinclair, A.R. West, *Adv. Mater.* 2 (1990) 132–138.
- [42] R. De Levie, *Electrochim. Acta.* 8 (1963) 751–780.
- [43] R. De Levie, *Electrochim. Acta.* 9 (1964) 1231–1245.
- [44] W. Li, Q.-A. Huang, Y. Li, Y. Bai, N. Wang, J. Wang, Y. Hu, Y. Zhao, X. Li, J. Zhang, *J. Energy Chem.* 77 (2023) 384–405.
- [45] J. Newman, W. Tiedemann, *AIChE J.* 21 (1975) 25–41.
- [46] G. Paasch, K. Micka, P. Gersdorf, *Electrochim. Acta.* 38 (1993) 2653–2662.
- [47] M. Doyle, T.F. Fuller, J. Newman, *J. Electrochim. Soc.* 140 (1993) 1526–1533.
- [48] T.F. Fuller, M. Doyle, J. Newman, *J. Electrochim. Soc.* 141 (1994) 1–10.
- [49] M. Doyle, J. Newman, A.S. Goetz, C.N. Schmutz, J.M. Tarascon, *J. Electrochim. Soc.* 143 (1996) 1890–1903.
- [50] J.P. Meyers, M. Doyle, R.M. Darling, J. Newman, *J. Electrochim. Soc.* 147 (2000) 2930–2940.
- [51] M. Doyle, J.P. Meyers, J. Newman, *J. Electrochim. Soc.* 147 (2000) 99–110.
- [52] G. Sikha, R.E. White, *J. Electrochim. Soc.* 154 (2007) A43–A54.
- [53] G. Sikha, R.E. White, *J. Electrochim. Soc.* 155 (2008) A893–A902.
- [54] J. Huang, J. Zhang, *J. Electrochim. Soc.* 163 (2016) A1983–A2000.
- [55] X. Kong, G.L. Plett, M.S. Trimboli, Z. Zhang, Y. Zheng, *J. Electrochim. Soc.* 167 (2020) 013539.
- [56] A. Shodiev, E.N. Primo, M. Chouchane, T. Lombardo, A.C. Ngandjoung, A. Rucci, A.A. Franco, *J. Power Sources.* 454 (2020) 227871.
- [57] M. Cronau, M. Kroll, M. Szabo, F. Sälzer, B. Roling, *Batteries Supercaps.* 3 (2020) 611–618.
- [58] S. Devan, V.R. Subramanian, R.E. White, *J. Electrochim. Soc.* 151 (2004) A905–A913.
- [59] Q. Guo, V.R. Subramanian, J.W. Weidner, R.E. White, *J. Electrochim. Soc.* 149 (2002) A307–A318.
- [60] M. Pathak, M.D. Murbach, C. Pathak, T.-J. Jang, Y. Qi, D.T. Schwartz, V.R. Subramanian, *J. Electrochim. Soc.* 165 (2018) A1324–A1337.
- [61] L. Teo, V.R. Subramanian, D.T. Schwartz, *J. Electrochim. Soc.* 168 (2021).
- [62] X. Zhou, R. Zhang, Y. Wang, *Energy Technol.* 11 (2023) 2300473.
- [63] N. Biju, H. Fang, *Appl. Energy.* 339 (2023) 120905.
- [64] J. Jannik, J. Maier, *Phys. Chem. Chem. Phys.* 3 (2001) 1668–1678.
- [65] Y. Li, M. Vilathgamuwa, T. Farrell, N.T. Tran, J. Teague, *Electrochim. Acta.* 299 (2019) 451–469.
- [66] Y. Liu, C. Zhang, J. Jiang, L. Zhang, W. Zhang, L. Lao, S. Yang, *Appl. Energy.* 331 (2023).
- [67] P.M. Gomadam, J.W. Weidner, T.A. Zawodzinski, A.P. Saab, *J. Electrochim. Soc.* 150 (2003) E371–E376.
- [68] Y. Zhao, V. Kumtepe, S. Ludwig, A. Jossen, *J. Power Sources.* 530 (2022) 231250.
- [69] C. Rabissi, A. Innocenti, G. Sordi, A. Casalegno, *Energy Technol.* 9 (2021) 2000986.
- [70] Z. Siroma, N. Fujiwara, S.-I. Yamazaki, M. Asahi, T. Nagai, T. Ioroi, *Electrochim. Acta.* 160 (2015) 313–322.
- [71] M. Adamić, S.D. Talian, A.R. Sinigoi, I. Humar, J. Moškon, M. Gaberšček, *J. Electrochim. Soc.* 166 (2019) A5045–A5053.
- [72] S. Drvacić Talian, J. Bobnar, A.R. Sinigoi, I. Humar, M. Gaberšček, *J. Phys. Chem. C.* 123 (2019) 27997–28007.
- [73] K. Zelić, T. Katrašnik, M. Gaberšček, *J. Electrochim. Soc.* 168 (2021) 070543.
- [74] M.E. Orazem, B. Tribollet, *ChemTexts.* 6 (2020) 12.
- [75] A.C. Lazanas, M.I. Prodromidis, *ACS Med. Sci. Au.* 3 (2023) 162–193.
- [76] R.R. Gaddam, L. Katzenmeier, X. Lamprecht, A.S. Bandarenka, *Phys. Chem. Chem. Phys.* 23 (2021) 12926–12944.
- [77] X. Wang, X. Wei, J. Zhu, H. Dai, Y. Zheng, X. Xu, Q. Chen, *eTransportation* 7 (2021) 100093.
- [78] J. Huang, Y. Gao, J. Luo, S. Wang, C. Li, S. Chen, J. Zhang, *J. Electrochim. Soc.* 167 (2020) 166503.
- [79] W. Wang, H.-S.-H. Chung, J. Zhang, *IEEE Trans. Power Electron.* 29 (2014) 5905–5920.
- [80] J. Li, R.G. Landers, J. Park, *J. Power Sources.* 456 (2020) 227950.
- [81] M. Heinrich, N. Wolff, N. Harting, V. Laue, F. Röder, S. Seitz, U. Kreuer, *Batteries Supercaps.* 2 (2019) 530–540.
- [82] X. Zhou, J. Huang, *J. Energy Storage.* 31 (2020) 101629.
- [83] D. Lu, M.S. Trimboli, G. Fan, Y. Wang, G.L. Plett, *J. Electrochim. Soc.* 169 (2022) 080504.
- [84] S.E. Li, B. Wang, H. Peng, X. Hu, *J. Power Sources.* 258 (2014) 9–18.
- [85] X. Duan, F. Liu, E. Agar, X. Jin, *J. Electrochim. Soc.* 169 (2022) 040561.
- [86] R. Tao, T. Zhang, S. Tan, C.J. Jafra, C. Li, J. Liang, X.G. Sun, T. Wang, J. Fan, Z. Lu, C.A. Bridges, X. Suo, C.-L. Do-Thanh, S. Dai, *Adv. Energy Mater.* 12 (2022) 2200519.
- [87] D.A. Harrington, *J. Electroanal. Chem.* 737 (2015) 30–36.
- [88] J.P. Schmidt, T. Chrobak, M. Ender, J. Illig, D. Klotz, E. Ivers-Tiffée, *J. Power Sources.* 196 (2011) 5342–5348.
- [89] M. Gaberšček, *Acta Chim. Slov.* 61 (2014) 480–487.
- [90] N. Ogihara, Y. Itou, T. Sasaki, Y. Takeuchi, *J. Phys. Chem. C.* 119 (2015) 4612–4619.
- [91] H. Gao, Q. Wu, Y. Hu, J.P. Zheng, K. Amine, Z. Chen, *J. Phys. Chem. Lett.* 9 (2018) 5100–5104.
- [92] N. Vicente, M. Haro, G. Garcia-Belmonte, *Chem. Commun.* 54 (2018) 1025–1040.
- [93] R. Suarez-Hernandez, G. Ramos-Sánchez, I.O. Santos-Mendoza, G. Guzmán-González, I. González, *J. Electrochim. Soc.* 167 (2020) 100529.
- [94] J. Inamoto, S. Komiyama, S. Uchida, A. Inoo, Y. Matsuo, *J. Phys. Chem. C.* 126 (2022) 16100–16108.
- [95] E. Barsoukov, J.H. Kim, J.H. Kim, C.O. Yoon, H. Lee, *Solid State Ionics.* 116 (1999) 249–261.
- [96] U. Tröltzsch, O. Kanoun, H.-R. Tränkler, *Electrochim. Acta.* 51 (2006) 1664–1672.
- [97] X. Zhou, Z. Pan, X. Han, L. Lu, M. Ouyang, *J. Power Sources.* 417 (2019) 188–192.
- [98] W. Hu, Y. Peng, Y. Wei, Y. Yang, *J. Phys. Chem. C.* 127 (2023) 4465–4495.
- [99] M. Gaberšček, *Nat. Commun.* 12 (2021) 6513.
- [100] L. Wang, J. Qiu, X. Wang, L. Chen, G. Cao, J. Wang, H. Zhang, X. He, *eScience* 2 (2022) 125–137.

- [101] T. Li, X.-Z. Yuan, L. Zhang, D. Song, K. Shi, C. Bock, *Electrochim. Energy Rev.* 3 (2020) 43–80.
- [102] X. Zhou, J. Huang, Z. Pan, M. Ouyang, *J. Power Sources.* 426 (2019) 216–222.
- [103] K. Ando, T. Matsuda, D. Imamura, *J. Energy Chem.* 53 (2021) 285–289.
- [104] P.-Y. Lee, A. Nagar, K. Yoo, J. Kim, *J. Electroanal. Chem.* 942 (2023) 117572.
- [105] Y. Guo, J. Cai, Y. Liao, J. Hu, X. Zhou, *J. Energy Storage.* 72 (2023).
- [106] Y. Liu, Q. Liu, Z. Li, Y. Ren, J. Xie, H. He, F. Xu, *J. Electrochim. Soc.* 161 (2014) A620–A632.
- [107] Y. Liu, J. Xie, *J. Electrochim. Soc.* 162 (2015) A2208–A2217.
- [108] X. Duan, F. Liu, E. Agar, X. Jin, *J. Electrochim. Soc.* 170 (2023).
- [109] X. Kong, G.L. Plett, M.S. Trimboli, Z. Zhang, D. Qiao, T. Zhao, Y. Zheng, *J. Energy Storage.* 27 (2020) 101085.
- [110] R. Ma, J. He, Y. Deng, *J. Energy Storage.* 54 (2022) 105346.
- [111] Y. Chen, Y. Kang, Y. Zhao, L. Wang, J. Liu, Y. Li, Z. Liang, X. He, X. Li, N. Tavajohi, B. Li, *J. Energy Chem.* 59 (2021) 83–99.
- [112] J. Duan, X. Tang, H. Dai, Y. Yang, W. Wu, X. Wei, Y. Huang, *Electrochim. Energy Rev.* 3 (2019) 1–42.
- [113] J. Kalhoff, G.G. Eshetu, D. Bresser, S. Passerini, *ChemSusChem.* 8 (2015) 2154–2175.
- [114] J. Wang, X. Guo, Z. Luo, H. Yang, M. Chen, K. Wang, *Electrochim. Acta.* 465 (2023) 142992.
- [115] K. Mc Carthy, H. Gullapalli, K.M. Ryan, T. Kennedy, *J. Electrochim. Soc.* 168 (2021) 080517.
- [116] M. Messing, T. Shoa, S. Habibi, *J. Energy Storage.* 43 (2021) 103210.
- [117] A. Straßer, A. Adam, J. Li, *J. Power Sources.* 580 (2023) 233366.
- [118] N. Harms, T.P. Heins, U. Schröder, *Energy Technol.* 4 (2016) 1514–1519.
- [119] R. Pollard, T. Comte, *J. Electrochim. Soc.* 136 (1989) 3734–3748.
- [120] Q.-A. Huang, S.-M. Park, *J. Phys. Chem. C.* 116 (2012) 16939–16950.
- [121] C.-F. Chen, P.P. Mukherjee, *Phys. Chem. Chem. Phys.* 17 (2015) 9812–9827.
- [122] T. Jacobsen, K. West, *Electrochim. Acta.* 40 (1995) 255–262.
- [123] Q.-A. Huang, Y. Bai, L. Wang, J. Wang, F. Zhang, L. Wang, X. Li, J. Zhang, *J. Energy Chem.* 67 (2022) 209–224.
- [124] X. Li, Q.-A. Huang, W.-H. Li, Y.-X. Bai, J. Wang, Y. Liu, Y.-F. Zhao, J. Wang, J.-J. Zhang, *J. Electrochim.* 27 (2021) 467–497.
- [125] M. Schönleber, C. Uhlmann, P. Braun, A. Weber, E. Ivers-Tiffée, *Electrochim. Acta.* 243 (2017) 250–259.
- [126] J. Moškon, J. Žuntar, S.D. Talian, R. Dominko, M. Gaberšček, *J. Electrochim. Soc.* 167 (2020) 140539.
- [127] J. Moškon, M. Gaberšček, *J. Power Sources Adv.* 7 (2021) 100047.
- [128] S.D. Talian, J. Moškon, R. Dominko, M. Gaberšček, *Electrochim. Acta.* 302 (2019) 169–179.
- [129] M. Torchio, L. Magni, R.B. Gopaluni, R.D. Braatz, D.M. Raimondo, *J. Electrochim. Soc.* 163 (2016) A1192–A1205.
- [130] L. Zhang, L. Wang, G. Hinds, C. Lyu, J. Zheng, J. Li, *J. Power Sources.* 270 (2014) 367–378.
- [131] F. Wang, Z. Lin, L. Liu, X. Wei, S. Lin, L. Dai, Y. Wei, C. Liang, B. Liaw, *J. Electrochim. Soc.* 167 (2020) 090549.
- [132] J.S. Edge, S. O’Kane, R. Prosser, N.D. Kirkaldy, A.N. Patel, A. Hales, A. Ghosh, W. Ai, J. Chen, J. Yang, S. Li, M.-C. Pang, L.B. Diaz, A. Tomaszewska, M.W. Marzook, K.N. Radhakrishnan, H. Wang, Y. Patel, B. Wu, G.J. Offer, *Phys. Chem. Chem. Phys.* 23 (2021) 8200–8221.
- [133] S.E.J. O’Kane, W. Ai, G. Madabattula, D. Alonso-Alvarez, R. Timms, V. Sulzer, J. S. Edge, B. Wu, G.J. Offer, M. Marinescu, *Phys. Chem. Chem. Phys.* 24 (2022) 7909–7922.
- [134] R. Fu, S.-Y. Choe, V. Agubra, J. Fergus, *J. Power Sources.* 261 (2014) 120–135.
- [135] R. Fu, S.-Y. Choe, V. Agubra, J. Fergus, *J. Power Sources.* 278 (2015) 506–521.
- [136] E. Teliz, C.F. Zinola, V. Díaz, *Electrochim. Acta.* 426 (2022) 140801.
- [137] R. Xiong, Y. Pan, W. Shen, H. Li, F. Sun, *Renewable Sustainable Energy Rev.* 131 (2020) 110048.
- [138] X. Zhang, X. Zhang, X. Sun, Y. An, S. Song, C. Li, K. Wang, F. Su, C.-M. Chen, F. Liu, Z.-S. Wud, Y. Ma, *J. Power Sources.* 488 (2021) 229454.
- [139] J. Huang, Z. Li, J. Zhang, S. Song, Z. Lou, N. Wu, *J. Electrochim. Soc.* 162 (2015) A585–A595.
- [140] A. Nyman, T.G. Zavalis, R. Elger, M. Behm, G. Lindbergh, *J. Electrochim. Soc.* 157 (2010) A1236–A1246.
- [141] Y. Ji, Y. Zhang, C.-Y. Wang, *J. Electrochim. Soc.* 160 (2013) A636–A649.
- [142] Y. Zhao, S. Kücher, A. Jossen, *Electrochim. Acta.* 432 (2022) 141174.
- [143] E. Woillez, M. Chandresris, *J. Electrochim. Soc.* 170 (2023) 070527.
- [144] J. Wang, Q.-A. Huang, W.-H. Li, J. Wang, Q.-C. Zhuang, J.-J. Zhang, *J. Electrochim.* 26 (2020) 607–627.
- [145] Q.-A. Huang, Y. Shen, Y. Huang, L. Zhang, J. Zhang, *Electrochim. Acta.* 219 (2016) 751–765.
- [146] S. Cruz-Manzo, P. Greenwood, *J. Electroanal. Chem.* 871 (2020) 114305.
- [147] F. Jiang, P. Peng, *Sci. Rep.* 6 (2016) 32639.
- [148] T. Huang, J. Ding, Z. Liu, R. Zhang, B. Zhang, K. Xiong, L. Zhang, C. Wang, S. Shen, C. Li, P. Yang, F. Qiu, *eScience 2* (2022) 319–328.
- [149] R. Xiong, L. Li, Z. Li, Q. Yu, H. Mu, *Appl. Energy.* 219 (2018) 264–275.
- [150] J. Li, D. Wang, L. Deng, Z. Cui, C. Lyu, L. Wang, M. Pecht, *J. Energy Storage.* 31 (2020) 101538.
- [151] N.A.-Z. R-Smith, M. Leitner, I. Alic, D. Toth, M. Kasper, M. Romio, Y. Surace, M. Jahn, F. Kienberger, A. Ebner, G. Gramse, *J. Power Sources.* 512 (2021) 230459.
- [152] R.R. Jaini, B.P. Setzler, T.F. Fuller, *J. Electrochim. Soc.* 165 (2018) A3125–A3135.
- [153] D. Gruet, B. Delobel, D. Sicsic, I.T. Lucas, V. Vivier, *Electrochim. Acta.* 295 (2019) 787–800.
- [154] R.W.J.M. Huang, F. Chung, E.M. Kelder, *J. Electrochim. Soc.* 153 (2006) A1459–A1465.
- [155] X. Lai, C. Deng, X. Tang, F. Gao, X. Han, Y. Zheng, *J. Cleaner Prod.* 339 (2022) 130786.
- [156] V. Miš, A. Ramanayagam, B. Roling, *ACS Appl. Mater. Interfaces.* 14 (2022) 38246–38254.
- [157] M. Cronau, A. Paulus, L.P. Pescara, M. Kroll, D. Renz, J.A. Mekontso, A. Marx, B. Roling, *Batteries Supercaps.* 5 (2022) e202200194.
- [158] X. Wang, Y. Sone, G. Segami, H. Naito, C. Yamada, K. Kibe, *J. Electrochim. Soc.* 154 (2007) A14–A21.
- [159] W. Kim, D. Jang, H.-J. Kim, *J. Power Sources.* 510 (2021) 230338.
- [160] J. Ma, H. Wang, C. Zheng, Z. Tao, Y. Fu, H. Bai, H. Xiao, *J. Phys. Conf. Ser.* 2557 (2023) 012028.